TECHNICAL REPORT

IEC TR 61282-9

First edition
2006-07

Fibre optic communication system design guides –

Part 9: Guidance on polarization mode dispersion measurements and theory

IECNORM.COM : Click to view the full PDF of IEC TR 61282-9:2006
Withdrawn

Reference number
IEC/TR 61282-9:2006(E)

Publication numbering

As from 1 January 1997 all IEC publications are issued with a designation in the 60000 series. For example, IEC 34-1 is now referred to as IEC 60034-1.

Consolidated editions

The IEC is now publishing consolidated versions of its publications. For example, edition numbers 1.0, 1.1 and 1.2 refer, respectively, to the base publication, the base publication incorporating amendment 1 and the base publication incorporating amendments 1 and 2.

Further information on IEC publications

The technical content of IEC publications is kept under constant review by the IEC, thus ensuring that the content reflects current technology. Information relating to this publication, including its validity, is available in the IEC Catalogue of publications (see below) in addition to new editions, amendments and corrigenda. Information on the subjects under consideration and work in progress undertaken by the technical committee which has prepared this publication, as well as the list of publications issued, is also available from the following:

- **IEC Web Site (www.iec.ch)**

- **Catalogue of IEC publications**

  The on-line catalogue on the IEC web site (www.iec.ch/searchpub) enables you to search by a variety of criteria including text searches, technical committees and date of publication. On-line information is also available on recently issued publications, withdrawn and replaced publications, as well as corrigenda.

- **IEC Just Published**

  This summary of recently issued publications (www.iec.ch/online_news/ justpub) is also available by email. Please contact the Customer Service Centre (see below) for further information.

- **Customer Service Centre**

  If you have any questions regarding this publication or need further assistance, please contact the Customer Service Centre:

  Email: custserv@iec.ch
  Tel: +41 22 919 02 11
  Fax: +41 22 919 03 00

IECNORM.COM : Click to view the full PDF of IEC TR 61282-9:2006
Withdrawn

TECHNICAL REPORT

IEC TR 61282-9

First edition
2006-07

IECNORM.COM : Click to view the full PDF of IEC TR 61282-9:2006
Withdrawn

Fibre optic communication system design guides –

Part 9: Guidance on polarization mode dispersion measurements and theory

© IEC 2006 — Copyright - all rights reserved

No part of this publication may be reproduced or utilized in any form or by any means, electronic or mechanical, including photocopying and microfilm, without permission in writing from the publisher.

International Electrotechnical Commission, 3, rue de Varembé, PO Box 131, CH-1211 Geneva 20, Switzerland
Telephone: +41 22 919 02 11 Telefax: +41 22 919 03 00 E-mail: inmail@iec.ch Web: www.iec.ch

Commission Electrotechnique Internationale
International Electrotechnical Commission
Международная Электротехническая Комиссия

PRICE CODE XF

For price, see current catalogue

CONTENTS

FOREWORD 5
1 Scope 7
2 Normative references 7
3 Acronyms and abbreviations 8
4 General information 9
4.1 Polarization modes 9
4.2 Birefringence 11
4.3 Beat length 12
4.4 Polarization transfer function 12
4.5 Stokes parameters and the Poincaré sphere 13
4.6 Principal states of polarization 15
4.7 Differential group delay 15
4.8 Polarization mode dispersion 15
4.9 Polarization dispersion and birefringence vectors 16
4.10 Polarization mode coupling 18
4.11 Second-order polarization mode dispersion 23
5 Mathematical formulations of the polarization mode dispersion test methods 26
5.1 Stokes parameter evaluation 26
5.2 Modulation phase shift 39
5.3 Polarization phase shift 42
5.4 Fixed analyser 45
5.5 Interferometric method 59
5.6 Poincaré sphere arc method 84
5.7 Poole formula method 87
5.8 Single-end test methods 88
6 Measurement issues 95
6.1 Degree of polarization and amplified spontaneous emission 95
6.2 Suppression of amplified spontaneous emission using optical or electrical filtering 97
6.3 The use of a broadband source 98
6.4 The Nyquist theorem and optical measurements 99
6.5 Continuously swept tuneable laser source and sampling theory 106
6.6 Tuneable laser source and noise 107
6.7 The selection of the states of polarization 107
6.8 Coherence interference effects and multiple path interference 107
6.9 Fibre pigtails 108
6.10 Power measurement resolution and linearity 108
6.11 Calibration of test instruments 108

Annex A (informative) Summary of various PMD test methods found in IEC standards 109
Annex B (Informative) Summary of key definitions 111
Annex C (Informative) Calculation of polarization mode dispersion value 114
Annex D (informative) Generalised Parseval theorem 117
Annex E (informative) Open issues 119

Bibliography 125

IECNORM.COM : Click to view the full PDF of IEC TR 61282-9:2006
Withdrawn

Figure 1 – Two electric field vector polarizations of the HE_{11} mode in an optical fibre along the a) *x*-direction and b) *y*-direction 10
Figure 2 – Cartesian and elliptical representation of a state of polarization 12
Figure 3 – Poincaré sphere representation of states of polarization 14
Figure 4 – Effect of polarization mode dispersion on transmission of an information-bit pulse in a device 16
Figure 5 – Polarization dispersion vector and principal states of polarization 17
Figure 6 – No or negligible mode coupling 18
Figure 7 – Random mode coupling 19
Figure 8 – Statistics of differential group delay and related Maxwell distribution [15] 22
Figure 9 – Polarization mode dispersion and differential group delay in negligible mode coupling 23
Figure 10 – Effects of first-order polarization mode dispersion (PMD_1) and second-order polarization mode dispersion (PMD_2) on the output state of polarization on the Poincaré sphere 24
Figure 11 – Rectangular system of co-ordinates defined by the response Stokes vectors, and direction angles of the polarization dispersion vector 29
Figure 12 – Arc of a circle described by the output state of polarization in the increment $[\omega, \omega+\Delta\omega]$ 30
Figure 13 – Functional diagram of Stokes parameter evaluation 36
Figure 14 – a) Differential group delay (DGD) as a function of the optical frequency (*f*) obtained through Poincaré sphere analysis (PSA) and Jones matrix analysis (JME), and b) Difference of DGDs. 38
Figure 15 – Trajectories of the principal states of polarization on the Poincaré sphere from a) Jones matrix eigenanalysis (JME) and b) Poincaré sphere analysis (PSA) 39
Figure 16 – Mueller states on Poincaré sphere 40
Figure 17 – Example of random mode coupling result with fixed analyser using Fourier transform technique [15] 49
Figure 18 – Polarization mode dispersion by Fourier analysis 54
Figure 19 – Mean cross-correlation and autocorrelation functions 58
Figure 20 – Generic set-up for the measurement of polarization mode dispersion using the interferometric test method 59
Figure 21 – Schematic diagram for GINTY analysis using input/output state-of-polarization scrambling 65
Figure 22 – Comparison between single-scan and scrambling uncertainties 69
a) With a polarization maintaining fibre and one I/O SOP) 70
b) With I/O-SOP scrambling (L/h << 1, DGD = 0,732 ps, σ_A = 50 fs, DGD/σ_A ~ 14,7) 70
Figure 23 – Example of negligible-mode-coupling result using a) TINTY analysis and b) GINTY analysis 70
Figure 24 – Example of random-mode-coupling result using TINTY analysis 71
Figure 25 – Example of random-mode-coupling result using GINTY analysis with I/O-SOP scrambling 75
Figure 26 – Equivalence between a) Stokes parameter evaluation method PSA analysis and b) GINTY analysis 76
Figure 27 – Example of mixed-mode-coupling result using GINTY analysis 79
Figure 28 – Comparison between polarization mode dispersion results from TINTY and GINTY analyses 81
Figure 29 – Relationship between beat length and state of polarization 85

IECNORM.COM : Click to view the full PDF of IEC TR 61282-9:2006
Withdrawn

Figure 30 – Relationship between Stokes parameter and state of polarization on the Poincaré sphere 85
Figure 31 – Relationship between fixed analyser method with circular analyser (—) and Poincaré sphere arc method (---) 86
Figure 32 – Relationship of state of polarization (SOP) analysis to normalised Stokes s_3 parameter 87
a) For wide SOP-to-birefringence axis angle 93
b) For a small SOP-to-birefringence axis angle 93
Figure 33 – Backscattered state of polarization (SOP) for short and long pulses versus distance 93
Figure 34 – Degree of polarization (DOP) vs. distance for a concatenation of three 500-m fibres, with a centre fibre that exhibits a high *h* value 94
Figure 35 – Power spectrum of a typical optical fibre amplifier output showing the amplified signal, the amplified spontaneous emission (ASE), and the optical signal-to-noise ratio (OSNR) 95
Figure 36 – Power ratio of amplified signal to total amplified spontaneous emission (ASE) versus the optical signal-to-noise ratio (OSNR) in 0,1-nm resolution bandwidth (RBW) 96
Figure 37 – Time varying signal 99
Figure 38 – Frequency spectrum of Figure 37 signal (its Fourier transform) a) in linear; b) in log scales 100
Figure 39 – Filtered signal with Nyquist-based defined bandwidth 101
Under-sampled signal (factor 2) 101
Figure 40 – Unfiltered signal with under-sampled (factor 2) defined bandwidth a 101
Figure 41 – Figure 37 signal with noise 102
Figure 42 – Frequency spectrum of Figure 41 signal 102
Figure 43 – Filtered noisy signal respecting the Nyquist theorem 103
Figure 44 – Un-filtered noisy signal spectrum not respecting the Nyquist theorem 103
Figure 45 – Signal frequency spectrum (of a filter as an example) 104
Figure 46 – Impulse response from Figure 45 signal 104
a) Signal frequency spectrum reconstructed following the Nyquist theorem 105
b) Under-sampled signal frequency spectrum 105
c) Under-sampled noisy signal spectrum 105
d) Reconstructed frequency spectrum of signal shown in (c) 105
Figure 47 – Reconstructed signal based on Figure 45 a) following the Nyquist theorem; b) not following the Nyquist theorem; c) including noise; d) based on c) 105

Table 1 – Example of Mueller set 41
Table 2 – Cosine Fourier transform calculations 57
Table 3 – Values of g_S for various types or degrees of coupling 80
Table 4 – Values of 45 ° power, Stokes parameters and SOP corresponding to Figure 29 85
Table A.1 – Applicability matrix for various polarization-mode-dispersion test methods 109
Table D.1 – Definition of the Fourier transform pairs 117

IECNORM.COM : Click to view the full PDF of IEC TR 61282-9:2006
Withdrawn

INTERNATIONAL ELECTROTECHNICAL COMMISSION

FIBRE OPTIC COMMUNICATION SYSTEM DESIGN GUIDES –

Part 9: Guidance on polarization mode dispersion measurements and theory

FOREWORD

1) The International Electrotechnical Commission (IEC) is a worldwide organization for standardization comprising all national electrotechnical committees (IEC National Committees). The object of IEC is to promote international co-operation on all questions concerning standardization in the electrical and electronic fields. To this end and in addition to other activities, IEC publishes International Standards, Technical Specifications, Technical Reports, Publicly Available Specifications (PAS) and Guides (hereafter referred to as "IEC Publication(s)"). Their preparation is entrusted to technical committees; any IEC National Committee interested in the subject dealt with may participate in this preparatory work. International, governmental and non-governmental organizations liaising with the IEC also participate in this preparation. IEC collaborates closely with the International Organization for Standardization (ISO) in accordance with conditions determined by agreement between the two organizations.
2) The formal decisions or agreements of IEC on technical matters express, as nearly as possible, an international consensus of opinion on the relevant subjects since each technical committee has representation from all interested IEC National Committees.
3) IEC Publications have the form of recommendations for international use and are accepted by IEC National Committees in that sense. While all reasonable efforts are made to ensure that the technical content of IEC Publications is accurate, IEC cannot be held responsible for the way in which they are used or for any misinterpretation by any end user.
4) In order to promote international uniformity, IEC National Committees undertake to apply IEC Publications transparently to the maximum extent possible in their national and regional publications. Any divergence between any IEC Publication and the corresponding national or regional publication shall be clearly indicated in the latter.
5) IEC provides no marking procedure to indicate its approval and cannot be rendered responsible for any equipment declared to be in conformity with an IEC Publication.
6) All users should ensure that they have the latest edition of this publication.
7) No liability shall attach to IEC or its directors, employees, servants or agents including individual experts and members of its technical committees and IEC National Committees for any personal injury, property damage or other damage of any nature whatsoever, whether direct or indirect, or for costs (including legal fees) and expenses arising out of the publication, use of, or reliance upon, this IEC Publication or any other IEC Publications.
8) Attention is drawn to the Normative references cited in this publication. Use of the referenced publications is indispensable for the correct application of this publication.
9) Attention is drawn to the possibility that some of the elements of this IEC Publication may be the subject of patent rights. IEC shall not be held responsible for identifying any or all such patent rights.

The main task of IEC technical committees is to prepare International Standards. However, a technical committee may propose the publication of a technical report when it has collected data of a different kind from that which is normally published as an International Standard, for example "state of the art".

IEC 61282-9, which is a technical report, has been prepared by subcommittee 86C: Fibre optic systems and active devices, of IEC technical committee 86: Fibre optics.

The text of this technical report is based on the following documents:

Enquiry draft	Report on voting
86C/696/DTR	86C/703/RVC

Full information on the voting for the approval of this technical report can be found in the report on voting indicated in the above table.

IECNORM.COM : Click to view the full PDF of IEC TR 61282-9:2006
Withdrawn

This publication has been drafted in accordance with the ISO/IEC Directives, Part 2.

A list of all parts of IEC 61282 series, published under the general title *Fibre optic communication system design guides,* can be found on the IEC website.

The committee has decided that the contents of this publication will remain unchanged until the maintenance result date indicated on the IEC web site under "http://webstore.iec.ch" in the data related to the specific publication. At this date, the publication will be

- reconfirmed,
- withdrawn,
- replaced by a revised edition, or
- amended.

A bilingual version of this publication may be issued at a later date.

Withdrawn
IECNORM.COM : Click to view the full PDF of IEC TR 61282-9:2006

FIBRE OPTIC COMMUNICATION SYSTEM DESIGN GUIDES –

Part 9: Guidance on polarization mode dispersion measurements and theory

1 Scope

This technical report applies to all commercially available fibre optic products sensitive to polarization mode dispersion (PMD).

This report presents general information about PMD, the mathematical formulation related to the application of the generally accepted methods to test PMD, and some considerations related to the sampling theory regarding the use of different light sources and detection systems.

This report is complementary to the International Standards describing the PMD procedures (IEC 60793-1-48, IEC 61280-4-4, IEC 61290-11-1, IEC 61290-11-2 and IEC 61300-3-32) and other design guides on PMD (IEC 61282-3 and IEC 61292-5).

2 Normative references

The following referenced documents are indispensable for the application of this document. For dated references, only the edition cited applies. For undated references, the latest edition of the referenced document (including any amendments) applies.

IEC 60793-1-48: *Optical fibres – Part 1-48: Measurement methods and test procedures – Polarization mode dispersion*

IEC 61280-4-4: *Fibre optic communication subsystem test procedures – Part 4-4: Cable plants and links – Polarization mode dispersion measurement for installed links*

IEC 61290-11-1: *Optical fibre amplifier test methods – Part 11-1: Polarization mode dispersion – Jones matrix eigenanalysis method (JME)*

IEC 61290-11-2: *Optical amplifiers – Test methods – Part 11-2: Polarization mode dispersion parameter – Poincaré sphere analysis method*

IEC 61300-3-2: *Fibre optic interconnecting devices and passive components – Basic test and measurement procedures – Part 3-2: Examinations and measurements – Polarization dependence of attenuation in a single-mode fibre optic device*

IEC 61300-3-32: *Fibre optic interconnecting devices and passive components – Basic test and measurement procedures – Part 3-32: Examinations and measurements – Polarization mode dispersion for passive optical components* [1]

IEC/TR 61282-3: *Fibre optic communication system design guides – Part 3: Calculation of polarization mode dispersion*

IEC/TR 61292-5: *Optical amplifiers – Part 5: Polarization mode dispersion parameter – General information*

---

1 To be published

IECNORM.COM : Click to view the full PDF of IEC TR 61282-9:2006
Withdrawn

3 Acronyms and abbreviations

ASE	amplified spontaneous emission
AWG	array waveguide grating
BBS	broadband source
BER	bit error rate or bit error ratio
Clh	circular left handed
Crh	circular right handed
CSO	composite second-order beat noise
DAS	differential attenuation slope
DGD	differential group delay
DOP	degree of polarization
DUT	device under test
DVV	polarization dispersion vector velocity
DWDM	dense wavelength division multiplexing
EC	extrema counting
EDFA	erbium doped fibre amplifier
FA	fixed analyser
FAFT	fixed analyser Fourier transform
FAEC	fixed analyser extrema counting
FCFT	fast cosine Fourier transform
ffs	for further study
FT	Fourier transform
FWHM	full width at half the maximum
GINTY	general analysis for the interferometric method
HMD	harmonic distortion
IMD	intermodulation distortion
INTY	interferometry
I/O	input/output
ISI	inter-symbol interference
JME	Jones matrix eigenanalysis
L	linear
LH	linear horizontal
LV	linear vertical
MMA	Mueller matrix analysis
MPS	modulation phase shift
OA	optical amplifier
OFA	optical fibre amplifier
OSA	optical spectrum analyser
OTDR	optical time domain reflectometer
P-	parallel polarization (to the plane of incidence)
PDCD	polarization dependent chromatic dispersion
PDD	polarization dependent delay
PDG	polarization dependent gain

IECNORM.COM : Click to view the full PDF of IEC TR 61282-9:2006
Withdrawn

PDL	polarization dependent loss
PDV	polarization dispersion vector
PM	polarization mode
PMD	polarization mode dispersion
PMD_1	first-order polarization mode dispersion
PMD_2	second-order polarization mode dispersion
PMF	polarization maintaining fibre
POTDR	polarization optical time domain reflectometer
POWA	planar optical waveguide amplifier
PPS	polarization phase shift
PS	Poincaré sphere
PSA	Poincaré sphere analysis
PSP	principal states of polarization
RBW	resolution bandwidth
RMS	root mean square
RTM	reference test method
S	source
SMSR	side mode suppression ratio
SOP	state of polarization
SPE	Stokes parameter evaluation
SRM	standard reference material
SSE	source spontaneous emission
TINTY	traditional analysis for the interferometric method
TLS	tuneable laser source
TSSE	total source spontaneous emission
WDM	wavelength division multiplexing

4 General information

The following text provides general information concerning the PMD theory and phenomenon. In that context, the word "device" or "device under test" (DUT) is used throughout the text in the sense of an optical path with an input and an output interface, such as an optical fibre, an optical fibre cable, an optical component, an optical amplifier, etc. The device may be connectorised.

4.1 Polarization modes

The solution of the wave equation has degenerated eigenvalues. This means that even the fundamental solution is degenerated. A single-mode fibre can therefore support several modes, the polarization modes (PM), and by analogy can be considered as a multi-(polarization) mode fibre. In particular, the lowest order mode, namely the fundamental HE_{11} (LP_{01}) mode, can be chosen to have its transverse electric field predominately along the x-direction; the orthogonal polarization is an independent mode, as shown in Figure 1.

IECNORM.COM : Click to view the full PDF of IEC TR 61282-9:2006
Withdrawn

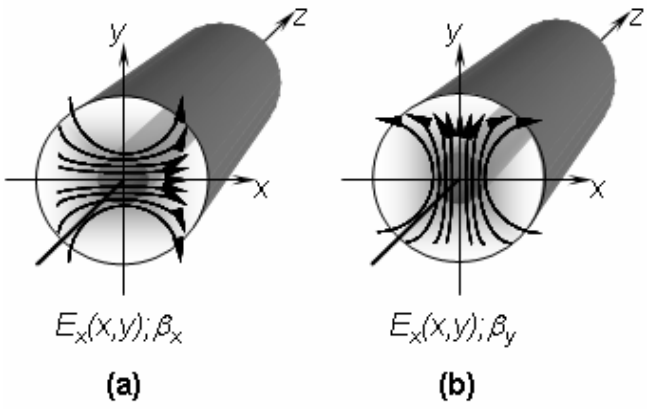

Figure 1 – Two electric field vector polarizations of the HE_{11} mode in an optical fibre along the a) x-direction and b) y-direction

In a lossless optical fibre, the electric field vector of a monochromatic electromagnetic wave propagating along the z-direction can be described by a linear superposition of these two PM in the x-y transverse plane as shown in Equation (1) and in Figure 1 [1,2][2].

$$E = \left\{\left[A_x(z)\cdot E_x(x,y)\right]+\left[A_y(z))\cdot E_y(x,y)\right]\right\}\cdot e^{-i\omega t} \quad (1)$$

where

$A_x(z)$ $= E_x e^{i\beta_x z}$, is the complex coefficient describing the amplitude E_x and the phase β_x of the PM along the x-direction propagating in the z-direction;

$A_y(z)$ $= E_y e^{i\beta_y z}$, is the complex coefficient describing the amplitude E_y and the phase β_y of the PM along the y-direction propagating in the z-direction;

$E_x(x,y)$ is the spatial variation (in the x-y transverse plane) of the electric field vector of the PM along the x-direction (see Figure 1(a);

$E_y(x,y)$ is the spatial variation (in the x-y transverse plane) of the electric field vector of the PM along the y-direction (see Figure 1(b);

β_x $= kn_x$, is the propagation constant (also called effective index or wavenumber) of the PM along the x-direction with the index of refraction n_x; β_x, through n_x has a dependence on optical angular frequency ω, or optical frequency ν, or wavelength λ;

β_y $= kn_y$, is the propagation constant (also called effective index or wavenumber) of the PM along the y-direction with the index of refraction n_y; β_y, through n_y has a dependence on angular optical frequency ω, or optical frequency ν, or wavelength λ;

k $= 2\pi\nu = 2\pi/\lambda = \omega/c$, is the propagation constant with the wavelength λ in vacuum;

ν is the optical frequency in s^{-1} or Hz;

ω is the angular optical frequency in rad/s;

c is the speed of light in vacuum;

z is the distance in the device along the optical axis; $z = L$ at the output of the device with length L.

The complex ratio $A_x(z)/A_y(z)$ describes the state of polarization (SOP) defined in the x-y plane of the wave propagating along the z-direction.

IECNORM.COM : Click to view the full PDF of IEC TR 61282-9:2006
Withdrawn

2 Figures in square brackets refer to the Bibliography.

In an ideal optical fibre with perfect circular symmetry,

- $\beta_y = \beta_x$;
- the two PM are degenerate;
- consequently, any wave with a defined input SOP will propagate unchanged along the z-direction throughout the output of the fibre.

However, in a practical optical fibre, imperfections produced by the fabrication process, cabling, field installation/use or the environment break the circular symmetry,

- $\beta_y \neq \beta_x$, implying a phase difference, and index of refraction difference Δn and a phase velocity difference Δv between the two PM;
- the degeneracy of the two PM is lifted;
- consequently, the SOP of an input wave will change along the z-direction throughout the output of the fibre.

The difference between β_y and β_x, namely $\Delta\beta$, is called the phase birefringence or simply the birefringence and has units of inverse length. Birefringence may also be referred to as the index difference, Δn. Index differences typically vary between 10^{-7} and 10^{-5} in commonly available single-mode fibres [2].

4.2 Birefringence

Birefringence is produced by an anisotropic distribution of the index of refraction in the propagating region of an optical device medium. As such, any device is susceptible to birefringence. For instance, birefringence is produced by asymmetry in the optical fibre core, meaning when the circular symmetry of the fibre core is broken [1,3].

It is well known that the asymmetry provides an index of refraction that is smaller along an axis, and as such that smaller index provides a faster phase velocity along that axis compared to the other one. That axis is consequently called the fast axis as opposed to the other one, which is called the slow axis, corresponding to a larger index and a slower phase velocity. The slower wave is also said to be retarded compared to the other one.

The asymmetry can result from geometrical deformation of the medium or material anisotropy through various elasto-optic, magneto-optic or electro-optic changes of the index of refraction. Geometrical deformation and asymmetric lateral stress via elasto-optic index changes may be produced during fabrication, for instance, and will typically produce linear birefringence. Bending, kinks and electro-optic Kerr effect will also typically produce linear birefringence. Twist and magneto-optic effect via Faraday effect will produce circular birefringence.

Several of these mechanisms may coexist and may be present in various numbers, strengths and distributions; and may vary with time and over environmental conditions. This makes the SOP along the propagating medium and at the output unpredictable and unstable and, consequently, PMD compensation difficult to achieve.

Birefringence can, however, be imposed, such as is the case for polarization maintaining fibre (PMF). This type of fibre has a strong birefringence maintained along the fibre length which can be created, for example, by introducing stress in one plane. This will keep the two PM non-degenerate. Any SOP launched aligned with the axis of one of these two PM will be maintained throughout the fibre. As opposed to PMF, commonly available single-mode fibres used for fibre optic transmissions in the field are weakly birefringent fibres.

IECNORM.COM : Click to view the full PDF of IEC TR 61282-9:2006
Withdrawn

4.3 Beat length

Birefringence makes the two PM slip in phase relative to one another as they propagate at different phase velocities. When the phase difference between the two PM is equal to an integer number of 2π, the two PM beat with one another, and at that periodic point along the z-direction, the input SOP is reproduced. The length corresponding to that periodicity is called the beat length L_b.

$$L_b = \frac{2\pi}{\Delta\beta} \text{ in units of length} \tag{2}$$

Beat lengths typically vary between 2 m and15 m in commonly available single-mode fibres [2].

Beat length should not be confused with coupling length, which will be explained later.

4.4 Polarization transfer function

Polarized light and its related SOP can be represented using Jones calculus [4] as a complex vector illustrating the x- and y- components of the electric field of the SOP at a point in space (see Figure 2).

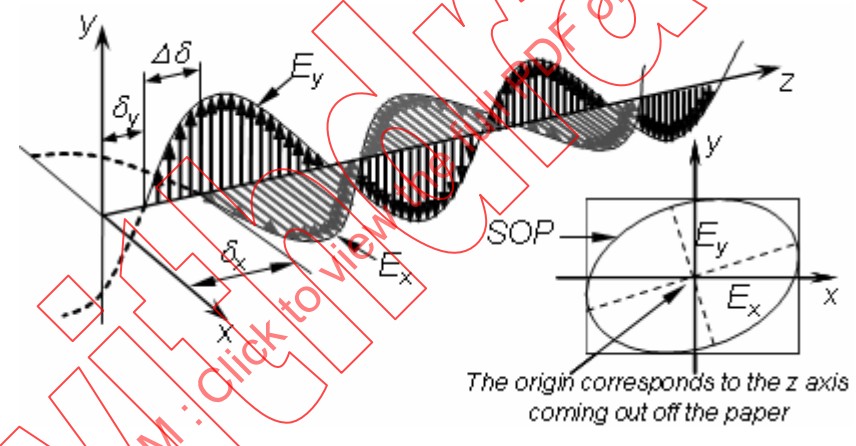

Figure 2 – Cartesian and elliptical representation of a state of polarization

NOTE In the presence of anisotropy, the y axis is the slow axis in Figure 2, while the x axis is the fast axis, and the wave propagating in the y-z plane is retarded. The resulting wave from the vector combination of the y-z plane wave and the x-z plane wave is shown in the x-y plane in the lower right corner of Figure 2

The Jones vector has the form (not considering any unit vector):

$$E = \begin{pmatrix} A_x \\ A_y \end{pmatrix} = \begin{pmatrix} E_x e^{i\delta_x} \\ E_y e^{i\delta_y} \end{pmatrix} \tag{3}$$

Equation (3) can easily be related to Equation (1) in case of anisotropy when δ becomes β. As polarized light traverses any DUT such as an optical fibre, its SOP undergoes a transformation. This transformation is described in Jones calculus by the complex 2x2 Jones matrix, T, so that the output Jones vector E_{out} is related to the input Jones vector E_{in} through E_{out} = T E_{in}. The Jones matrix is determined by measuring the output Jones vectors in response to any three unique input vectors. The calculation is simplest when the stimuli are linear horizontal (LH) 0 º (E_y = 0; δ_x = 0), linear vertical (LV) 90 º (E_x = 0, δ_y = 0) and linear (L) +45 º ($E_y = E_x$; δ_y = δ_x = 0) SOPs. If the responses to the three stimuli are:

IECNORM.COM : Click to view the full PDF of IEC TR 61282-9:2006
Withdrawn

$$\begin{pmatrix} X_1 \\ Y_1 \end{pmatrix}, \begin{pmatrix} X_2 \\ Y_2 \end{pmatrix}, \begin{pmatrix} X_3 \\ Y_3 \end{pmatrix} \tag{4}$$

the Jones matrix is

$$T = C^* \begin{bmatrix} K_1 K_4 & K_2 \\ K_4 & 1 \end{bmatrix} \tag{5}$$

$$K_1 = \frac{X_1}{Y_1};\ K_2 = \frac{X_2}{Y_2};\ K_3 = \frac{X_3}{Y_3};\ K_4 = \frac{K_3 - K_2}{K_1 - K_3} \tag{6}$$

where C is a complex constant.

The magnitude of C can be calculated from intensities measured with the DUT removed from the optical path. Most measurements do not require the calculation of C.

4.5 Stokes parameters and the Poincaré sphere

While Jones calculus is very useful in explaining SOPs, it is problematic in practice to measure the electric field of a light wave. An alternative expression for the SOPs is the Stokes vector, as shown in Equation (7):

$$S = \begin{bmatrix} S_0 \\ S_1 \\ S_2 \\ S_3 \end{bmatrix} \tag{7}$$

where

S_0 $= E_x^2 + E_y^2$ is the total power including the polarized and unpolarized parts;

NOTE The degree of polarization (DOP) is equal to the ratio of the polarized part of the power to S_0.

S_1 $= E_x^2 - E_y^2$ is the power difference between the LH and LV SOPs;

S_2 $= 2\mathrm{Re}(E_x E_y^*)$ is the power difference between the L +45 º and the L –45 º SOPs;

S_3 $= 2\mathrm{Im}(E_x E_y^*)$ is the power difference between the circular right-handed (Crh) and circular left-handed (Clh) SOPs.

The magnitude of the Stokes vector is the square root of the sum of the squares of S_1, S_2 and S_3.

The Poincaré sphere uses the normalised S parameters s ($s_1 = S_1/S_0$, $s_2 = S_2/S_0$, $s_3 = S_3/S_0$) as a three-real component unit vector co-ordinate system to represent any possible SOP [5,6]. The LH 0 º SOP is represented as (1,0,0), LV 90 º as (–1,0,0), L +45 º as (0,1,0), L –45 º as (0,-1,0), Crh as (0,0,1), and Clh as (0,0,-1).

Withdrawn
IECNORM.COM : Click to view the full PDF of IEC TR 61282-9:2006

$$E = \begin{pmatrix} E_x * e^{i\delta x} \\ E_y * e^{i\delta y} \end{pmatrix} \Rightarrow \begin{bmatrix} S_0 \\ S_1 \\ S_2 \\ S_3 \end{bmatrix} = \begin{bmatrix} E_x^2 + E_y^2 \\ E_x^2 - E_y^2 \\ 2\mathrm{Re}(E_x E_y^*) \\ 2\mathrm{Im}(E_x E_y^*) \end{bmatrix} = \begin{bmatrix} E_x^2 + E_y^2 \\ E_x^2 - E_y^2 \\ 2E_x E_y \cos\Delta\delta \\ 2E_x E_y \sin\Delta\delta \end{bmatrix} \quad (8)$$

$$\begin{bmatrix} s_1 \\ s_2 \\ s_3 \end{bmatrix} = \begin{bmatrix} S_1/S_0 \\ S_2/S_0 \\ S_3/S_0 \end{bmatrix} = \begin{bmatrix} (E_x^2 - E_y^2)/(E_x^2 + E_y^2) \\ 2\mathrm{Re}(E_x E_y^*)/(E_x^2 + E_y^2) \\ 2\mathrm{Im}(E_x E_y^*)/(E_x^2 + E_y^2) \end{bmatrix} = \begin{bmatrix} (E_x^2 - E_y^2)/(E_x^2 + E_y^2) \\ 2E_x E_y \cos\Delta\delta/(E_x^2 + E_y^2) \\ 2E_x E_y \sin\Delta\delta/(E_x^2 + E_y^2) \end{bmatrix} \quad (9)$$

In polar coordinates,

$$E = \begin{bmatrix} (\cos\theta)e^{-i\mu/2} \\ (\sin\theta)e^{i\mu/2} \end{bmatrix} e^{i\phi} \quad (10)$$

$$\begin{bmatrix} s_1 \\ s_2 \\ s_3 \end{bmatrix} = \begin{bmatrix} \cos 2\theta \\ (\sin 2\theta)(\cos\mu) \\ (\sin 2\theta)(\sin\mu) \end{bmatrix} \quad (11)$$

where $\Delta\delta = \delta_x - \delta_y$, is the difference in phase between the x (LH) and y (LV) SOPs.

The use of the Stokes vector parameters is best illustrated via the use of the Poincaré sphere (see Figure 3). Stokes vectors can be converted to Jones vectors using the respective E-field formulae.

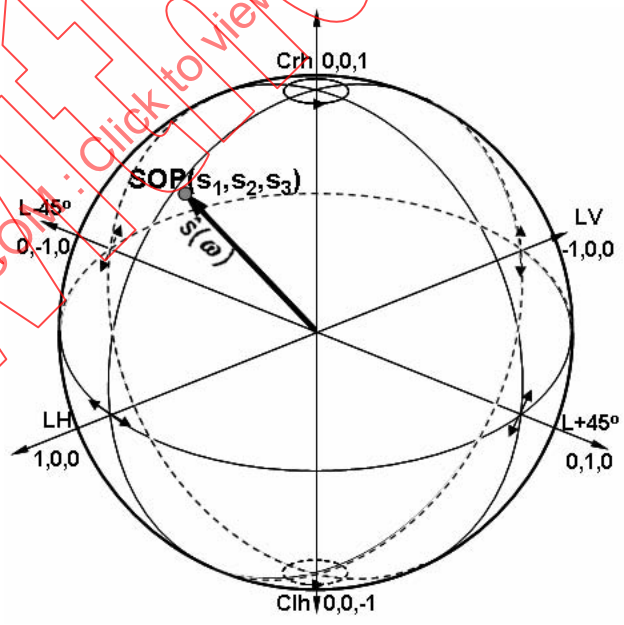

Figure 3 – Poincaré sphere representation of states of polarization

NOTE The *LH* axis usually faces the observer/receiver

IECNORM.COM : Click to view the full PDF of IEC TR 61282-9:2006
Withdrawn

For a fully polarized field (DOP = 100 %), $\sqrt{s_1^2 + s_2^2 + s_3^2}$ is unitary, and a SOP is represented by a dot on the surface of the sphere (the tip of the SOP vector). The observer looks at the LH SOP. Any SOP laying on the equator of the sphere is linear. The north pole of the sphere is Crh SOP, and the south pole is Clh SOP. Any other SOP anywhere else on the sphere is elliptical.

4.6 Principal states of polarization

In a device that exhibits PMD, there are two SOPs called principal states of polarization (PSPs) [7,8] having the property that the SOP measured at the output of the device is invariant with optical frequency (or wavelength) to first order (over a small optical frequency or wavelength increment) for any output SOP aligned with these PSPs. Of the two PSPs, the one called the fast PSP gives the fastest group velocity and consequently the shortest propagation delay; the other, called the slow PSP, gives the slowest group velocity and consequently the longest propagation delay. These two PSPs will be orthogonal in the absence of polarization dependent loss (PDL) or polarization dependent gain (PDG) and non-linear effects. In a device with polarization-mode coupling such as a single-mode optical fibre used to transport fibre optic telecommunications, the PSPs are, in general, different from the eigenstates of the device; in a non-mode-coupled device such as a PMF, the PSPs are identical to the eigenstates of the device. The eigenstates are the eigenvectors of the Jones matrix, i.e. the two SOPs which propagate through the device without modification.

NOTE 1 The two PSPs are an intrinsic function of the material birefringence and induced external and internal stresses acting on the device.

NOTE 2 An output signal whose SOP is aligned with one of the two PSPs will have been undistorted by PMD, at least to first order.

4.7 Differential group delay

The difference between the two PSP arrival times is the differential group delay (DGD). The resultant pulse broadening or splitting is the source of signal distortion.

The definition provided above is in the context of 1st order PMD without PDL. In the case of PDL, there is an open issue regarding the definition (see also E.2.1).

NOTE Depending on the device, DGD varies with wavelength, and for a randomly mode coupled device, the pattern of variation changes randomly with device deployment and small temperature changes (~0,1 °C). The average DGD across a wavelength range remains moderately stable, depending on the device construction and the wavelength range that is sampled.

4.8 Polarization mode dispersion

PMD is the temporal distortion of an optical signal induced by the interaction of the source polarization and spectral characteristics with the transport of the signal through a device that includes two orthogonal SOPs (i.e. PSPs) with differing group velocities. The term "PMD" is used both in this general sense of a “phenomenon” of pulse width broadening, as well as specific “numeric values” of broadening (in time) that characterise a device.

4.8.1 Phenomenon

When an optical signal pulse passes through a device, the pulse may change. PMD refers to the change in shape, particularly in the root-mean-square (RMS) width of the pulse, due to the average propagation delay difference between the two PSPs, i.e. DGD, and/or waveform distortion for each PSP (see Figure 4). PMD together with PDL and PDG, when applicable, may introduce waveform distortion leading to an unacceptable increase in bit error ratio (BER).

IECNORM.COM : Click to view the full PDF of IEC TR 61282-9:2006
Withdrawn

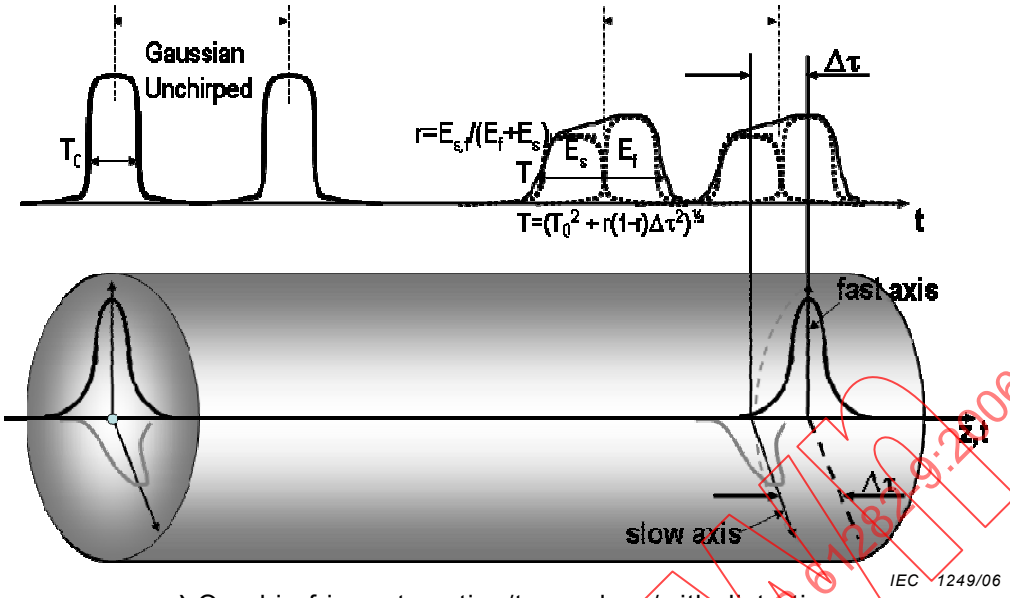

a) One birefringent section/two pulses/with distortion

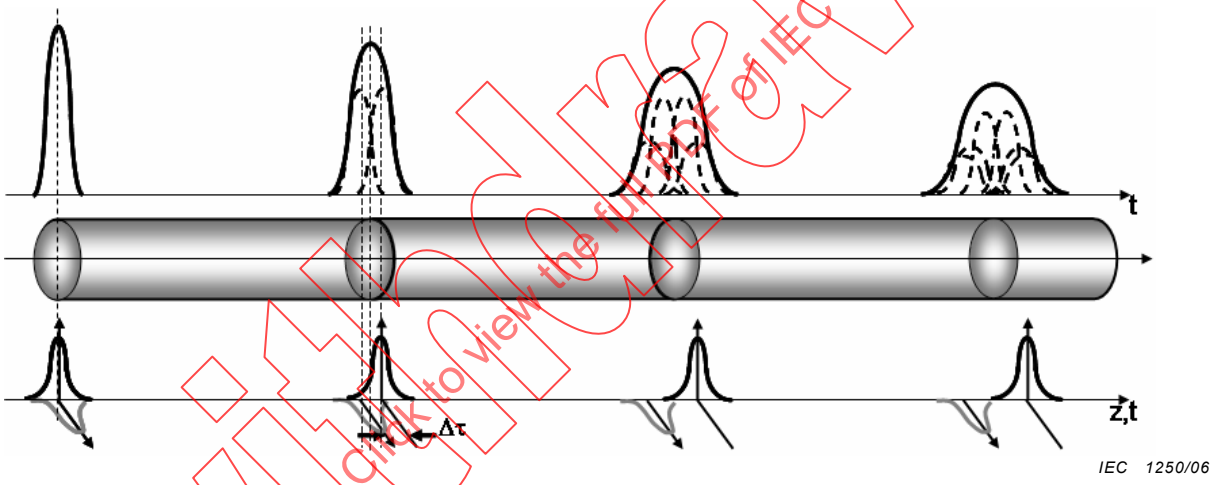

b) Multi-birefringent sections/one pulse/no distortion (only broadening)

Figure 4 – Effect of polarization mode dispersion on transmission of an information-bit pulse in a device

IECNORM.COM : Click to view the full PDF of IEC TR 61282-9:2006
Withdrawn

4.8.2 Numerical value

The PMD value (in units of time) is specified and measured depending on the type of device and its contribution to the overall signal link distortion. In some cases, either the average or RMS DGD over an optical frequency (or wavelength) range is used to define the PMD value. In other cases, the maximum DGD occurring in the optical frequency or wavelength range is used.

4.9 Polarization dispersion and birefringence vectors

From Poole [6,9,10], the polarization dispersion vector (PDV), $\hat{\Omega}$, and the birefringence vector, $\hat{\Delta\beta}$ are a compact way of representing PMD. The variation of the SOP, $\hat{s}$, as a function of the optical angular frequency, ω and z, inside the device obeys the equations of motion described in (12) and (13) respectively (see Figure 5).

$$\frac{d\hat{s}(\omega)}{d\omega} = \hat{\Omega}(\omega) x \hat{s}(\omega) \tag{12}$$

$$\frac{d\hat{s}(\omega)}{dz} = \Delta\hat{\beta}(\omega) x \hat{s}(\omega) \tag{13}$$

where

$\hat{s}$ is the SOP vector with three components, s_1, s_2 and s_3, defined in Equation (9), unitless and depending on ω and z;

$\hat{\Omega}$ is the PDV with three components, Ω_1, Ω_2 and Ω_3, depending on ω and z, and having units of time; $\hat{\Omega}$ depends on the DUT properties along the entire optical path;

$\hat{\Delta\beta}$ is the birefringence vector with three components, $\Delta\beta_1$, $\Delta\beta_2$ and $\Delta\beta_3$, depending on ω and z, and having units of inverse length; $\hat{\Delta\beta}$ depends on the DUT properties at position z;

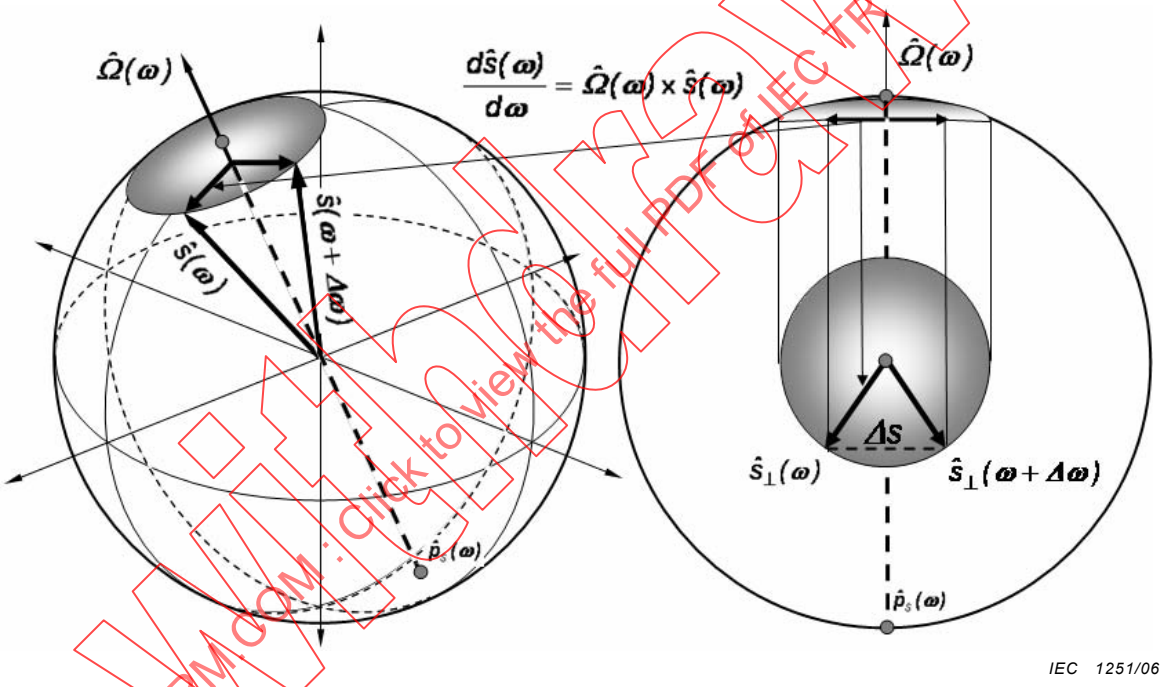

Figure 5 – Polarization dispersion vector and principal states of polarization

A relationship exists between the PDV and the birefringence vector, and this relationship has important consequences [6,10]:

$$\frac{d\hat{\Omega}}{dz} = \frac{d\hat{\Delta\beta}}{d\omega} + \left(\hat{\Delta\beta} x \hat{\Omega}\right) \tag{14}$$

where

$d\Delta\hat{\beta}/d\omega$ is the modal birefringence (vector), B, at position z along the DUT and has units of delay time per unit length;

$\Delta\hat{\beta} x \hat{\Omega}$ is the term indirectly affecting the growth of the polarization dispersion by causing the PDV to change direction with $d\Delta\hat{\beta}/d\omega$, causing dephasing between the two vectors.

IECNORM.COM : Click to view the full PDF of IEC TR 61282-9:2006
Withdrawn

$$B = \frac{1}{v}\left(\frac{\Delta v}{v}\right) \tag{15}$$

where

v is the average group velocity;

Δv is the differential group velocity between the fast and slow PM (PSPs), so that $v + ½\Delta v$ is the fast group velocity and $v - ½\Delta v$ is the slow group velocity [11].

Modal birefringence is responsible for the growth of the polarization dispersion along the DUT length.

When looking into the ω domain, the direction of $\hat{\Omega}$ is collinear with the PSP (in the direction of the fast PSP, $\hat{s}_p$, as shown in Figure 5). The magnitude of $\hat{\Omega}$ (its modulus) is equal to the DGD, i.e. (see Figure 5)

$$\hat{\Omega}(\omega) = \Delta\tau(\omega) \bullet \hat{s}_p(\omega) \tag{16}$$

where [7]

$$\hat{s}_p^{slow}(\omega) = -s_p^{fast}(\omega) \tag{17}$$

$$\left|\hat{\Omega}(\omega)\right| = \Delta\tau(\omega) = DGD \tag{18}$$

4.10 Polarization mode coupling

The two PM and output PSPs of a simple birefringent element result from two input PSPs whose fast and slow axes are maintained throughout the element (see Figure 6). A short optical fibre is often modelled as a simple birefringent element for which the two output PSPs do not change appreciably with optical frequency and throughout the fibre.

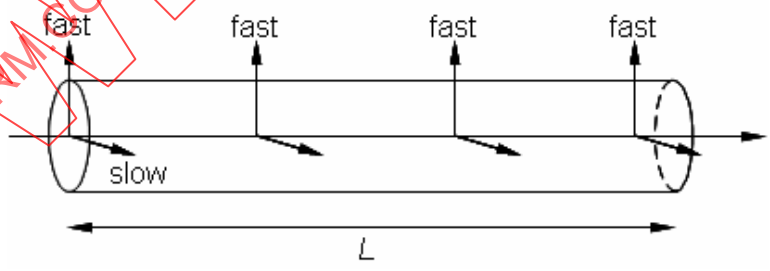

IEC 1252/06

Figure 6 – No or negligible mode coupling

In that case, the modal birefringence, B, is modelled as a constant vector (B,0,0). This is the case for PMF in which birefringence is strong.

If two such elements are concatenated, i.e. they are jointed with random axis orientation, the output PSPs of the first element may not align with the input PSPs of the second element, as shown in Figure 7. The distance between such concatenations is associated with the coupling length, h (also called the h-parameter).

IECNORM.COM : Click to view the full PDF of IEC TR 61282-9:2006
Withdrawn

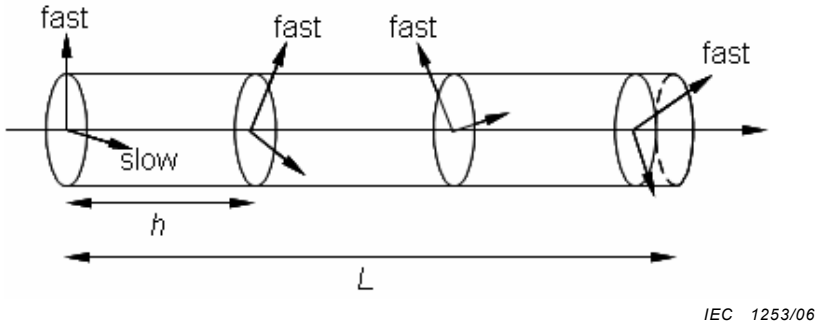

Figure 7 – Random mode coupling

Under this condition, mode coupling occurs: part of the energy of one local PM is transferred to the other one [11]. The mode coupling resulting from the repeated concatenation of many elements produces a continuous variation of the fast and slow axes along the DUT and a random variation, with optical frequency, of the output PSPs and DGD of the concatenation.

In a long single-mode optical fibre, the birefringence is generally too weak to maintain the polarization as compared to a PMF and is typically modelled as a weak but constant background birefringence $(\Delta\beta,0,0)$ together with a small random stepsize fluctuating perturbation $(\delta\Delta\beta_1,\delta\Delta\beta_2,\delta\Delta\beta_3)$ [6,10]. The distributions of the $\delta\Delta\beta_i$ are Gaussian and uncorrelated.

The local fast-axis PSP PM and the slow-axis PSP PM can easily couple together under the influence of external factors like fibre twist, or bending. That DUT is often modelled as the concatenation of several randomly oriented simple birefringent elements (short fibres) of randomly varying lengths. The h parameter is a metric used to quantify the average length of these elementary sections as shown in Figure 7.

In presence of random coupling, many PM exist across the frequency spectrum and a natural definition for PMD delay would be the mean square deviation of the time of flight of the various PMs. The many PMs exist because many frequencies exist. If only one frequency is present, only one pair of PMs would be present as well. The output time intensity leads to the telegrapher equation, describing the probability density function (PDF), ρ, of time of flight, τ, as a function of distance, z, in a DUT such as an optical fibre [11-13]:

$$\frac{\partial^2\rho}{\partial z^2}=\left(B^2\frac{\partial^2\rho}{\partial\tau^2}\right)-\left(\frac{2}{h}\frac{\partial\rho}{\partial z}\right) \tag{19}$$

The PMD delay is expressed by the RMS width of the PM time of flight distribution [6,14,15] and is expressed in units of ps:

$$PMD=\frac{Bh}{\sqrt{2}}\left(\frac{2L}{h}-1+e^{-2L/h}\right)^{1/2} \tag{20}$$

where h is the PM mean coupling length [11].

Equation (20) has two limit conditions [11]:

a) when $L << h$, the PMD distribution function (PDF of times of flight, τ) is flat:

$$PMD = BL \tag{21}$$

and PMD increases linearly with L.

IECNORM.COM : Click to view the full PDF of IEC TR 61282-9:2006
Withdrawn

b) when $L >> h$, the PMD distribution function (PDF of times of flight, τ) becomes essentially Gaussian:

$$PDF(\tau) = \left(\sqrt{\frac{1}{2\pi \langle \tau^2 \rangle}} \right) e^{-\tau^2 / 2\langle \tau^2 \rangle} \tag{22}$$

where $<\tau^2>^{1/2}$ is the PMD delay.

In that case,

$$PMD = B\sqrt{hL} \tag{23}$$

and PMD increases with the square root of L.

4.10.1 Random mode coupling

When the DGD statistically varies as a function of wavelength (or optical frequency), the PMD phenomenon is in general considered stochastic. The PMD phenomenon is defined as a stochastic process because of the random mode coupling between the two PSPs.

NOTE The expression *strong mode coupling* is also used in the literature and in some International Standards for *random mode coupling*. As a preference, the expression *random mode coupling* will be used in this document.

At any one optical frequency or wavelength, there are net PSPs for the entire DUT length (such as a long fibre) that depend on the totality of local disturbances, with DGD between fast and slow PSPs. Averaging the PSPs over a wavelength range, thermal range or time then yields the concept of sampling the population of disturbances and their spatial distribution (in relation to the local birefringence). The PMD is then essentially a statistical parameter characterised by the statistics of the PSPs and the statistics of DGD. In the former case, the PDV components $(\Omega_1, \Omega_2, \Omega_3)$ are known to obey a PDF following a Gaussian distribution similar to Equation (22), while in the latter case, the DGD (the square root of the sum of the squared Ω_i) is known to obey a PDF following a Maxwell distribution:

$$PDF(\Delta\tau) = \left(\sqrt{\frac{2}{\pi}} \right) \frac{\Delta\tau^2}{\sigma^3} e^{-\Delta\tau^2 / 2\sigma^2} \tag{24}$$

If the quadratic mean value $<\Delta\tau^2>$ is considered, then

$$\sigma = \frac{\langle \Delta\tau^2 \rangle^{1/2}}{\sqrt{3}} \tag{25}$$

and [5]

$$PDF(\Delta\tau) = 3\left(\sqrt{\frac{6}{\pi}} \right) \frac{\Delta\tau^2}{\langle \Delta\tau^2 \rangle^3} e^{-3\Delta\tau^2 / 2\langle \Delta\tau^2 \rangle} \tag{26}$$

and PMD will be equal to the RMS DGD:

$$PMD = <\Delta\tau^2>^{1/2} \tag{27}$$

IECNORM.COM : Click to view the full PDF of IEC TR 61282-9:2006
Withdrawn

If the mean value $<\Delta\tau>$ is considered, then

$$\sigma = \left(\sqrt{\frac{\pi}{8}}\right)\langle\Delta\tau\rangle \tag{28}$$

and

$$PDF(\Delta\tau) = \frac{32}{\pi^2}\frac{\Delta\tau^2}{\langle\Delta\tau\rangle^3}e^{-4\Delta\tau^2/\pi\langle\Delta\tau\rangle^2} \tag{29}$$

and the PMD is equal to the mean value of the DGD (see Figure 8).

$$PMD = <\Delta\tau> \tag{30}$$

The RMS DGD, $<\Delta\tau^2>^{1/2}$, and the mean DGD $<\Delta\tau>$ are both related as follows [9,16]:

$$\left\langle\Delta\tau^2\right\rangle = \frac{3\pi}{8}\langle\Delta\tau\rangle^2 \tag{31}$$

The statistics of mean or RMS value of the DGD variation is analysed over a wavelength (or optical frequency[3]) range (as wide as possible) (see Figure 8).

IECNORM.COM : Click to view the full PDF of IEC TR 61282-9:2006
Withdrawn

[3] The RMS value of the spectral variation of the DGD (or PDV length or modulus) $PMD_{\mathrm{RMS}} = \sqrt{\langle\left|\hat{\Omega}(\omega)\right|^2\rangle}$ is generally more representative of the mathematics of the PMD.

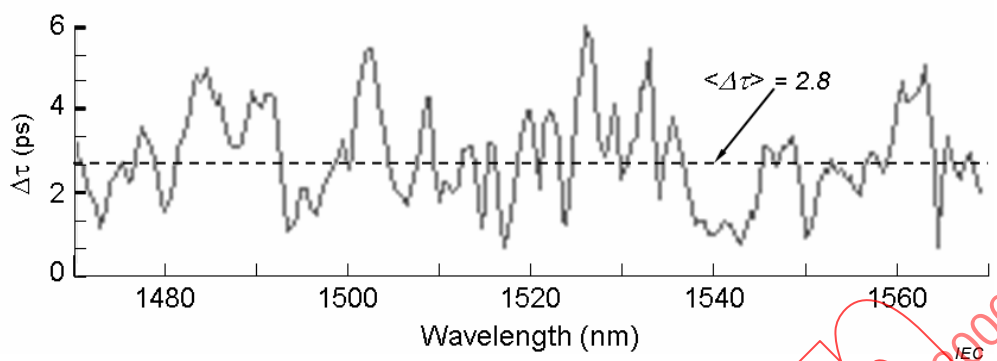

a) Differential group delay (Δτ) as a function of wavelength

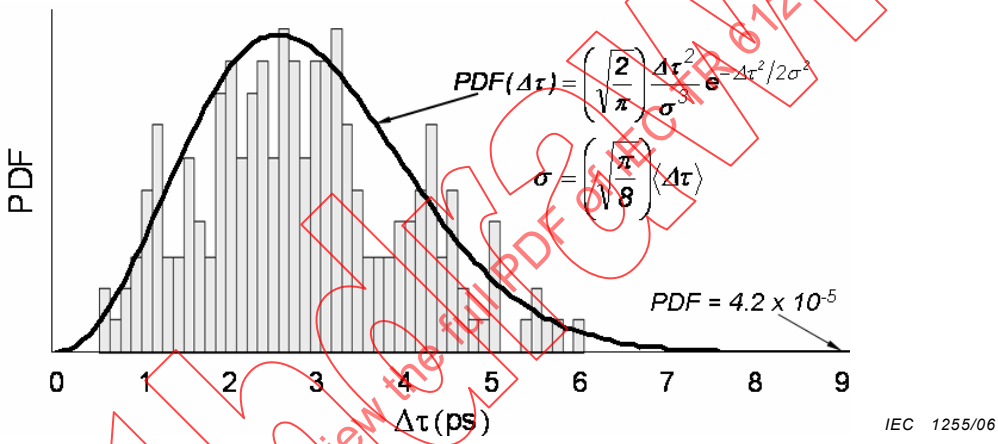

b) Probability density function (PDF) (histogram) as a function of $\Delta\tau$ from (a). Maxwell PDF is fit to the experimental results

Figure 8 – Statistics of differential group delay and related Maxwell distribution [15]

IECNORM.COM : Click to view the full PDF of IEC TR 61282-9:2006
Withdrawn

4.10.2 Negligible mode coupling

In the case where the birefringence inside the DUT remains relatively fixed (fixed PSP orientation along the DUT as shown in Figure 6), the two PSP PMs are not coupled or negligibly coupled together.

NOTE The expression *weak mode coupling* is also used in the literature and in some International Standards for negligible mode coupling. As a preference, the expression *negligible mode coupling* will be used in this document.

As a consequence, DGD does not vary as a function of wavelength (or optical frequency), as shown in Figure 9.

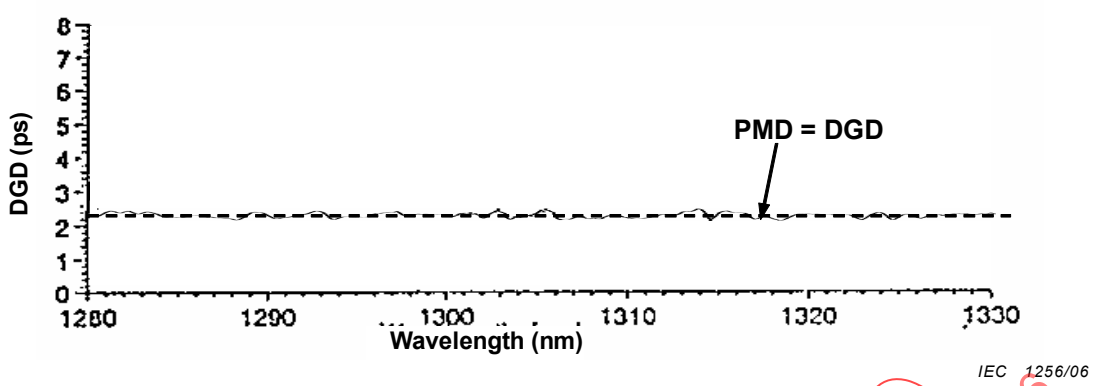

Figure 9 – Polarization mode dispersion and differential group delay in negligible mode coupling

As most optical components have extremely small physical lengths as compared to fibre lengths, PMD of such components may then be reported in units of ps only. In complex components and optical amplifiers, the DGD may vary as a function of wavelength (or frequency) even if this variation is smooth, small or sometimes predictable. In that case, the concept of PMD expressed as the RMS value of the variation of the DGD as a function of wavelength (or optical frequency) and the concept of maximum value of that DGD variation can be used.

There can also be intermediate cases where the device has a few birefringent sections, and the DGD can vary less strongly as a function of wavelength, such as a monotonous or sine wave variation. Some components, such as some array waveguide gratings (AWG), may exhibit such behaviour. In that case, the PMD is still the mean or RMS value of the DGD distribution, and the phenomenon is still somehow deterministic, but the mode coupling is neither negligible nor random.

There are also DUT classes where the issue of random mode coupling or not is irrelevant. Such a device is one with multiple optical paths for different frequencies, such as an optical multiplexer, where the DGD for each frequency is largely independent of the others. Some Bragg grating DUT could also fit into this category. Clause C.4 describes the treatment of such a device.

4.11 Second-order polarization mode dispersion

If the DGD and PSPs were wavelength independent, their knowledge would be sufficient to characterise propagation through a DUT, whatever the spectral width of the input signal. However, the DGD can change within a frequency increment. Moreover, as PMD increases in random mode coupling, the DGD varies more rapidly in its magnitude and the PSPs more rapidly in their orientation. Considering that first-order PMD (PMD_1) is found from Equations (16) and (18), second-order PMD (PMD_2) is this variation of the DGD and PSPs with optical frequency (or wavelength), as shown in Equation (32), when deriving Equation (16).

$$\frac{\mathrm{d}\hat{\Omega}(\omega)}{\mathrm{d}\omega} = \left(\hat{s}_p \frac{d\Delta\tau(\omega)}{d\omega}\right) + \left(\Delta\tau \frac{d\hat{s}_p(\omega)}{d\omega}\right) \qquad (32)$$

PMD_2 term

PMD_2 was identified and described in some detail several years ago [17], but more recent work has provided a deeper appreciation of its potential importance for realistic communications links [5,18].

IECNORM.COM : Click to view the full PDF of IEC TR 61282-9:2006
Withdrawn

There has been a common misconception that PMD_2 was simply derived from the slope of a DGD-versus-ω plot. The fact that the derivative is of a vector (see Equation (32)) rather than a scalar introduces an additional term proportional to the frequency dependence of the PSP orientation. For the very practical case of a long telecommunication fibre, this contribution can be shown to account for about 8/9 of the total PMD_2 effect [18].

On the right-hand side of Equation (32), there are two terms present in the definition of PMD_2. The first term is in the direction of the fast PSP and is often refered to as the parallel term, while the second term is in the direction perpendicular to the PSP and is often refered to as the perpendicular term.

As an example, a single waveplate or PMF does not (ideally) exhibit any PMD_2, since its DGD does not change significantly over a wavelength range (see Figure 9) (apart from the small variation due to chromatic dispersion), and since the orientation of its fast and slow axes do not change as the input wavelength is varied (see Figure 6). This will be the case for a simple component where the DGD barely varies as a function of wavelength. If the waveplate orientation was changed in response to changes in wavelength, this would introduce PMD_2, which could be the case for more complex devices.

On a more rigorous mathematical basis, the combined effect of PMD_1 and PMD_2 on the output-SOP can be easily pictured on the Poincaré sphere (see Figure 10).

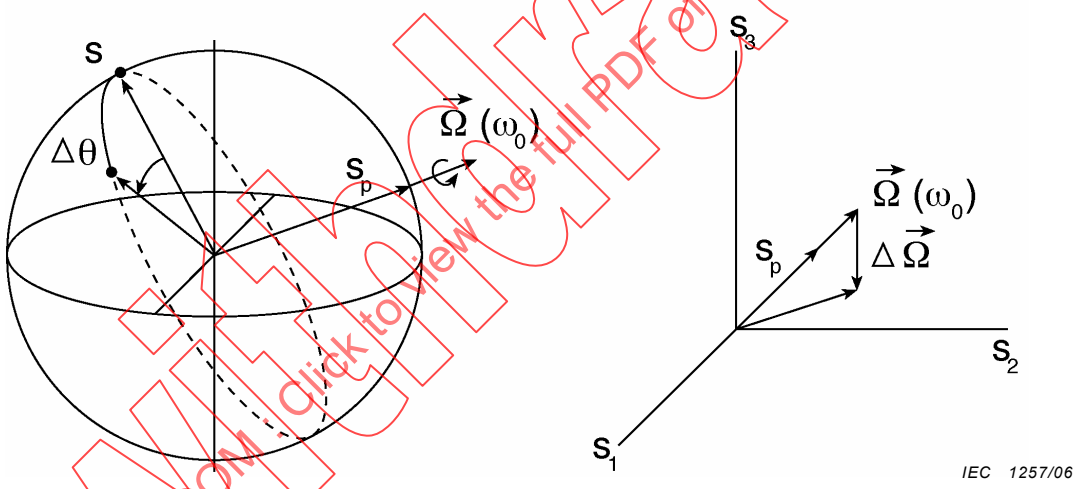

Figure 10 – Effects of first-order polarization mode dispersion (PMD_1) and second-order polarization mode dispersion (PMD_2) on the output state of polarization on the Poincaré sphere

At a given angular optical frequency, ω_0, PMD_1 is characterised by the PDV as shown in Equations (16) and (18).

The vector, $\hat{\Omega}$, lies along the direction of the output fast PSP, $\hat{s}_p$, and its modulus, $\left|\hat{\Omega}\right|$, is equal to the DGD as shown in Equation (18). Specifically, PMD_1 is defined in terms of the RMS value of the modulus of $\hat{\Omega}$, viz

$$PMD_1 = \sqrt{\left\langle \left|\hat{\Omega}\right|^2 \right\rangle} = \sqrt{\left\langle \Delta\tau^2 \right\rangle} \tag{33}$$

IECNORM.COM : Click to view the full PDF of IEC TR 61282-9:2006
Withdrawn

On the sphere, $\hat{s}$ "precesses" around $\hat{\Omega}$ at a rate $d\theta/d\omega = \Delta\tau$ (like a spin around a static magnetic field). On the other hand, PMD_2 is characterised by the ω-derivative of $\hat{\Omega}$, its velocity vector, and its modulus is the PDV velocity (DVV). From Equation (32), we note again that both the variations of DGD and PSPs are included. Following [18], PMD_2 is defined in analogy to PMD_1 as proportional to the RMS value of the ω-derivative of $\hat{\Omega}$ Equation (32) or the RMS value of the DVV.

$$PMD_2 = \sqrt{\left\langle \left| \frac{d\hat{\Omega}}{d\omega} \right|^2 \right\rangle} \tag{34}$$

The fundamental units of PMD_2 are s^2, as for chromatic dispersion. More convenient units are ps^2 or ps/nm with a slightly different formula (see Equation (35)).

$$PMD_2 = \frac{2\pi c}{\lambda^2} \sqrt{\left\langle \left| \frac{d\hat{\Omega}}{d\omega} \right|^2 \right\rangle} \tag{35}$$

As with chromatic dispersion, if the derivative of the PDV with respect to frequency is measured, a minimum and maximum value will be found. The polarization dependent chromatic dispersion (PDCD) is related to the DVV (the modulus of the ω-derivative of $\hat{\Omega}$, the PDV) as follows:

$$PDCD = CD_{max} - CD_{min} = DVV = \left| \frac{d\hat{\Omega}}{d\omega} \right| \tag{36}$$

Equation (36) holds in case of negligible PDL/PDG.

From the above discussion, it is clear that it is the behaviour of the $\hat{\Omega}$ vector, both in its magnitude and in its optical-frequency dependence, which underlies both PMD_1 and PMD_2. Thus, it is not surprising that the measurable effects of both phenomena can be related to each other in terms of this vector. In fact, it can be shown [5,18] that in the (very realistic) limit of fibres with length much longer than the coupling length (random mode coupling), the following relation holds:

$$\left\langle \left| \frac{d\hat{\Omega}}{d\omega} \right|^2 \right\rangle = \frac{1}{3} \left\langle \left| \hat{\Omega} \right|^2 \right\rangle^2 \tag{37}$$

Combining Equations (34), (35) and (37), the following relation is obtained between PMD_1 and PMD_2:

$$PMD_2 = \frac{1}{\sqrt{3}} (PMD_1)^2 \tag{38}$$

IECNORM.COM : Click to view the full PDF of IEC TR 61282-9:2006
Withdrawn

5 Mathematical formulations of the polarization mode dispersion test methods

This clause is organized to present first the Stokes parameter evaluation (polarimetric), then the methods most similar (in polarimetry), then those in the frequency domain, and finally the time domain method.

There are two generic categories of PMD test methods: one that determines DGD and PMD, and another that only determines PMD.

DGD and PMD determination is covered by the following methods:

- Stokes parameter evaluation (SPE):
  - o Jones matrix eigenanalysis (JME),
  - o Poincaré sphere analysis (PSA);
- Modulation phase shift (MPS);
- Polarization phase shift (PPS);
- Poincaré sphere arc method (PS);
- Poole formula.

PMD-only determination is covered by the following methods:

- Fixed analyser (FA):
  - o Extrema counting (EC),
  - o Fourier transform (FT);
- Interferometric method (INTY).

5.1 Stokes parameter evaluation

The SPE method determines PMD by measuring a polarimetric response of a DUT to a change of narrowband light across a wavelength range. For each wavelength, three distinct and known SOPs, the easiest being the linear (orthogonal on the Poincaré sphere) SOPs at nominally 0 °, 45 °, and 90 °, are launched into the DUT, and the output Stokes vectors transmitted through the DUT are obtained. The change of these Stokes vectors with angular optical frequency, ω (or wavelength) and, with change in input SOPs, yields the DGD as a function of wavelength through relationships that are based on Equations (12) and (18).

In the JME approach, the output Stokes vectors are transformed into Jones matrices [4], with an appropriate combination of the matrices at adjacent wavelengths. The resulting eigenvalues are calculated followed by the application of an argument function to obtain the DGD at the base frequency.

In the PSA approach, matrix algebra is performed on the normalised output Stokes vectors to infer the output Stokes vector associated with circular birefringence at two adjacent wavelengths, followed by the application of an arcsine formula to obtain the DGD at the base frequency.

For both JME and PSA, the average of the DGD values for a given wavelength range yields the PMD value over that range. The JME and PSA approaches are mathematically and formalistically equivalent.

IECNORM.COM : Click to view the full PDF of IEC TR 61282-9:2006
Withdrawn

5.1.1 Jones matrix eigenanalysis

Any Jones vector can be completely specified by a magnitude, an absolute phase as shown in Equation (3), and the Jones matrix of a DUT can be determined following 4.4. Typically, a linear SOP parallel to the x (0 º) axis, a linear SOP parallel to the y (90 º) axis, and parallel to the bisector of the angle between the positive x and y axes (45 º) are used as stimuli to the DUT.

To obtain the output Jones vectors, the output Stokes vectors are measured using the stimuli, then normalised to unit length. These are then converted to Jones vectors using Equations (8) and (9), assuming, for example, that $0 \leq \theta \leq \pi$. Following Equation (6), four complex ratios, not affected by the assumption on θ, and independent of the intensities of the three SOPs, can then.be formed

The transmission Jones matrix, T, is then given by Equation (5).

By definition of the PSP, a general device has associated with it a pair of input principal SOPs. $\hat{x}(\omega)$, which, as the input SOP is held constant while the angular optical frequency, ω, is changed by a small increment, results in a pair of output PSPs whose unit vectors are invariant to first order over ω. For a general transmission Jones matrix, $T(\omega)$, an output PSP can be expressed as a magnitude, $\sigma(\omega)$, and absolute phase, $\phi(\omega)$, times a unit vector, $\hat{y}(\omega)$, which specifies the output PSP:

$$y(\omega)=T(\omega)\hat{x}(\omega)=\sigma(\omega)e^{i\phi(\omega)}\hat{y}(\omega) \tag{39}$$

$\sigma(\omega)$ and $\phi(\omega)$ may vary with ω, but $\hat{y}(\omega)$ is frequency-invariant to first order by definition of the output PSP. Using primes to denote differentiation with respect to ω, differentiation of Equation (39) results in:

$$y'(\omega)=T'(\omega)\hat{x}(\omega)=\left(\frac{\sigma'}{\sigma}+i\phi'\right)y+\sigma(\omega)e^{i\phi(\omega)}\hat{y}'(\omega) \tag{40}$$

The first derivative of the absolute phase ϕ' is the group delay, τ_g, through the device. If the device is not perfectly polarizing, its transmission matrix, T, is non-singular, and the input can be expressed in terms of the output as $\hat{x} = T^{-1}y$. Explicitly setting $\hat{y}'$ to zero, the following eigenvalue relation is obtained:

$$\sigma(\omega)e^{i\phi(\omega)}\hat{y}'(\omega)=\left[T'T^{-1}-\left(\frac{\sigma'}{\sigma}+i\tau_g\right)I\right]y=0 \tag{41}$$

where I is the identity matrix, a square matrix with values of one on the diagonal and zero elsewhere.

The imaginary parts of the eigenvalues of the matrix product are the group delays associated with the PSPs, and the DGD $\Delta\tau$ which leads to PMD is given by the difference of the imaginary parts of the two eigenvalues. The output PSP themselves are the eigenvectors of $T'T^{-1}$, which may be non-unitary for devices with PDL, in which case the output PSPs are not necessarily orthogonal.

IECNORM.COM : Click to view the full PDF of IEC TR 61282-9:2006
Withdrawn

Measurement of T' and T, including measurement of the absolute phase, would allow direct calculation of the two group delays and $\Delta\tau$, but in practice, two restrictions are imposed by the Jones matrix measurement technique previously described. Instead of measuring T' directly, T' must be approximated as $T' \approx [T(\omega+\Delta\omega) - T(\omega)]/\Delta\omega$ for a finite $\Delta\omega$. If the angular optical frequency increment $\Delta\omega$ is small enough so that each output PSP suffers nearly the same loss at ω and $\omega + \Delta\omega$, then $\sigma'\Delta\omega/\sigma \approx 0$ and Equation (42) can be rewritten as

$$\left[T(\omega+\Delta\omega)T^{-1}(\omega)-\left(1+i\tau_g\Delta\omega\right)I\right]y=0 \tag{42}$$

The second restriction arises from the fact that $T(\omega+\Delta\omega)T^{-1}(\omega)$, and therefore its associated eigenvalues ρ_1 and ρ_2 can be determined only to within a complex constant, preventing determination of the two group delays individually. When the loss through the device is independent of polarization, the eigenvalues of $T(\omega+\Delta\omega)T^{-1}(\omega)$ are determined to be $\beta\rho_1$ and $\beta\rho_2$, where β is a complex constant and $\rho k = exp(i\tau_{g,k}\Delta\omega)$. The DGD $\Delta\tau$ can therefore be expressed as

$$\Delta\tau = \left|\tau_{g,1}-\tau_{g,2}\right| = \left|\frac{Arg\left(\frac{\rho_1}{\rho_2}\right)}{\Delta\omega}\right| \tag{43}$$

where ρ_1 and ρ_2 are the eigenvalues of $T(\omega+\Delta\omega)T^{-1}(\omega)$ and Arg denotes the argument function, that is, $Arg(\alpha e^{i\theta}) = \theta$. In the presence of PDL, the eigenvalues can still be approximated as

$$\rho_k = 1+i\tau_{g,k}\Delta\omega \approx e^{i\tau_{g,k}\Delta\omega} \tag{44}$$

In practice, the impact of PDL on the measurement of $\Delta\tau$ can be reduced by using smaller $\Delta\omega$ increments. In all cases, the condition $\Delta\tau \bullet \Delta\omega < \pi$ must be satisfied in order to avoid the ambiguities of the multiple-valued argument function.

NOTE The JME method does not correspond to the fundamental Jones mathematical treatment, such as

$$\frac{d|E\rangle}{d\omega} = A|E\rangle \tag{45}$$

where

A is the matrix of equivalent device defined as

$$A = \left(\frac{dT}{d\omega}\right)\bullet T^{-1} \tag{46}$$

where

T is the Jones transfer matrix

By definition,

DGD = |Im(eigenvalue difference of A)|

eigenvalue difference of $A = a_1 - a_2$ (47)

where

a_1 is one eigenvalue of A;

a_2 is the other eigenvalue of A.

PSPs = 2 eigenvectors of $A = \pm\dfrac{\hat{\Omega}}{|\hat{\Omega}|}$ (48)

IECNORM.COM : Click to view the full PDF of IEC TR 61282-9:2006
Withdrawn

The JME method uses the following approximation:

$$\left[\frac{T(\omega+\Delta\omega)-T(\omega)}{\Delta\omega}\right]\bullet T(\omega)^{-1}=\frac{\left\{\left[T(\omega+\Delta\omega)\right]\bullet T(\omega)^{-1}\right\}-1}{\Delta\omega}=A_{measured}\approx A \tag{49}$$

JME is measuring $T(\omega+\Delta\omega)T(\omega)^{-1}$ and by definition,

$$DGD_{\text{measured}} = |\text{Im(eigenvalue difference of } A_{\text{measured}}| \tag{50}$$

eigenvalue difference of $A_{measured}$ = $(a_1 - a_2)_{\text{measured}}$ = $\rho_1 - \rho_2$

The JME method is not based on finite differences.

JME measures the polarizations, not the intensities, nor the phases and does not obtain the true Jones matrix, but with a factor β (complex number, not constant with λ):

$$\begin{aligned} a_1(or\ \rho_1) &= \beta_1 e^{i\left(\frac{DGD\Delta\omega}{2}\right)} \\ a_2(or\ \rho_2) &= \beta_2 e^{i\left(\frac{DGD\Delta\omega}{2}\right)} \\ \frac{a_1}{a_2} &= \left(\frac{\beta_1}{\beta_2}\right)e^{iDGD\Delta\omega} = \left|\frac{\beta_1}{\beta_2}\right| e^{i\left[\arg\left(\frac{a_1}{a_2}\right)\right]} \end{aligned} \tag{51}$$

then

$$DGD=\left|\text{Im}(a_1-a_2)\right|=\frac{\left|\arg\left(\frac{a_1}{a_2}\right)\right|}{\Delta\omega} \tag{52}$$

5.1.2 Poincaré sphere analysis

Let $\hat{h}$ and $\hat{q}$ be the output Stokes vectors measured for two linear input SOPs oriented at 45 ° from each other (90 ° on the Poincaré sphere), and $\hat{c}=\hat{h}\times\hat{q}$ the cross product of the two measured response vectors, as shown in Figure 11 [19].

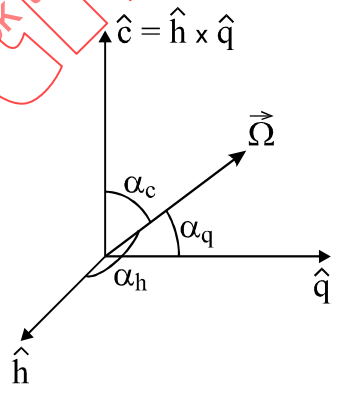

IEC 1258/06

Figure 11 – Rectangular system of co-ordinates defined by the response Stokes vectors, and direction angles of the polarization dispersion vector

Assuming negligible PDL, the transformation of Stokes vectors from input to output is a rotation (angles between vectors are preserved), and the equation of motion of any one of the response Stokes vector (including $\hat{c}$) is given by Equation (12) with

$$\hat{s}=\hat{h},\hat{q}\text{ or }\hat{c} \tag{53}$$

IECNORM.COM : Click to view the full PDF of IEC TR 61282-9:2006
Withdrawn

The square modulus of the derivative in Equation (12) can be written as

$$\left(\frac{d\hat{s}}{d\omega}\right)^2 = \left|\hat{\Omega}\right|^2 \sin^2(\alpha) \tag{54}$$

where α is the angle between $\hat{s}$ and $\hat{\Omega}$.

But $\hat{h}$ and $\hat{q}$ are mutually orthogonal, since angles are preserved from input to output. Thus $\hat{h}$, $\hat{q}$ and $\hat{c}$ define a rectangular system of co-ordinates (see Figure 11) in which $\cos(\alpha_h)$, $\cos(\alpha_q)$ and $\cos(\alpha_c)$ are the direction cosines of $\hat{\Omega}$. Using the sum rule,

$$\cos^2(\alpha_h) + \cos^2(\alpha_q) + \cos^2(\alpha_c) = 1 \tag{55}$$

In Equation (56), the following expression of DGD is obtained:

$$\left|\hat{\Omega}\right| = \sqrt{\frac{1}{2}\left[\left(\frac{d\hat{h}}{d\omega}\right)^2 + \left(\frac{d\hat{q}}{d\omega}\right)^2 + \left(\frac{d\hat{c}}{d\omega}\right)^2\right]} \tag{56}$$

If only finite differences $\Delta\hat{s}/\Delta\omega$ are known instead of derivatives ($\Delta\omega \to 0$), an approximation of DGD must be obtained that is more accurate than Equation (56). Assuming that the PDV is independent of ω over the increment $[\omega,\ \omega+\Delta\omega]$, the output SOP follows an arc of a circle as shown in Figure 12.

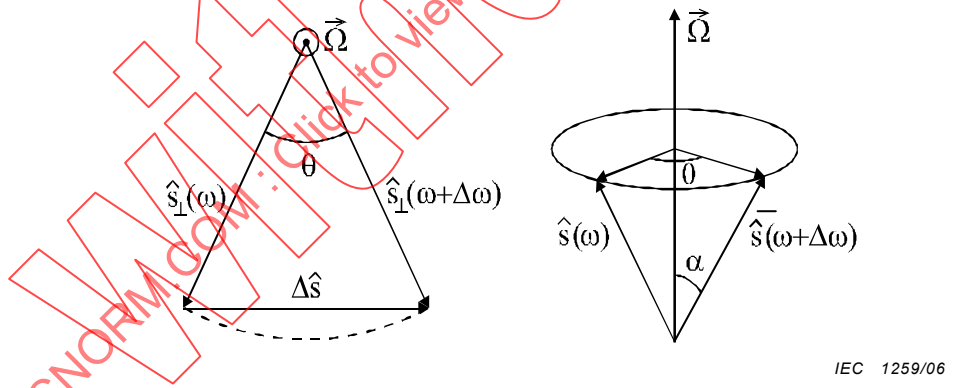

Figure 12 – Arc of a circle described by the output state of polarization in the increment $[\omega,\ \omega+\Delta\omega]$

In Figure 12, $\hat{s}_\perp$ is the component of $\hat{s}$ perpendicular to $\hat{\Omega}$ and θ the angle swept by $\hat{s}_\perp$. Also, as a consequence of the equation of motion (12), we have

$$\left|\hat{s}_\perp\right| = \left|\sin(\alpha)\right| \tag{57}$$

$$\theta = \left|\hat{\Omega}\right|\Delta\omega \tag{58}$$

IECNORM.COM : Click to view the full PDF of IEC TR 61282-9:2006
Withdrawn

Through simple geometry (see Figure 12),

$$\left|\Delta\hat{s}\right| = 2\left|\hat{s}_{\perp}\right|\left|\sin\left(\frac{\theta}{2}\right)\right| \tag{59}$$

is obtained, so that

$$\left|\Delta\hat{s}\right| = 2\left|\sin(\alpha)\sin\left(\frac{\left|\hat{\Omega}\right|\Delta\omega}{2}\right)\right| \tag{60}$$

The sum of the square modulus of $\Delta\hat{h}$, $\Delta\hat{q}$ and $\Delta\hat{c}$ is then written as

$$\Delta\hat{h}^2 + \Delta\hat{q}^2 + \Delta\hat{c}^2 = 4\sin^2\left(\frac{\left|\hat{\Omega}\right|\Delta\omega}{2}\right)\cdot\left[\sin^2(\alpha_h) + \sin^2(\alpha_q) + \sin^2(\alpha_c)\right] \tag{61}$$

Finally, we apply the sum rule of Equations (56) to (61) to obtain the following expression of DGD:

$$\left|\hat{\Omega}\right| = \frac{2}{\Delta\omega}\arcsin\left[\frac{1}{2}\sqrt{\frac{1}{2}\left(\Delta\hat{h}^2 + \Delta\hat{q}^2 + \Delta\hat{c}^2\right)}\right] \tag{62}$$

$$PSP = \frac{\pm\hat{u}}{\left|\hat{u}\right|} \quad \text{with} \quad \hat{u} = (\bar{c}\cdot\Delta\hat{q})\,\bar{h} + (\bar{h}\cdot\Delta\hat{c})\,\bar{q} + (\bar{q}\cdot\Delta\hat{h})\,\bar{c} \tag{63}$$

where $\bar{c}$, $\bar{h}$ and $\bar{q}$ are the mean of the Stokes vectors measured at ω and (ω+Δω), i.e.

$$\bar{s} = \frac{\hat{s}(\omega) + \hat{s}(\omega+\Delta\omega)}{2}$$

5.1.3 Calculation of differential group delay

In the following example, the DGD of a DUT is found from the Jones matrix or directly from the Stokes vectors obtained at a pair of input optical frequencies or wavelengths. The hypothetical DUT is described in terms of Mueller matrices at these optical frequencies or wavelengths.

The DUT chosen for this example has linear PSPs at +45 º and –45 º in the wavelength range of interest. The 4x4 Mueller matrix, M, for such DUT is [20]

$$M(\omega) = \begin{bmatrix} 1 & 0 & 0 & 0 \\ 0 & \cos\delta & 0 & -\sin\delta \\ 0 & 0 & 1 & 0 \\ 0 & \sin\delta & 0 & \cos\delta \end{bmatrix} \tag{64}$$

where is the retardance at the angular optical frequency ω in rad/s.

IECNORM.COM : Click to view the full PDF of IEC TR 61282-9:2006
Withdrawn

Assuming the DUT is non-dispersive for the two PSPs, the retardance is related to the DGD $\Delta\tau$ by

$$\delta = \omega\Delta\tau \tag{65}$$

Assuming that the Jones matrix or the Stokes vectors of the DUT are obtained at frequencies ω_1 = 1,21x10^{15} rad/s (1 556,734 nm) and $\omega_2 = \omega_1+\Delta\omega$ = 1,22x10^{15} rad/s (1 543,974 nm), and that the DGD of the DUT is $\Delta\tau(\omega_1)$ = 100 fs, the Mueller matrices at these optical frequencies are

$$M_1 = M(\omega_1) = \begin{bmatrix} 1 & 0 & 0 & 0 \\ 0 & \cos 121 & 0 & -\sin 121 \\ 0 & 0 & 1 & 0 \\ 1 & \sin 121 & 0 & \cos 121 \end{bmatrix}$$

$$M_2 = M(\omega_2) = \begin{bmatrix} 1 & 0 & 0 & 0 \\ 0 & \cos 122 & 0 & -\sin 122 \\ 0 & 0 & 1 & 0 \\ 0 & \sin 122 & 0 & \cos 122 \end{bmatrix} \tag{66}$$

Of course, these matrices are unknown beforehand.

5.1.3.1 Jones matrix eigenanalysis

In the JME approach, PMD determination requires a Jones matrix at each of two wavelengths. The Jones matrix at a particular wavelength is found from the output SOPs corresponding to each of three input SOPs. The three chosen input SOPs are as follows:

$$0^o \Rightarrow x_a = \begin{bmatrix} 1 \\ 1 \\ 0 \\ 0 \end{bmatrix} \qquad 45^o \Rightarrow x_b = \begin{bmatrix} 1 \\ 0 \\ 1 \\ 0 \end{bmatrix} \qquad 90^o \Rightarrow x_c = \begin{bmatrix} 1 \\ -1 \\ 0 \\ 0 \end{bmatrix} \tag{67}$$

The three output SOPs, related to the input ones by $y = M_1 x$, are obtained at ω_1:

$$y_{a1} = \begin{bmatrix} 1 \\ \cos 121 \\ 0 \\ \sin 121 \end{bmatrix} \qquad y_{b1} = \begin{bmatrix} 1 \\ 0 \\ 1 \\ 0 \end{bmatrix} \qquad y_{c1} = \begin{bmatrix} 1 \\ -\cos 121 \\ 0 \\ -\sin 121 \end{bmatrix} \tag{68}$$

The three other output SOPs, related to the input ones by $y = M_2 x$, are obtained at ω_2:

$$y_{a2} = \begin{bmatrix} 1 \\ \cos 122 \\ 0 \\ \sin 122 \end{bmatrix} \qquad y_{b2} = \begin{bmatrix} 1 \\ 0 \\ 1 \\ 0 \end{bmatrix} \qquad y_{c2} = \begin{bmatrix} 1 \\ -\cos 122 \\ 0 \\ -\sin 122 \end{bmatrix} \tag{69}$$

The Jones matrix T_1 is calculated at ω_1, starting by converting the three output SOPs at ω_1 to the following Jones vectors:

$$v_{a1} = \begin{bmatrix} 0{,}689687 \\ 0{,}724108i \end{bmatrix} \qquad v_{b1} = \begin{bmatrix} 0{,}707107 \\ 0{,}707107 \end{bmatrix} \qquad v_{c1} = \begin{bmatrix} 0{,}724108 \\ 0{,}689687i \end{bmatrix} \tag{70}$$

IECNORM.COM : Click to view the full PDF of IEC TR 61282-9:2006
Withdrawn

From the Jones vectors, the following complex ratios are formed in order to populate the Jones matrix:

$$k_1 = \frac{0{,}689687}{0{,}724108i} = -0{,}952465i \qquad k_2 = \frac{0{,}707107}{0{,}707107} = 1 \tag{71}$$

$$k_3 = \frac{0{,}724108}{-0{,}689687i} = 1{,}049910i \quad k_4 = \frac{k_3 - k_2}{k_1 - k_3} = -0{,}524332 - 0{,}499408i$$

The following Jones matrix T_1 is obtained, where β_1 is an unknown complex constant:

$$T_1 = \beta_1 \begin{bmatrix} k_1 k_4 & k_2 \\ k_4 & 1 \end{bmatrix} = \begin{bmatrix} (-0{,}475668 + 0{,}499408i) & 1 \\ (-0{,}524332 - 0{,}499408i) & 1 \end{bmatrix} \tag{72}$$

Similarly, the Jones matrix T_2 is obtained by converting the Stokes output vectors at ω_2 to Jones vectors:

$$v_{a2} = \begin{bmatrix} 0.258102 \\ 0{,}966118i \end{bmatrix} \qquad v_{b2} = \begin{bmatrix} 0{,}707107 \\ 0{,}707107 \end{bmatrix} \qquad v_{c2} = \begin{bmatrix} 0{,}966118 \\ 0{,}258102i \end{bmatrix} \tag{73}$$

Again, from the Jones vectors, the following complex ratios are formed in order to populate the found Jones matrix T_2 where β_2 is an unknown complex constant:

$$k_1 = \frac{0{,}258102}{0{,}966118i} = -0{,}267153i \qquad k_2 = \frac{0{,}707107}{0{,}707107} = 1 \tag{74}$$

$$k_3 = \frac{0{,}966118}{-0{,}258102i} = 3{,}74317i \quad k_4 = \frac{k_3 - k_2}{k_1 - k_3} = -0{,}933384 - 0{,}249357i$$

$$T_2 = \beta_2 \begin{bmatrix} k_1 k_4 & k_2 \\ k_4 & 1 \end{bmatrix} = \begin{bmatrix} (-0{,}0666165 + 0{,}249357i) & 1 \\ (-0{,}933384 - 0{,}249357i) & 1 \end{bmatrix} \tag{75}$$

Since β_1 and β_2 do not affect the eigenvalue ratio or the eigenvectors, they are dropped.

Next, the product $T_2 T_1^{-1}$ is calculated:

$$A = T_2 T_1^{-1} = \begin{bmatrix} (0{,}770151 - 0{,}420735i) & (0{,}229849 + 0{,}420735i) \\ (0{,}229849 + 0{,}420735i) & (0{,}770151 - 0{,}420735i) \end{bmatrix} \tag{76}$$

The eigenvalues of A are ρ_1 = 1 and ρ_2 = 0,540302 – 0,841471 i.

The corresponding eigenvectors are

$$z_1 = \begin{bmatrix} 0{,}707107 \\ 0{,}707107 \end{bmatrix} \qquad z_2 = \begin{bmatrix} 0{,}707107 \\ -0{,}707107 \end{bmatrix} \tag{77}$$

This can be seen by confirming that $\rho_1 z_1 = A z_1$ and $\rho_2 z_2 = A z_2$ (the set of solutions is unique).

Eigenvectors z_1 and z_2 are Jones vector representations of +45 º and –45 º linear SOPs, so they correctly identify the output PSPs.

IECNORM.COM : Click to view the full PDF of IEC TR 61282-9:2006
Withdrawn

Now the DGD $\Delta\tau$ is found from

$$\Delta\tau(\omega_1) = \left| \frac{Arg\left(\frac{\rho_1}{\rho_2}\right)}{\omega_2 - \omega_1} \right| = \left| \frac{Arg\left(\frac{1}{0{,}540302 - 0{,}841471i}\right)}{0{,}01\,x\,10^{15}\ rad/s} \right| \tag{78}$$

The expression 1/(0,540302 – 0,841471i) has magnitude 1 and polar angle 1 rad.

$$\Delta\tau(\omega_1) = \left| \frac{1\,rad}{0{,}01\,x\,10^{15}\ rad/s} \right| = 100\,fs \tag{79}$$

The DGD has correctly been found.

5.1.3.2 Poincaré sphere analysis

From the Stokes vectors $\hat{h}$, $\hat{v}$ and $\hat{q}$, the vector products $\hat{c} = \hat{h} \times \hat{q}$ and $\hat{c}' = \hat{q} \times \hat{v}$ are formed at each wavelength. For each wavelength increment, the finite differences are computed:

$$\begin{aligned} &\Delta\hat{h} = \hat{h}(\omega + \Delta\omega) - \hat{h}(\omega) && \Delta\hat{q} = \hat{q}(\omega + \Delta\omega) - \hat{q}(\omega) && \Delta\hat{v} = \hat{v}(\omega + \Delta\omega) - \hat{v}(\omega) \\ &\Delta\hat{c} = \hat{c}(\omega + \Delta\omega) - \hat{c}(\omega) && \Delta\hat{c}' = \hat{c}'(\omega + \Delta\omega) - \hat{c}'(\omega) \end{aligned} \tag{80}$$

The DGD $\Delta\tau$ is found for a particular wavelength increment from the following expression:

$$\Delta\tau = \frac{1}{\Delta\omega} \cdot \left\{ \arcsin\left[\frac{1}{2} \sqrt{\frac{1}{2}\left(\Delta\hat{h}^2 + \Delta\hat{q}^2 + \Delta\hat{c}^2\right)} \right] + \arcsin\left[\frac{1}{2} \sqrt{\frac{1}{2}\left(\Delta\hat{q}^2 + \Delta\hat{v}^2 + \Delta\hat{c}'^2\right)} \right] \right\} \tag{81}$$

Each DGD value is taken to represent the DGD at the midpoint of the corresponding wavelength increment.

Now the mean Stokes vectors are formed as follows:

$$\begin{aligned} &\hat{h} = \frac{\hat{h}(\omega) + \hat{h}(\omega + \Delta\omega)}{2} && \hat{q} = \frac{\hat{q}(\omega) + \hat{q}(\omega + \Delta\omega)}{2} && \hat{v} = \frac{\hat{v}(\omega) + \hat{v}(\omega + \Delta\omega)}{2} \\ &\hat{c} = \frac{\hat{c}(\omega) + \hat{c}(\omega + \Delta\omega)}{2} && \hat{c}' = \frac{\hat{c}'(\omega) + \hat{c}'(\omega + \Delta\omega)}{2} \end{aligned} \tag{82}$$

and the scalar products are computed as follows:

$$u_h = \hat{c} \cdot \Delta\hat{q} \qquad u_q = \hat{h} \cdot \Delta\hat{c} \qquad u_c = \hat{q} \cdot \Delta\hat{h} \tag{83}$$

The PSPs are found from the following expression:

$$PSP = \frac{\pm\hat{u}}{|\hat{u}|} \qquad \hat{u} = u_h\,\hat{h} + u_q\,\hat{q} + u_c\,\hat{c} \tag{84}$$

IECNORM.COM : Click to view the full PDF of IEC TR 61282-9:2006
Withdrawn

Now in the case of the hypothetical DUT defined previously, the six output Stokes vectors are

$$\hat{h}(\omega)=\begin{bmatrix}\cos(121)\\0\\\sin(121)\end{bmatrix}\qquad \hat{v}(\omega)=\begin{bmatrix}-\cos(121)\\0\\-\sin(121)\end{bmatrix}\qquad \hat{q}(\omega)=\begin{pmatrix}0\\1\\0\end{pmatrix}$$

$$\hat{h}(\omega+\Delta\omega)=\begin{bmatrix}\cos(122)\\0\\\sin(122)\end{bmatrix}\qquad \hat{v}(\omega+\Delta\omega)=\begin{bmatrix}-\cos(122)\\0\\-\sin(122)\end{bmatrix}\qquad \hat{q}(\omega+\Delta\omega)=\begin{pmatrix}0\\1\\0\end{pmatrix} \tag{85}$$

From Equation (85), the vector products $\hat{c}=\hat{h}\times\hat{q}$ and $\hat{c}'=\hat{q}\times\hat{v}$ are computed at ω and $(\omega+\Delta\omega)$:

$$\hat{c}(\omega)=\begin{bmatrix}-\sin(121)\\0\\\cos(121)\end{bmatrix}\qquad \hat{c}(\omega+\Delta\omega)=\begin{bmatrix}-\sin(122)\\0\\\cos(122)\end{bmatrix}$$

$$\hat{c}'(\omega)=\begin{bmatrix}-\sin(121)\\0\\\cos(121)\end{bmatrix}\qquad \hat{c}'(\omega+\Delta\omega)=\begin{bmatrix}-\sin(122)\\0\\\cos(122)\end{bmatrix} \tag{86}$$

and the square modulus of the finite differences is found as follows:

$$\begin{aligned}
\Delta\hat{v}^2 &= \left|\hat{v}(\omega+\Delta\omega)-\hat{v}(\omega)\right|^2 = [\cos(122)-\cos(121)]^2+[\sin(122)-\sin(121)]^2 = 4\sin^2(1/2)\\
\Delta\hat{q}^2 &= \left|\hat{q}(\omega+\Delta\omega)-\hat{q}(\omega)\right| = 0\\
\Delta\hat{c}^2 &= \left|\hat{c}(\omega+\Delta\omega)-\hat{c}(\omega)\right|^2 = [\sin(122)-\sin(121)]^2+[\cos(122)-\cos(121)]^2 = 4\sin^2(1/2)\\
\Delta\hat{c}'^2 &= \left|\hat{c}'(\omega+\Delta\omega)-\hat{c}'(\omega)\right|^2 = [\sin(122)-\sin(121)]^2+[\cos(122)-\cos(121)]^2 = 4\sin^2(1/2)\\
\Delta\hat{h}^2 &= \left|\hat{h}(\omega+\Delta\omega)-\hat{h}(\omega)\right|^2 = [\cos(122)-\cos(121)]^2+[\sin(122)-\sin(121)]^2 = 4\sin^2(1/2)
\end{aligned} \tag{87}$$

and the DGD is found from

$$\Delta\tau=\frac{1}{\Delta\omega}\cdot\left(\arcsin\left\{\frac{1}{2}\sqrt{\frac{1}{2}\left[4\sin^2\left(\frac{1}{2}\right)+0+4\sin^2\left(\frac{1}{2}\right)\right]}\right\}+\arcsin\left\{\frac{1}{2}\sqrt{\frac{1}{2}\left[0+4\sin^2\left(\frac{1}{2}\right)+4\sin^2\left(\frac{1}{2}\right)\right]}\right\}\right) \tag{88}$$

$$\Delta\tau=\frac{1}{\Delta\omega}\cdot 2\cdot\arcsin\left[\sin\left(\frac{1}{2}\right)\right]=\frac{1}{\Delta\omega}=100\ \text{fs}$$

This calculation yields the correct value of $\Delta\tau$ = 100 fs.

The PSPs can also be computed from the following mean Stokes vectors:

$$\hat{h}=\frac{\hat{h}(\omega)+\hat{h}(\omega+\Delta\omega)}{2}=\begin{pmatrix}-0{,}458\\0\\0{,}749\end{pmatrix}\qquad \hat{q}=\frac{q(\omega)+\hat{q}(\omega+\Delta\omega)}{2}=\begin{pmatrix}0\\1\\0\end{pmatrix} \tag{89}$$

IECNORM.COM : Click to view the full PDF of IEC TR 61282-9:2006
Withdrawn

$$\hat{c} = \frac{\hat{c}(\omega) + \hat{c}(\omega + \Delta\omega)}{2} = \begin{pmatrix} -0{,}749 \\ 0 \\ -0{,}458 \end{pmatrix}$$

and the scalar products:

$$u_h = \left(\hat{c} \cdot \Delta\hat{q}\right) = 0 \qquad u_q = \left(\hat{h} \cdot \Delta\hat{c}\right) = -0{,}841 \qquad u_c = \left(\hat{q} \cdot \Delta\hat{h}\right) = 0 \tag{90}$$

The PSPs are found:

$$PSP = \frac{\pm\hat{u}}{\left|\hat{u}\right|} = \begin{pmatrix} 0 \\ \pm 1 \\ 0 \end{pmatrix} \tag{91}$$

The linear SOPs, PSPs have correctly been found at +45 ° and –45 °.

5.1.4 Formalistic equivalence of Poincaré sphere analysis and Jones matrix eigenanalysis

The test procedures for PSA and JME are the same. The two methods determine the DGD and the PSPs from the same raw data, i.e. the normalised Stokes vectors at the output of the device under test as a function of the angular optical frequency ω for a number of input SOPs. The PSA is performed directly in the Stokes parameter representation of the SOP, while the JME is performed in the SOP vector (or normalised Jones vector) representation, after transformation of the Stokes vectors into SOP vectors (see Figure 13).

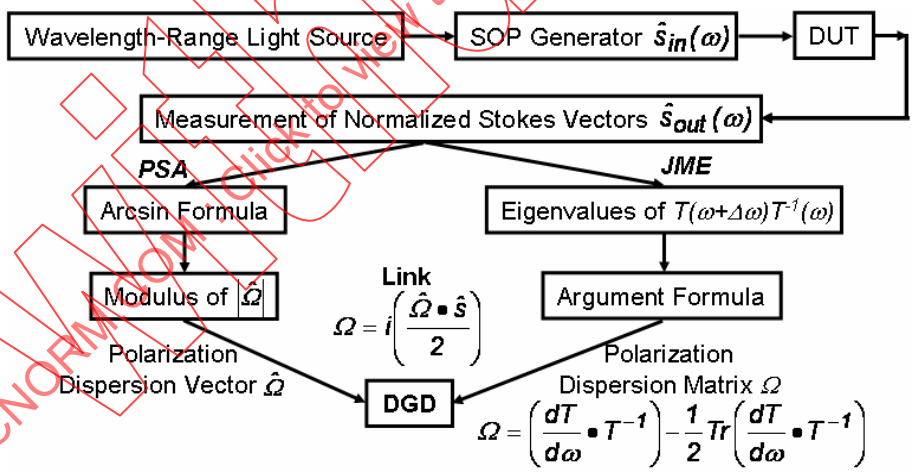

Figure 13 – Functional diagram of Stokes parameter evaluation

In the following sections, PSA and JME are demonstrated to be formally equivalent [21]. The *polarization dispersion matrix* is identified in the Jones vector representation that is equivalent to *the complex or generalised PDV* in the Stokes vector representation. A simple expression of the polarization dispersion matrix as a function of the PDV establishes the conceptual link between the two analyses. A formula is also provided for a simple calculation of DGD in low PDL conditions, which is the equivalent of the "exponential approximation" used in JME.

IECNORM.COM : Click to view the full PDF of IEC TR 61282-9:2006
Withdrawn

5.1.4.1 Fundamental link between Poincaré sphere analysis and Jones matrix eigenanalysis

The normalised Jones vector can be viewed as the quantum mechanical state-vector representing the SOP of each individual photon of a fully polarized wave. On the other hand, the normalised Stokes vector, $\hat{s}$, can be defined as the mean value of the photon angular momentum (in units of $\hbar$). Hence, $\hat{s} = \langle e|\hat{\sigma}|e\rangle$ where $|e\rangle$ is the normalised Jones vector, and $\hat{\sigma}$ is the Pauli operator.

JME and PSA are based on the equations of motion of the SOP at the output of the device under test, as a function of angular optical frequency, ω. The derivative of $\hat{s}$, $d\hat{s}/d\omega$ can be found from $d|e\rangle/d\omega$, starting from $\hat{s} = \langle e|\hat{\sigma}|e\rangle$. In order to obtain formally identical equations, it is convenient to use the polarization density matrix $\rho = |e\rangle\langle e|$ instead of the SOP-vector. This eliminates the cumbersome phase factor that appears in $|e\rangle$. The equation of motions can be written as

$$\frac{d\hat{s}}{d\omega} = \frac{1}{2}\left[\hat{\Omega} - \mathrm{i}\left(\hat{\Omega}\times\hat{s}\right)\right]\times\hat{s} + c.c. \qquad \frac{d\rho}{d\omega} = \left[\Omega - \mathrm{Tr}(\Omega\rho)\right]\rho + h.c. \tag{92}$$

where

$c.c.$ is a complex conjugate expression;

$h.c.$ is the hermitian conjugate.

The complex or generalised polarization dispersion vector $\hat{\Omega}$ and the polarization dispersion matrix Ω are related to the Jones matrix (T) through the following relations:

$$W = \frac{dT}{d\omega}T^{-1} \qquad \Omega = W - \frac{1}{2}Tr(W)I \tag{93}$$

$$\Omega = \frac{i}{2}\left(\hat{\Omega}\bullet\hat{\sigma}\right) \tag{94}$$

where

Tr is the trace of the matrix;

I is the identity matrix.

In the basic theory of JME, the PSPs and DGD are defined as the eigenvectors and difference-of-eigenvalues of W (imaginary part). From Equation (93), the eigenvectors and difference-of-eigenvalues of Ω can be seen to be the same as those of W. The link establishing the conceptual equivalence of PSA and JME is the expression of Ω as a function of $\hat{\Omega}$ Equation (94). Simply, knowing $\hat{\Omega}$, the vector obtained via PSA, one can deduce Ω, the matrix that defines the DGD and PSPs in JME.

5.1.4.2 Comparison of results obtained through Poincaré sphere analysis and Jones matrix eigenanalysis

To illustrate the identity of the two analyses, the DGD was calculated from both PSA and JME, as a function of the optical frequency. The simulation was performed with a concatenation of 20 waveplates with random delays and orientations of the birefringence axes. In PSA, the DGD was deduced from the finite differences $\Delta\hat{s}_a$ corresponding to input SOP's a = i, j, k through the following formula:

IECNORM.COM : Click to view the full PDF of IEC TR 61282-9:2006
Withdrawn

$$DGD = \frac{2}{\Delta\omega}\arcsin\left[\frac{1}{2}\sqrt{\frac{1}{2}\sum_{a}\Delta\hat{s}_a^2}\right] \tag{95}$$

where $\Delta\omega$ is the angular optical frequency increment.

The relative frequency increment was $\Delta\omega\cdot\Delta\tau_{\max} = 0{,}2\pi$. The following section provides the derivation of Equation (95). Equation (95) is obtained using the equivalent of the JME exponential approximation, which consists of assuming that the polarization dispersion matrix (vector) is constant over the frequency increment, so that the Jones matrix can be written as an exponential, i.e.

$$T(\omega+\Delta\omega) = T(\omega)\cdot e^{W\Delta\omega} \tag{96}$$

The equivalent in PSA is to take into account that the path followed by the SOP between two points is not along $\Delta\hat{s}$ but along an arc of a circle subtended by $\Delta\hat{s}$. Angles between Stokes vectors being preserved in absence of PDL (rotation), the third result (k) corresponding to circular input SOP can be deduced from the first two measurements (i,j) with linear input SOP's oriented at 0 º and 45 º from a given reference axis. The DGD curves obtained from the two analyses are shown in Figure 14(a).

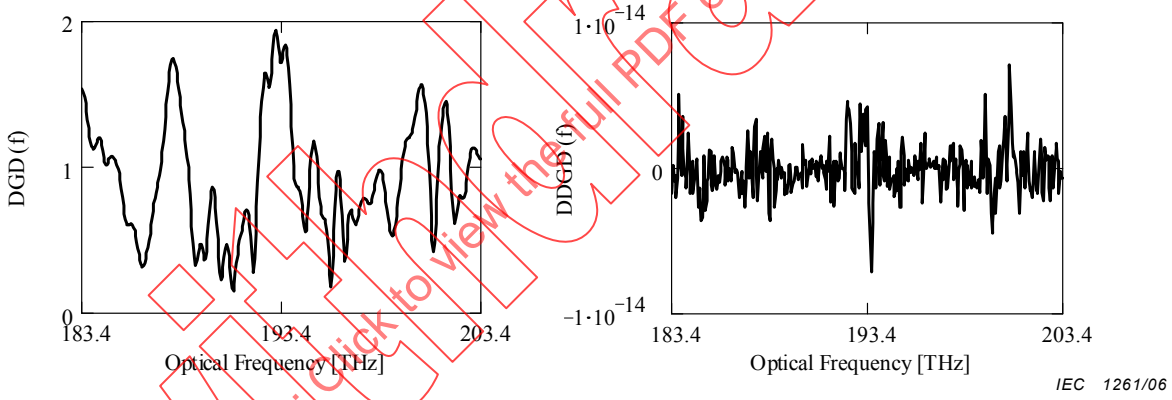

NOTE This simulation uses 20 concatenated waveplates with random delays and orientations of the birefringence axes. The PMD (RMS DGD) is found to be 1,01 ps when averaged over a range of 20 THz centred at 193,4 THz (1 550 nm). The relative frequency increment is $\delta f \cdot DGD_{\max} = 0{,}1$.

Figure 14 – a) Differential group delay (DGD) as a function of the optical frequency (*f*) obtained through Poincaré sphere analysis (PSA) and Jones matrix analysis (JME), and b) Difference of DGDs.

The two curves are superimposed on the graph. The difference of PMD values is ΔPMD = 2,2 × 10^{-16}. The difference between DGD's (ΔDGD) is shown in Figure 14(b) as a function of the optical frequency. Its RMS value is ΔDGD_{RMS} = 1,6 × 10^{-15}. These residual differences are accounted for by rounding errors.

The PSPs obtained from both analyses are shown in Figure 15 (trajectories).

IECNORM.COM : Click to view the full PDF of IEC TR 61282-9:2006
Withdrawn

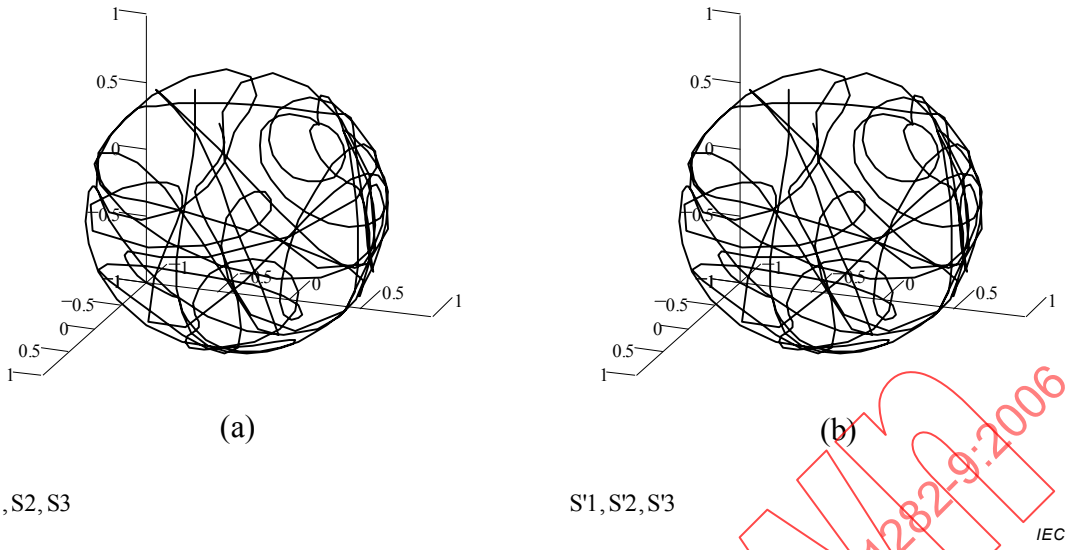

Figure 15 – Trajectories of the principal states of polarization on the Poincaré sphere from a) Jones matrix eigenanalysis (JME) and b) Poincaré sphere analysis (PSA)

There is no difference between the PSP trajectories and also no difference between the three Stokes parameters within numerical rounding errors.

5.2 Modulation phase shift

This clause includes a method for determining DGD using time domain analysis [22].

In this procedure, a modulated light source at a given wavelength is coupled into the DUT, and the phase of the modulated signal exiting the DUT at a first SOP is compared with the phase at a second, orthogonal, SOP. The maximum phase difference is then determined corresponding to the input SOPs aligned with the two PSPs of the device. This phase difference is then converted to a delay difference and reported as the DGD for the device at the given wavelength. The reported result is strictly the DGD at that particular wavelength.

Two techniques are used, one based on a full search of input SOPs and one based on the measurement of the output SOPs associated with a Mueller set of input SOPs. The full search procedure can be implemented with either a simple polarization controller or with a polarization modulator in combination with the controller.

5.2.1 Full search procedure

For any pair of orthogonal input SOPs, there will be a phase shift difference for a given wavelength. The DGD at the wavelength is derived from the maximum phase shift for any pair of orthogonal input SOPs. The state of the pair at which this maximum phase shift occurs is the PSP.

There are several strategies for determining the correct DGD between the fast/slow PSPs when the PSPs themselves are arbitrary, as described above. In the SOP-search methods, a source of uncertainty is the alignment error of the input SOPs with the true PSPs. For example, a 5 º alignment error will give rise to a 0,4 % uncertainty in the DGD value. The polarization search alignment error will have to be well controlled and minimised.

IECNORM.COM : Click to view the full PDF of IEC TR 61282-9:2006
Withdrawn

Examples of suitable implementations are:

- the use of the polarization controller in a search mode at each wavelength. At a given wavelength, the polarization controller is used to scan the launch SOP, recording the phase shift for each SOP. Once sufficient SOPs are covered, the maximum and minimum of the recorded phase shifts will correspond to light launched along the PSPs. The DGD at the current wavelength is then proportional to the difference between the maximum and minimum phase shifts. This difference is referred to as the differential phase shift. The DGD at this wavelength is the difference in delay between these two SOPs;
- in the case of polarization modulation, the search mode may be adapted, so that as the polarization controller is scanned, the differential phase shift can be detected directly. This simplifies the search to looking for the maximum differential phase shift, which is proportional to the DGD by the relationship of 5.2.3. At this point, the PSPs have been found.

The maximum phase shift difference for a given wavelength is:

$$\Delta\phi_{\max}(\lambda) = \max\left|\Delta\phi_i(\lambda) - \Delta\phi_i'(\lambda)\right| \tag{97}$$

where

i is an index representing the various input SOPs;

$\Delta\phi$ is the phase shift of one orthogonal SOP;

$\Delta\phi'$ is the phase shift of the other orthogonal SOP.

5.2.2 Mueller set analysis

A Mueller set of input SOPs can be described using the Poincaré sphere (see Figure 16).

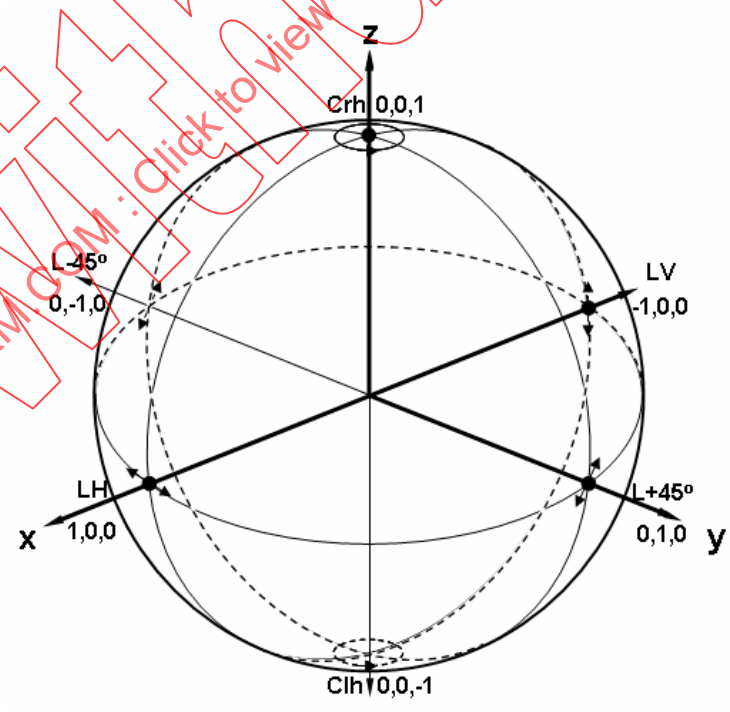

Figure 16 – Mueller states on Poincaré sphere

IECNORM.COM : Click to view the full PDF of IEC TR 61282-9:2006
Withdrawn

Orthogonal SOPs are 180 ° apart on the sphere. Three of the SOPs are on the sphere equator and are mutually separated by 90 °. Starting from the horizontal SOP on the equator, 45 º and vertical SOPs follow by adding, successively, 90 °. A circular right handed SOP is orthogonal to the other points and oriented "up" (north pole) using the right hand rule. The system of spherical coordinates is used to describe the normalised input Stokes vector s_0, the parameters used to define an example of a Mueller set where the great circle is on the equator as shown in Figure 16. The parameter θ is the linear orientation of the associated normalised Jones vector j_0. The parameter μ is the phase difference of the x and y elements of that vector as shown in Equation (98) and Table 1.

$$\begin{bmatrix} s_1 \\ s_2 \\ s_3 \end{bmatrix} = \begin{bmatrix} \cos 2\theta \\ \sin 2\theta \cos \mu \\ \sin 2\theta \sin \mu \end{bmatrix} \qquad j_0 = \begin{bmatrix} \cos\theta \exp\left(-\frac{i\mu}{2}\right) \\ \sin\theta \exp\left(\frac{i\mu}{2}\right) \end{bmatrix} \tag{98}$$

Table 1 – Example of Mueller set

θ	μ	Description
0	0	Linear polarizationat 0 ° (horizontal)
$\pi/4$	0	Linear polarization at 45 ° (45 °)
$\pi/2$	0	Linear polarization at 90 ° (vertical)
$\pi/4$	$\pi/2$	Circular polarization (spherical)

For each wavelength, the phase shifts $\Delta\phi_A(\lambda)$, $\Delta\phi_B(\lambda)$, $\Delta\phi_C(\lambda)$, $\Delta\phi_D(\lambda)$, respectively, will be recorded for each SOP in units of rad. Using these quantities, the maximum phase shift difference for the given wavelength will be found following Equation (97).

5.2.3 Differential group delay computation

Both DGD calculation techniques can result in a series of DGD values versus wavelength as shown in Figure 8a). Alternatively, the DGD values may be displayed in a histogram format shown in Figure 8b).

5.2.3.1 Differential group delay calculation using full scan technique

The DGD value in units of ps is computed at each wavelength λ in units of nm, from the maximum phase difference $\Delta\phi_{Max}(\lambda)$ in units of rad and modulation frequency f in units of GHz as follows:

$$DGD(\lambda) = \frac{10^3}{2\pi} \frac{\Delta\phi_{Max}(\lambda)}{f} \tag{99}$$

5.2.3.2 Differential group delay calculation using Mueller set technique

The average phase of the two PSPs $\phi_{RF}(\lambda)$ is obtained from:

$$\phi_{RF}(\lambda) = \frac{\Delta\phi_A(\lambda) + \Delta\phi_C(\lambda)}{2} \tag{100}$$

IECNORM.COM : Click to view the full PDF of IEC TR 61282-9:2006
Withdrawn

The measured phase values are adjusted by the average phase as:

$$\phi_{RF,A}(\lambda) = \Delta\phi_A(\lambda) - \phi_{RF}(\lambda)$$
$$\phi_{RF,B}(\lambda) = \Delta\phi_B(\lambda) - \phi_{RF}(\lambda) \quad (101)$$
$$\phi_{RF,D}(\lambda) = \Delta\phi_D(\lambda) - \phi_{RF}(\lambda)$$

The phase difference $\delta_{RF}(\lambda)$ is calculated as:

$$\delta_{RF}(\lambda) = 2\arctan\left\{\left[\tan^2(\phi_{RF,A}(\lambda)) + \tan^2(\phi_{RF,B}(\lambda)) + \tan^2(\phi_{RF,D}(\lambda))\right]^{1/2}\right\} \quad (102)$$

The DGD in units of ps is calculated using $\delta_{RF}(\lambda)$ in units of rad and the modulation frequency f in units of GHz as:

$$DGD(\lambda) = 10^3 \frac{\delta_{RF}(\lambda)}{2\pi f} \quad (103)$$

5.2.4 Polarization mode dispersion calculation

The PMD value for a wavelength range is the average of the DGD values for this range.

5.3 Polarization phase shift

This method [23-26] uses a pair of orthogonal SOPs (the 0º and 90º linearly SOPs). The 0 º and 90 º linearly SOPs are launched into the DUT and the outputs are separated into two SOP components by the polarization splitter. After that, the amplitude and group delay for each SOP (the P- and S- polarized light) at a specific measurement wavelength are measured. That is, the P- and S-polarized light amplitudes ($|T_{11}|^2_{mea}$ and $|T_{21}|^2_{mea}$, respectively) and the group delays ($d\Phi_{11}/d\omega_{mea}$ and $d\Phi_{21}/d\omega_{mea}$, respectively) for the 0 º linearly SOP are measured. And for the 90 º linearly SOP, the P- and S-polarized light amplitudes ($|T_{12}|^2_{mea}$ and $|T_{22}|^2_{mea}$) and the group delays ($d\Phi_{12}/d\omega_{mea}$ and $d\Phi_{22}/d\omega_{mea}$) are measured.

5.3.1 Differential group delay calculations

The calculation technique can result in a series of DGD values versus wavelength as shown in Figure 8a).

The following parameters are calculated using measured values.

$$\bar{\alpha}_1 = \frac{\Delta\Theta}{\Delta\omega} = \frac{\Delta\Theta}{2\pi c \cdot \delta\lambda} \cdot \lambda_i\lambda_f$$
$$\bar{\beta}_1 = \frac{1}{4}\left(\frac{d\Phi_{11}}{d\omega} - \frac{d\Phi_{22}}{d\omega} - \frac{d\Phi_{21}}{d\omega} + \frac{d\Phi_{12}}{d\omega}\right)$$
$$\bar{\gamma}_1 = \frac{1}{4}\left(\frac{d\Phi_{11}}{d\omega} - \frac{d\Phi_{22}}{d\omega} + \frac{d\Phi_{21}}{d\omega} - \frac{d\Phi_{12}}{d\omega}\right) \quad (104)$$
$$\Theta = \frac{1}{2}\cos^{-1}\left(\frac{|T_{11}|^2 - |T_{21}|^2}{|T_{11}|^2 + |T_{21}|^2}\right)$$
$$\cos 2\Theta_0 = \frac{|T_{11}|^2 - |T_{21}|^2}{|T_{11}|^2 + |T_{21}|^2}$$

IECNORM.COM : Click to view the full PDF of IEC TR 61282-9:2006
Withdrawn

where

λ_i is the initial wavelength;

λ_f is the final wavelength;

$\delta\lambda$ is the wavelength range.

$$|T_{kl}|^2 = \frac{|T_{kl}|^2_{mea}}{|T_{11}|^2_{cal}} \qquad \frac{d\Phi_{kl}}{d\omega} = \left[\frac{d\Phi_{kl}}{d\omega}\right]_{mea} - \left[\frac{d\Phi_{11}}{d\omega}\right]_{cal} \qquad kl = 11 \text{ and } 12 \tag{105}$$

$$|T_{mn}|^2 = \frac{|T_{mn}|^2_{mea}}{|T_{22}|^2_{cal}} \qquad \frac{d\Phi_{mn}}{d\omega} = \left[\frac{d\Phi_{mn}}{d\omega}\right]_{mea} - \left[\frac{d\Phi_{22}}{d\omega}\right]_{cal} \qquad mn = 21 \text{ and } 22 \tag{106}$$

The DGD value for each wavelength is calculated using $\bar{\alpha}_1$, $\bar{\beta}_1$, $\bar{\gamma}_1$ and Θ_0 as:

$$DGD(\lambda) = 2\sqrt{\bar{\alpha}_1^2 + \bar{\beta}_1^2 + \bar{\gamma}_1^2 + 2\bar{\beta}_1\bar{\gamma}_1\cos 2\Theta_0} \tag{107}$$

5.3.2 Differential group delay determination

The definition of DGD concerning this method is hereinafter described. The optical transfer function matrix can be expressed as:

$$\begin{aligned} T(\omega) &= \begin{bmatrix} |T_{11}|\cdot\exp(-j\Phi_{11}) & |T_{12}|\cdot\exp(-j\Phi_{12}) \\ |T_{21}|\cdot\exp(-j\Phi_{21}) & |T_{22}|\cdot\exp(-j\Phi_{22}) \end{bmatrix} \\ &= \begin{bmatrix} \cos\Theta\cdot\exp(-j\phi - j\psi) & -\sin\Theta\cdot\exp(-j\phi + j\psi) \\ \sin\Theta\cdot\exp(+j\phi - j\psi) & \cos\Theta\cdot\exp(+j\phi + j\psi) \end{bmatrix}\cdot\exp(-j\Phi) \end{aligned} \tag{108}$$

where

Θ is the polarization angle;

ϕ is the phase difference between T_{11} and T_{21};

ψ is the phase difference between T_{11} and T_{12};

Φ is the polarization-independent phase shift.

The output of polarization vector $E^{out}(\omega)$ is expressed using $T(\omega)$ as:

$$E^{out}(\omega) = T(\omega)\cdot E^{in}(\omega) \tag{109}$$

where $E^{in}(\omega)$ is the FT of an optical input signal.

$E^{out}(\omega)$, which is described by Taylor expansion around the optical carrier frequency ω_0, is expressed as:

$$E^{out}(\omega) = E^{out}(\omega_0) + \left.\frac{dE^{out}}{d\omega}\right|_{\omega=\omega_0}\delta\omega + \frac{1}{2!}\left.\frac{d^2E^{out}}{d\omega^2}\right|_{\omega=\omega_0}\delta\omega^2 \tag{110}$$

where

$$\delta\omega = \omega - \omega_0 \tag{111}$$

IECNORM.COM : Click to view the full PDF of IEC TR 61282-9:2006
Withdrawn

The first order PMD operator $D(\omega)$, that should be called a transfer function differential operator, is expressed as:

$$D(\omega) = \frac{dT(\omega)}{d\omega} \cdot T(\omega)^{-1} \tag{112}$$

Therefore, the following expression is obtained by substituting Equation (112) for Equation (110).

$$\begin{aligned} E^{out}(\omega) &= \left\{1 + D\delta\omega + \frac{1}{2}D^2\delta\omega^2 + \frac{1}{2}\frac{dD}{d\omega}\delta\omega^2\right\} \cdot E^{out}(\omega_0) \\ &\cong \exp\left\{D\delta\omega + \frac{1}{2}\frac{dD}{d\omega}\delta\omega^2\right\} \cdot E^{out}(\omega_0) \end{aligned} \tag{113}$$

where

$D(\omega)$ is the first order PMD operator;

$\frac{dD(\omega)}{d\omega}$ is the second order PMD operator.

They are not commutative with each other, and the high order term is negligible.

The following expression is obtained by diagonalising $D(\omega)$ with the unitary operator X.

$$\begin{aligned} X^{-1} \cdot E^{out}(\omega) &= X^{-1}\exp(D \cdot \delta\omega) X \cdot X^{-1} E^{out}(\omega_0) \\ &= \begin{bmatrix} \exp(-j\Gamma_+ \cdot \delta\omega) & 0 \\ 0 & \exp(-j\Gamma_- \delta\omega) \end{bmatrix} \cdot X^{-1} E^{out}(\omega_0) \end{aligned} \tag{114}$$

where

$-j\Gamma_{+/-}$ are the eigenvalues of $D(\omega)$;

Γ_+ is the maximum group delay;

Γ_- is the minimum group delay.

That is, the difference between the imaginary parts of the eigenvalues of $D(\omega)$, Γ_+-Γ_- is the first order PMD called DGD.

Four independent parameters, Θ, ϕ, ψ and Φ, described in Equation (109) make the following expression using Taylor expansion.

$$\begin{aligned} \Theta &= \Theta_0 + \bar{\alpha}_1\delta\omega + \frac{1}{2}\bar{\alpha}_2\delta\omega^2 \\ \phi &= \phi_0 + \bar{\beta}_1\delta\omega + \frac{1}{2}\bar{\beta}_2\delta\omega^2 \\ \psi &= \psi_0 + \bar{\gamma}_1\delta\omega + \frac{1}{2}\bar{\gamma}_2\delta\omega^2 \\ \Phi &= \Phi_0 + \beta_1\delta\omega + \frac{1}{2}\beta_2\delta\omega^2 \end{aligned} \tag{115}$$

where

$$\delta\omega = \omega - \omega_c \tag{116}$$

IECNORM.COM : Click to view the full PDF of IEC TR 61282-9:2006
Withdrawn

Θ_0 is the value of Θ at $\omega - \omega_c$;

ϕ_0 is the value of ϕ at $\omega - \omega_c$;

ψ_0 is the value of ψ at $\omega - \omega_c$;

Φ_0 is the values of Φ at $\omega - \omega_c$;

$\bar{\alpha}_1$ is the first order coefficient of Taylor expansion of Θ;

$\bar{\beta}_1$ is the first order coefficient of Taylor expansion of ϕ;

$\bar{\gamma}_1$ is the first order coefficient of Taylor expansion of ψ;

β_1 is the first order coefficient of Taylor expansion Φ;

$\bar{\alpha}_2$ is the second order coefficient of Taylor expansion of Θ;

$\bar{\beta}_2$ is the second order coefficient of Taylor expansion of ϕ;

$\bar{\gamma}_2$ is the second order coefficient of Taylor expansion of ψ;

β_2 is the second order coefficient of Taylor expansion of Φ.

The first order PMD operator $D(\omega)$ is expressed using Equation (105) as:

$$D(\omega) = -j\beta_1 \begin{bmatrix} 1 & 0 \\ 0 & 1 \end{bmatrix} - j \begin{bmatrix} \bar{\beta}_1 + \bar{\gamma}_1 \cos 2\Theta & (-j\bar{\alpha}_1 + \bar{\gamma}_1 \sin 2\Theta) \cdot e^{-j2\phi} \\ (+j\bar{\alpha}_1 + \bar{\gamma}_1 \sin 2\Theta) \cdot e^{+j2\phi} & -\bar{\beta}_1 - \bar{\gamma}_1 \cos 2\Theta \end{bmatrix} \tag{117}$$

Therefore, the eigenvalues of $D(\omega)$ are expressed as:

$$j\Gamma_{\pm} = -j\beta_1 \pm j\sqrt{\bar{\alpha}_1^2 + \bar{\beta}_1^2 + \bar{\gamma}_1^2 + 2\bar{\beta}_1\bar{\gamma}_1 \cos 2\Theta} \tag{118}$$

where β_1 is the polarization-independent group delay.

The DGD, $\Delta\tau$, is given by the difference between the imaginary parts of the two eigenvalues as:

$$\Delta\tau = \Gamma_+ - \Gamma_- = 2\sqrt{\bar{\alpha}_1^2 + \bar{\beta}_1^2 + \bar{\gamma}_1^2 + 2\bar{\beta}_1\bar{\gamma}_1 \cos 2\Theta} \tag{119}$$

5.3.3 Polarization mode dispersion calculation

The PMD value within the measured wavelength range is given by the DGD average value over the measured wavelength range.

5.4 Fixed analyser

This method [16,27,28] requires calculation of the power ratio $R(\lambda)$ from the received power as $P_A(\lambda)$ with a polarization analyser in the light path, and the received power as $P_{Tot}(\lambda)$ with the analyser removed from the light path.

$$R(\lambda) = \frac{P_A(\lambda)}{P_{Tot}(\lambda)} \tag{120}$$

IECNORM.COM : Click to view the full PDF of IEC TR 61282-9:2006
Withdrawn

An alternative procedure is to leave the analyser in place on the second scan, but rotate it 90 °, and record the power as $P_B(\lambda)$. The formula for the power ratio $R(\lambda)$ is then:

$$R(\lambda) = \frac{P_A(\lambda)}{P_A(\lambda) + P_B(\lambda)} \tag{121}$$

There are two techniques for calculating PMD from the R function:

- extrema counting (EC);
- Fourier transform (FT).

5.4.1 Extrema counting

The procedure is also called cycle counting.

The function $R(\lambda)$ should be obtained at equally spaced wavelength increments from a minimum wavelength of λ_1 to a maximum wavelength of λ_2. E is the number of extrema (both maxima and minima) within the wavelength range $\lambda_1 < \lambda < \lambda_2$. Alternatively, the wavelength range can be redefined so that λ_1 and λ_2 coincide with extrema, in which case E is the number of extrema (including λ_1 and λ_2) minus one. The formula for the PMD value, $<\Delta\tau>$, is:

$$<\Delta\tau> = \frac{kE\lambda_1\lambda_2}{2c(\lambda_2 - \lambda_1)} \tag{122}$$

where

c is the speed of light in vacuum;

k is a mode-coupling factor which equals 1,0 in negligible mode coupling and 0,82 in random mode coupling.

5.4.1.1 Accuracy

The best accuracy is obtained by making $(\lambda_2 - \lambda_1)$ large enough to insure that $E >> 1$. This is especially important when there is random mode coupling and less so otherwise. Values of E in the range of 7 to 40 are typical. When E is at the low end of this range, the percentage uncertainties in both E and the PMD become large. At the upper end of the range, finite wavelength increment or instrumental spectral width may result in some adjacent peaks not being resolved.

Ideally, the scan window should be centred on the fibre's wavelength of use, and the wavelength range made wide enough to insure that E is greater than about 10 for the maximum PMD value of interest (where pass/fail is an issue).

5.4.1.2 Peak identification algorithm for extrema counting

In the presence of noise and/or random mode coupling, the identification of extrema in $R(\lambda)$ may sometimes be ambiguous. The following mathematical algorithm is used to make this identification objective.

5.4.1.2.1 Smoothing

At an evenly spaced set of wavelengths $\{\lambda_1, \lambda_2, \ldots \lambda_N\}$ the power ratio $R(\lambda)$ is obtained. To reduce the effect of noise, these $\{f_1, f_2, \ldots f_N\}$ data are smoothed with a running least-square procedure. For each λ_i, a low-order polynomial is fitted to the $2m+1$ measured values $\{f_{i-m}, \ldots f_i, \ldots f_{i+m}\}$ centred at λ_i. A cubic polynomial with $m = 8$ has been found to work well on most PMD data.

IECNORM.COM : Click to view the full PDF of IEC TR 61282-9:2006
Withdrawn

A cubic polynomial centred at λ_i has the general form:

$$R_i(\lambda) = a_i + b_i(\lambda_i - \lambda) + c_i(\lambda_i - \lambda)^2 + d_i(\lambda_i - \lambda)^3 \quad (123)$$

Using the method of least squares to calculate the coefficients,

$$a_i = \gamma_0^{(m)} f_i + \sum_{j=1}^{m} \gamma_j^{(m)}(f_{i+j} + f_{i-j}) \quad (124)$$

$$b_i = \frac{1}{h}\sum_{j=1}^{m} a_j^{(m)}(f_{i+j} + f_{i-j}) \quad (125)$$

where

h is the spacing between wavelengths.

$$\gamma_j^{(m)} = 3\frac{3m^2 + 3m - 5j^2 - 1}{(2m+1)(2m-1)(2m+3)} \quad (126)$$

$$a_j^{(m)} = \frac{5j\,[7j^2(3m^2 + 3m - 1) - 5(3m^4 + 6m^3 - 3m + 1)]}{m(m+1)(2m+1)(4m^4 + 8m^3 - 7m^2 - 11m + 6)} \quad (127)$$

Once a_i and b_i are evaluated, we find:

$$c_i = \frac{3}{h^2}\frac{\Sigma_{j=-m}^{m} f_{i+j} - (2m+1)a_i}{m(m+1)(2m+1)} \quad (128)$$

$$d_i = -\frac{5}{h^3}\frac{3\Sigma_{j=-m}^{m} jf_{i+j} + hb_i m(m+1)(2m+1)}{m(m+1)(2m+1)(3m^2+3m-1)} \quad (129)$$

The smoothed value $R_i(\lambda_i)$ then replaces the measured value f_i. In addition to this single value $R_i(\lambda_i)$, the smoothed function $R_i(\lambda)$ from Equation (123) is needed in order to calculate the derivative at $\lambda = \lambda_i$ in the following clause.

5.4.1.2.2 Definition of an extremum

Once the smoothed functions $R_i(\lambda)$ have been calculated, their derivatives $dR_i/d\lambda$ can be calculated. Whenever the sign of the derivative changes between the following adjacent values,

$$\frac{dR_{K-1}}{dl}(\lambda_{K-1}) \text{ and } \frac{dR_K}{dl}(\lambda_K) \quad (130)$$

The midpoint $(\lambda_{K-1} + \lambda_K)/2$, or an interpolated point, is identified as an extremum.

5.4.1.2.3 Robustness

Some extrema may be the result of small spurious oscillations that are unrelated to PMD (e.g., measurement noise). These can be eliminated by subjecting all of the identified extrema to a test. For each local maximum value $R\,(max)$, calculate the ratio:

IECNORM.COM : Click to view the full PDF of IEC TR 61282-9:2006
Withdrawn

$$\frac{R(\max) - R(\text{nearest min})}{R(\text{global max}) - R(\text{global min})} \quad (131)$$

where "global" refers to the entire data range from λ_1 to λ_N.

$R(max)$ is an acceptable maximum only if this ratio exceeds some predetermined value (which might typically be a few percent). Similarly, $R(min)$ is an acceptable minimum only if the ratio:

$$\frac{R(\text{nearest max}) - R(\min)}{R(\text{global max}) - R(\text{global min})} \quad (132)$$

exceeds the same predetermined value.

5.4.1.2.4 Goodness-of-fit

A goodness-of-fit test is useful in assuring that the smoothed values $R_i(\lambda_i)$ faithfully represent the measured power ratios f_i. As an example, one could require the mean square error

$$D^2 = \frac{1}{N} \sum_{j=1}^{N} [f_i - R_i(\lambda_i)]^2 \quad (133)$$

to be less than 0,3. If this condition is violated, some change may be necessary, for example repeating the measurement with more data points per period of the oscillation.

5.4.2 Fourier transform

The procedure is also called Fourier analysis.

In this method, a Fourier analysis of $R(\lambda)$, usually expressed in the domain of optical frequency ν, is used to derive PMD. The FT transforms this optical frequency domain data to the time domain. The FT yields direct information on the distribution of light arrival times $\delta\tau$. These data are post-processed as described below to derive the expected PMD $<\Delta\tau>$ for the DUT. This method is applicable to fibres with negligible or random mode coupling. Figure 17 shows an example of random mode coupling result with the FA method using the FT technique.

IECNORM.COM : Click to view the full PDF of IEC TR 61282-9:2006
Withdrawn

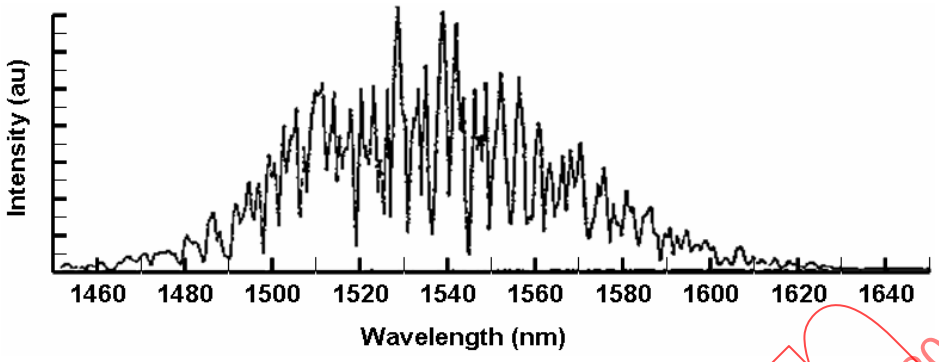

a) Spectral intensity

IEC 1264/06

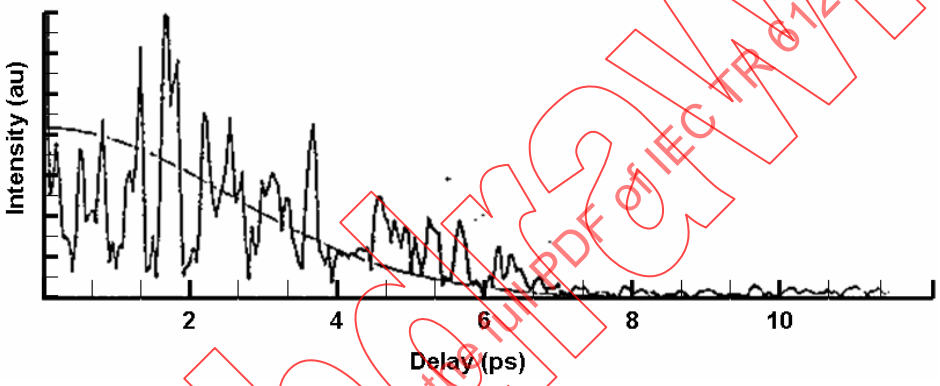

b) Fourier transform of intensity

IEC 1265/06

Figure 17 – Example of random mode coupling result with fixed analyser using Fourier transform technique [15]

5.4.2.1 Data pre-processing and Fourier transformation

To use this method, the FT normally requires equal increments in optical frequency so that $R(\lambda)$ data are collected at λ values so that they form equal increments in the optical frequency domain. Alternatively, data taken at equal λ increments may be fitted (for example, by using a cubic spline fit) and interpolation used to generate these points, or more advanced spectral estimation techniques can be used. In each instance, the ratio $R(\lambda)$ at each λ value used is calculated using Equation (120) or (121) as appropriate.

Zero-padding or data interpolation and d.c. level removal may be performed on the ratio data, $R(\lambda)$. Windowing the data may also be used as a pre-conditioning step before the FT. The Fourier transformation is then carried out, to yield the amplitude data distribution $P(\delta\tau)$ for each value of $\delta\tau$.

5.4.2.2 Transform data fitting

FT data at zero $\delta\tau$ has little meaning since, unless carefully removed, d.c. components in $R(\lambda)$ may be partially due to insertion loss of the analyser, for example. When the d.c. level is not removed, up to two data points are generally bypassed (not used) in any further calculations. A variable j can be defined so that the 'first valid bin' above zero $\delta\tau$ that is included in calculations corresponds to j = 0.

IECNORM.COM : Click to view the full PDF of IEC TR 61282-9:2006
Withdrawn

In order to remove measurement noise from subsequent calculations, $P(\delta\tau)$ is compared to a threshold level T_1, typically set to 200 % of the RMS noise level of the detection system. It is now necessary to determine if the mode coupling is negligible or random.

If it is found that the first X valid points of $P(\delta\tau)$ are all below T_1, this indicates that $P(\delta\tau)$ must have discrete spike features characteristic of negligible mode coupling. The value of X is equal to three, unless zero-padding is used in the Fourier analysis. In that case, the value of X can be determined from

$$X = \frac{3 \bullet (number\_original\_data\_points)}{total\_length\_of\_array\_after\_zeropadding} \tag{134}$$

PMD is calculated using Equation (135) for a negligible mode coupling fibre, or PMD is calculated using Equation (136) for a random mode coupling fibre.

5.4.2.3 Polarization mode dispersion calculation for negligible mode coupling

In the case of negligible mode coupling or a simple birefringent device, the ratio $R(\lambda)$ may be derived as a simple chirped sine wave in the wavelength domain. If the data is plotted in the optical frequency domain, the chirp is removed, and the 'frequency' of the resulting sine wave is related to the relative pulse arrival time $\delta\tau$, or simply the PMD value $<\Delta\tau>$ associated with the birefringence that produces the oscillation. Fourier transformation will give a $P(\delta\tau)$ output containing a discrete spike at a position corresponding to the relative pulse arrival time $\delta\tau$, the centroid of which is the PMD value $<\Delta\tau>$.

To define the spike centroid $<\Delta\tau>$ those points where $P(\delta\tau)$ exceeds a second pre-determined threshold level T_2, typically set to 200 % of the RMS noise level of the detection system are used in the equation:

$$<\Delta\tau> = \frac{\sum_{e=0}^{M'} [P_e(\delta\tau)\delta\tau_e]}{\sum_{e=0}^{M'} P_e(\delta\tau)} \tag{135}$$

where $M'+1$ is the number of data points of P within the spike which exceed T_2.

$<\Delta\tau>$ in Equation (135) is typically quoted in units of ps. If the DUT is a fibre of length L, the PMD coefficient may be calculated using $<\Delta\tau>/L$. If no spike is detected (i.e., $M' = 0$), then PMD is zero. Other parameters such as the RMS spike width and/or spike peak value may be reported.

If the DUT contains one or more birefringent elements, more than one spike will be generated. For a number n concatenated fibres/devices, up to $2^{(n-1)}$ spikes will be obtained.

5.4.2.4 Polarization mode dispersion calculation for random mode coupling

In the case of random mode coupling many pulse arrival times, $\delta\tau$, are present with different relative strengths, and $R(\lambda)$ becomes an extremely complex function. This leads to the concept that if an unweighted analysis of the spectral content (e.g. the fast FT) of $R(\lambda)$ is performed, the autocorrelation function $P(\delta\tau)$ of the distribution of the individual pulse arrivals and their relative strengths will be obtained. The second moment of this distribution $P(\delta\tau)$ will define the expected value of PMD, $<\Delta\tau>$. The statistics of random coupling dictates that the distribution $P(\delta\tau)$, should fall on a Gaussian curve, so comparing the distribution to a Gaussian permits the degree of randomness in the coupling to be inferred.

IECNORM.COM : Click to view the full PDF of IEC TR 61282-9:2006
Withdrawn

Counting up from j = 0, the first point of P is determined which exceeds T_1 and which is followed by at least X data points which fall below T_1. This point represents the last significant point in (i.e. the 'end' of) the distribution $P(\delta\tau)$ for a random mode coupling that is not substantially affected by measurement noise. The $\delta\tau$ value for this point is denoted $\delta\tau_{last}$, and the value of j at $\delta\tau_{last}$ is denoted M''.

The square root of the second moment, σ_R, of this distribution defines the fibre PMD $<\Delta\tau>$ and is given by

$$<\Delta\tau^2>^{1/2} = \sigma_R = \left\{ \frac{\sum_{j=0}^{M''} [P_j(\delta\tau)\delta\tau_j^2]}{\sum_{j=0}^{M''} P_j(\delta\tau)} \right\}^{\frac{1}{2}} \quad (136)$$

$<\Delta\tau>$ in Equation (136) is typically quoted in units of ps. If the DUT is a fibre of length L, the PMD coefficient may be calculated using $<\Delta\tau>/\sqrt{L}$.

5.4.2.5 Polarization mode dispersion calculation for mixed mode coupling

There may be instances where both negligibly coupled devices and randomly coupled device(s) are concatenated to form the system under test. In this case, both centroid determination (Equation (135)) and the second moment derivation (Equation (136)) may be required. Note that spikes in $P(\delta\tau)$ may only be determined beyond the $\delta\tau_{last}$ computed.

5.4.2.6 Fourier analysis theoretical background

The DUT, for instance a fibre, may be simulated theoretically by a simple model. If a simple birefringent device (i.e., negligible mode coupling case) is placed between crossed polarizers, each at 45 º to the DUT birefringence axes, the light transmission ratio R' as a function of wavelength λ is given by

$$R' = \sin^2\left(\frac{\pi\Delta nL}{\lambda}\right) \quad (137)$$

where

Δn is the DUT birefringence;

L is the DUT length (for instance a fibre length).

Formulating Equation (137) in optical frequency ν, we obtain:

$$R' = \sin^2\left[\pi\nu\left(\frac{\Delta n \cdot L}{c_0}\right)\right] \quad (138)$$

where c_0 is the velocity of light in free space.

Now, the PMD of the device is defined as:

$$\delta\tau = \frac{\Delta n \cdot L}{c_0} \quad (139)$$

Any (usually small) dispersion term in Δn has been neglected in Equation (139) for clarity.

IECNORM.COM : Click to view the full PDF of IEC TR 61282-9:2006
Withdrawn

Using Equation (139) in Equation (138) and reformulating:

$$R' = \frac{1-\cos(2\pi\nu \cdot \delta\tau)}{2} \tag{140}$$

Examination of Equation (140) reveals that R' is a cosine wave with an oscillation 'frequency' F given by:

$$F = \delta\tau \tag{141}$$

In other words the spectral content of R' has a single component at $\delta\tau$. Since the spectral content may be obtained by Fourier transformation of R', the FT of R' would show a single 'spike' at $\delta\tau$ in the transform domain (in this case the time domain). The FT operates from the optical frequency domain to the time domain. The effect of the dispersive term omitted in Equation (140) is to slightly broaden or 'smear' the spike in the time domain. The PMD of the device is then simply the centroid position of this spike within the transform. The spike intensity will depend on the orientations of the polarizer and analyser relative to the device polarization axes at input and output. However, it can be shown that the position $\delta\tau$, i.e., the PMD indication, does not change with polarizer/analyser orientations. Thus PMD may be measured independently of fibre splice rotation, polarizer position, etc.

Extending this analysis to the case where the mode coupling is random, we can see that the individual 'path' pulse arrival times arising from the mode coupling will each give rise to a corresponding spike in the FT, with an amplitude dependent on relative polarization orientation to the polarizer/analyser and on the relative power being carried by that path, with no other weighting factors. The FT is therefore compatible with the statistical nature of PMD in fibres, and the data represents the autocorrelation of the pulse arrival time distribution.

The model of PMD in fibres with random coupling shows that a short input pulse will emerge from the fibre as a broadened light pulse with a nominally Gaussian shape. The probability distribution of the output pulse is centred on the mean arrival time of the light pulse (the average group delay), where $\delta\tau = 0$. Therefore for randomly coupled fibres, we expect a distribution $P(\delta\tau)$ within the Fourier spectrum which is Gaussian, centred around $\delta\tau = 0$ (i.e., centred at zero 'frequency'). Since the FT of a real function is symmetric about zero “frequency”, the resulting transform is a one-sided Gaussian.

It can be determined whether the amplitude data $P(\delta\tau)$ is sufficiently close to Gaussian that the mode coupling may be assumed to be random. This is to determine if the PMD coefficient may be calculated from the PMD $<\Delta\tau>$ divided by the square root of the device length. One method that can be used is a chi-squared test assuming a fitted Gaussian equation.

The Gaussian equation fitted has the form

$$P'_j(\delta\tau) = A_{median} e^{-\left(\frac{\delta\tau_j^2}{2\sigma_R^2}\right)} \tag{142}$$

where

A_{median} is a constant;

$P'_j(\delta\tau)$ is the predicted probability function at time value $\delta\tau_j$.

The procedure is as follows:

a) rearranging Equation (142), an estimate of the value of A, A_j is obtained from each data point $P_j(\delta\tau)$ from j = 0 to $j = M$", using

IECNORM.COM : Click to view the full PDF of IEC TR 61282-9:2006
Withdrawn

$$A_j = P'_j(\delta\tau)e^{\left(\frac{\delta\tau_j^2}{2\sigma_R^2}\right)} \tag{143}$$

where j = 0, 1, …M''.

b) taking the A_j values, the final value of A is obtained from their median value, A_{median}, given by first arranging A_j in ascending order and using

$$M'' \text{ even: } A_{median} = A_{\left(\frac{M''}{2}\right)} \tag{144}$$

$$M'' \text{ odd: } A_{median} = \frac{\left[A_{\left(\frac{M''-1}{2}\right)} + A_{\left(\frac{M''+1}{2}\right)}\right]}{2} \tag{145}$$

c) using A_{median} in Equation (143), the predicted (Gaussian) distribution values $P'_j(\delta\tau)$ are determined, and the chi-squared test carried out using the equation:

$$X^2 = \sum_{j=0}^{M''} 2\left[\frac{P_j(\delta\tau)}{P'_j(\delta\tau)}\right]^2 \tag{146}$$

d) if

$$X^2 < X_a^2 \tag{147}$$

and

$$X^2 > X_{1-a}^2 \tag{148}$$

where X_a^2 is the critical value of the chi-squared distribution at level a (e.g. 0,01).

For $2(M''+1)$ degrees of freedom, the Gaussian fit is accepted, and the data is therefore random. The PMD coefficient may then be calculated using the square root of the DUT length (random mode coupling).

If the condition is not met, the data is deemed to be non-random, and the PMD coefficient may then not be calculated using the square root of the DUT length. The PMD coefficient is not defined in this case.

The statistical uncertainty in the chi-squared test is defined by the level a (in this case 1 %). Thus 1 % of tests can give the wrong decision whether the data is sufficiently random for the PMD coefficient to be determined using the square root of the DUT length. Multiple PMD measurements may be used to improve the measurement uncertainty. Individual measurements may or may not pass the chi-squared test, and in this instance the mean of the PMD $<\Delta\tau>$ values is calculated. Length normalisation using the DUT length or using the square root of the DUT length is then applied; the choice of length normalisation is made by whether the majority of single measurements in the set fail or pass the chi-squared test respectively. Regardless of the choice of equation, note that the second moment will always define the PMD, $<\Delta\tau>$.

IECNORM.COM : Click to view the full PDF of IEC TR 61282-9:2006
Withdrawn

An example of the FT output obtained in a fibre of length 25 km with random mode coupling is shown in Figure 18. In this case M" was determined to be 9, and Equation (146) gave X^2 = 22,61. Since for 2(M"+1) = 20, X_a^2 is 37,6, and X_{1-a}^2 is 8,26, both conditions of Equations (147) and (148) are met. The data is therefore Gaussian, randomly coupled, so that the PMD coefficient may be determined using the square root of a fibre length.

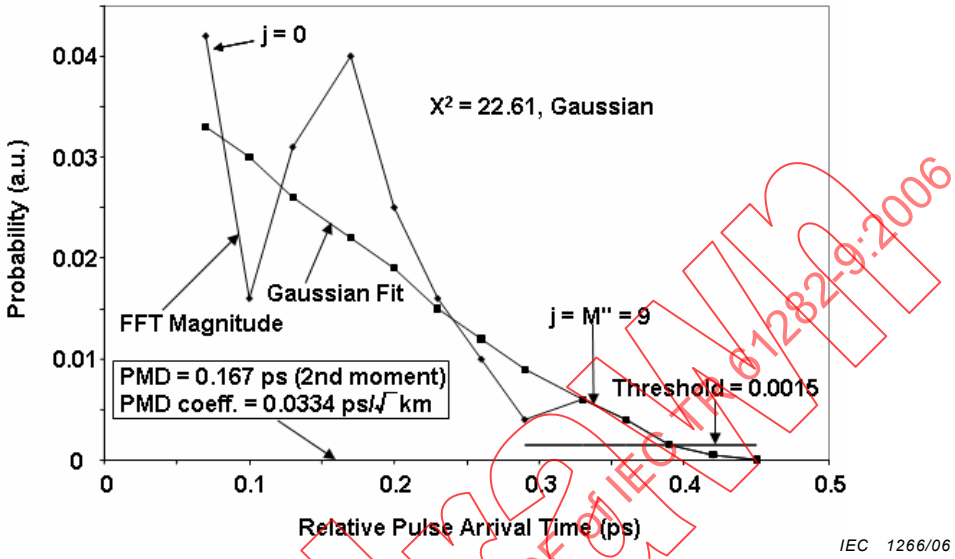

Figure 18 – Polarization mode dispersion by Fourier analysis

5.4.3 Cosine Fourier transform analysis

This analysis is based on the fact that the cosine Fourier transform of the spectrum emitted from the analyser is the fringe pattern of the interferogram that is obtained from GINTY (see 5.5.3.1.1.2). The difference between fringe patterns generated by the analyser being set at two orthogonal settings is the cross-correlation function. For an infinite spectrum into the analyser, the autocorrelation function would have zero width. In practice, the finite source spectrum in the optical frequency domain acts as a windowing function which produces a non-zero autocorrelation function width in the time domain.

The analysis of the squared cross-correlation and autocorrelation functions found in the GINTY analysis [31,62] shows that the difference in squared RMS widths of these functions is proportional to the square of the spectrally weighted RMS (by squared power) of the DGD values. (See Equation (214))

The result from the GINTY is independent of the spectral shape, which means that the details of the windowing function are fully taken into account. It is also independent of the degree of mode coupling, which means that no changes in algorithm are needed to treat the different mode coupling regimes.

The result is limited by the spectral width and optical frequency increment that is measured. As the PMD increases, the frequency increment must be decreased.

The analysis reports the PMD_{RMS} metric. If ideal random mode coupling is present, the result can be converted to PMD_{AVG} using Equation (31).

IECNORM.COM : Click to view the full PDF of IEC TR 61282-9:2006
Withdrawn

5.4.3.1 Overview

The measurement of powers emitted from the analyser set at two orthogonal settings is required. The ratio, R, associated with Equation (121) is modified to:

$$R(\nu)=\frac{P_A(\nu)-P_B(\nu)}{P_A(\nu)+P_B(\nu)} \tag{149}$$

where $\nu = c/\lambda$ is the optical frequency (THz)

If a polarimeter is used, the three normalised output Stokes vector elements are equivalent to three independent normalized ratios equivalent to that represented by Equation (149). Each Stokes vector element is the difference in powers between orthogonal analyser settings. The three elements are different in that the base settings are also orthogonal.

The data are multiplied by a windowing function, $W(\nu)$, that goes to zero smoothly at the edges. Both $R(\nu)W(\nu)$ and $W(\nu)$ are put into arrays with zero padding at lower, unmeasured frequencies. Fast Cosine Fourier Transforms (FCFT) are applied to each array to obtain the time domain fringe envelopes, $r(t)w(t)$ and $w(t)$. These are squared to obtain the squared cross-correlation and autocorrelation envelopes, E_x^2 and E_0^2, respectively. When multiple ratio functions (N) are available from different combinations of input polarizer setting and base analyser settings (or different Stokes output vector elements), using for instance input/output (I/O) SOP scrambling, form the mean square envelopes as:

$$\overline{E}_x^2=\frac{1}{N}\sum_i E_{xi}^2 \tag{150}$$

$$\overline{E}_0^2=\frac{1}{N}\sum_i E_{0i}^2 \tag{151}$$

Using the RMS calculation of 5.5.3.1.1.2, calculate the RMS widths, σ_x and σ_0 of these two functions. The PMD_{RMS} value is calculated as:

$$PMD_{\mathrm{RMS}}=\left[\frac{3}{2}\left(\sigma_x^2-\sigma_0^2\right)\right]^{1/2} \tag{152}$$

It is related to the spectrally weighted (by squared window value) RMS of the DGDs as:

$$\left\langle PMD_{\mathrm{RMS}}\right\rangle=\frac{\int\Delta\tau^2(\nu)W^2(\nu)d\nu}{\int W^2(\nu)d\nu} \tag{153}$$

The expected value operator is with respect to random I/O SOPs.

5.4.3.2 Details

This clause explains some of the details with respect to the measured frequency window, the frequency increment, $\Delta\nu$, frequency shifting and the result of the FCFT. An example of a FCFT algorithm may be found in [60].

The data must be available in uniform frequency increments. The number of data points, including zero pad values, must be $1+2^k$, with k an integer.

IECNORM.COM : Click to view the full PDF of IEC TR 61282-9:2006

If the nm measured data points are not taken in uniform frequency increments, they may be fitted to a polynomial such as a spline for interpolation. A cubic spline [61] with nm – 3 uniform segments will fit all the data perfectly and allow interpolation.

Given that the measured data are bounded by $\nu_{\min M}$ and $\nu_{\max M}$ and the fact that the minimum optical frequency is well above zero, the application of frequency shifting can be used to reduce the size of the arrays that are processed. The boundaries of the frequencies used in the calculation array can be selected by any choice of n so that:

$$\nu_{\max}\frac{n-1}{n} = \nu_{\min} \le \nu_{\min M} \quad , \quad \nu_{\max} = \nu_{\max M} \, , \tag{154}$$

where n is a positive integer.

The frequency values less than the measured frequency are filled with zeros.

Following the FCFT, the array will contain the time domain fringe pattern from times of 0 to $t_{\max} = \Delta t 2^k$, where the time increment, Δt, is given as:

$$\Delta t = \frac{n}{2\nu_{\max}} = \frac{1}{2(\nu_{\max} - \nu_{\min})} \tag{155}$$

The fringe pattern that would be obtained from interferometry extends to negative time values as well as positive time values. The value at a given negative time is equal to the value at the positive time. The function is even and symmetric about zero.

The selection of the frequency shift should be done keeping in mind that the RMS width calculation needs some time domain values that are less than the minimum PMD_{RMS} that is measurable.

The frequency increment, $\Delta\nu$, is also related to the number of points sampled, the frequency shift, and the maximum PMD_{RMS} that is to be measured. It is given as the following, along with the constraint as:

$$\Delta\nu = \frac{\nu_{\max} - \nu_{\min}}{2^k} \le \frac{1}{24 PMD_{RMS-\max}} \tag{156}$$

The spectral width of the filtered source should be half of this value. When the actual scan is done in equal wavelength increments, the wavelength increment at the lower end of the range should be consistent with the constraint of Equation (156).

The windowing function, $W(\nu)$, can technically be any function, including a square function. The function that is chosen should be one that minimises the value of σ_0. Functions that do this proceed to zero at the edges in a continuous way and should also have the first derivative proceed to zero at the edges. This will minimise the ringing that can increase σ_0.

5.4.3.3 Examples

Table 2 shows a sample calculation spreadsheet. The wavelength extrema and k are entered. For each of several possible frequency shift values, n, the other parameters are calculated. $minPMD$ is calculated as $3\Delta t$. The increment in terms of $\Delta\lambda$ at the lower wavelength limit is also presented. Clearly there are tradeoffs, depending on the range of PMD_{RMS} values that are to be measured. In general, the broader the wavelength range and the smaller the frequency increment, the better.

IECNORM.COM : Click to view the full PDF of IEC TR 61282-9:2006
Withdrawn

Table 2 – Cosine Fourier transform calculations

Frequency shift						
n	freqmin calc (THz)	del-t (ps)	delfreq (THz)	minPMD (ps)	maxPMD (ps)	wave increment (nm)
1	0	0.002168	0.112602	0.006504	0.370034	0.635076
2	115.3048077	0.004336	0.225205	0.013009	0.185017	1.270772
3	153.7397436	0.006504	0.337807	0.019513	0.123345	1.90709
4	172.9572115	0.008673	0.450409	0.026018	0.092508	2.544031
5	184.4876923	0.010841	0.563012	0.032522	0.074007	3.181596
6	192.1746795	0.013009	0.675614	0.039027	0.061672	3.819785
7	197.6653846	0.015177	0.788216	0.045531	0.052862	4.458599
8	201.7834135	0.017345	0.900819	0.052036	0.046254	5.098039

Wavelengths (nm)		Frequencies (THz)
max	1700	230.6096154
min	1300	176.3485294

c =	299792.5	nm/ps
k =	11	
npt =	2048	

Figure 19 illustrates the results for what might be obtained from a fibre with PMD_{RMS} = 0,2 ps. The mean cross-correlation and mean autocorrelation envelopes are shown for a single scan using a windowing function that is Gaussian with a standard deviation of 23 nm. The result is from a simulation of a fibre with ideal random mode coupling. The measured result for this simulation was 0,185 ps.

IECNORM.COM : Click to view the full PDF of IEC TR 61282-9:2006
Withdrawn

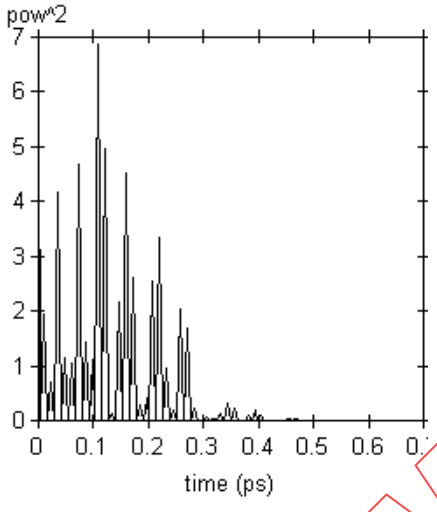

a) Mean cross-correlation envelope

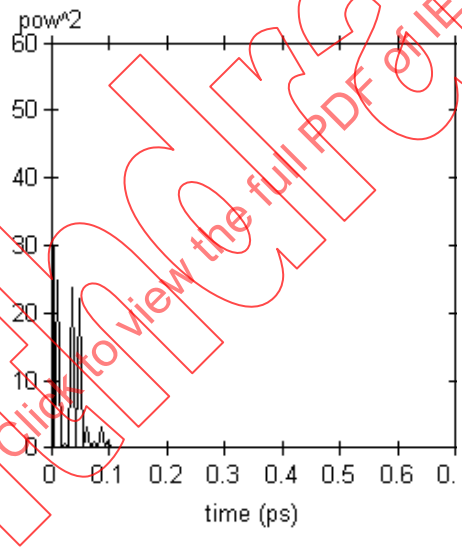

b) Mean autocorrelation envelope

Figure 19 – Mean cross-correlation and autocorrelation functions

IECNORM.COM : Click to view the full PDF of IEC TR 61282-9:2006
Withdrawn

5.4.4 Spectral range

For random mode coupling, sufficient spectral range must be used to form the spectral ensemble (average) with sufficient precision. The statistical uncertainty may be minimised by using the widest possible spectral range (e.g. at least 200 nm). The precision required and therefore spectral range must be specified prior to the measurement.

In addition, very low $\delta\tau$ values will give very long periods in $R(\lambda)$, and the spectral range λ_1 to λ_2 should cover at least two complete 'cycles'. The spectral range covered defines the smallest $\delta\tau$ value that can be resolved in $P(\delta\tau)$, $\delta\tau_{\text{min}}$:

$$\delta\tau_{\text{min}} = \frac{2\lambda_1\lambda_2}{(\lambda_2 - \lambda_1)c_0} \qquad (157)$$

The factor 2 is introduced in Equation (156) to allow for the fact that two data points in P at and adjacent to zero are generally ignored. For example, for λ_1 = 1 270 nm, λ_2 = 1 700 *nm*, $\delta\tau_{min}$ = 0,033 ps.

For negligible mode coupling, the requirement for spectral averaging described above may be relaxed, and the spectral range reduced (e.g. $(\lambda_2 - \lambda_1)$ ~ 30 nm) in order to allow variation of PMD with wavelength to be examined.

5.5 Interferometric method

The interferometric method (INTY) is based on a broadband light source (BBS) that is linearly polarized and an interferometer at the input or inside of which some form of polarizing analyser is used (see the generic INTY set-up shown in Figure 20). The cross-correlation of the electromagnetic field emerging from the DUT is determined by the interference pattern of the output light, i.e. the interferogram. The determination of the PMD delay for the wavelength range associated with the source spectrum is based on the envelope of the fringe pattern interferogram (see Figure 20). Two analyses are available to obtain the PMD delay:

- a traditional analysis (TINTY) [11,29,30] using a set of specific operating conditions for its successful applications and a basic set-up;
- a general analysis (GINTY) [31] using no limiting operating conditions but in addition to the same basic set-up also using a modified set-up compared to TINTY.

5.5.1 Generic set-up and definitions

Figure 20 provides an example of a generic set-up for INTY with the related definitions.

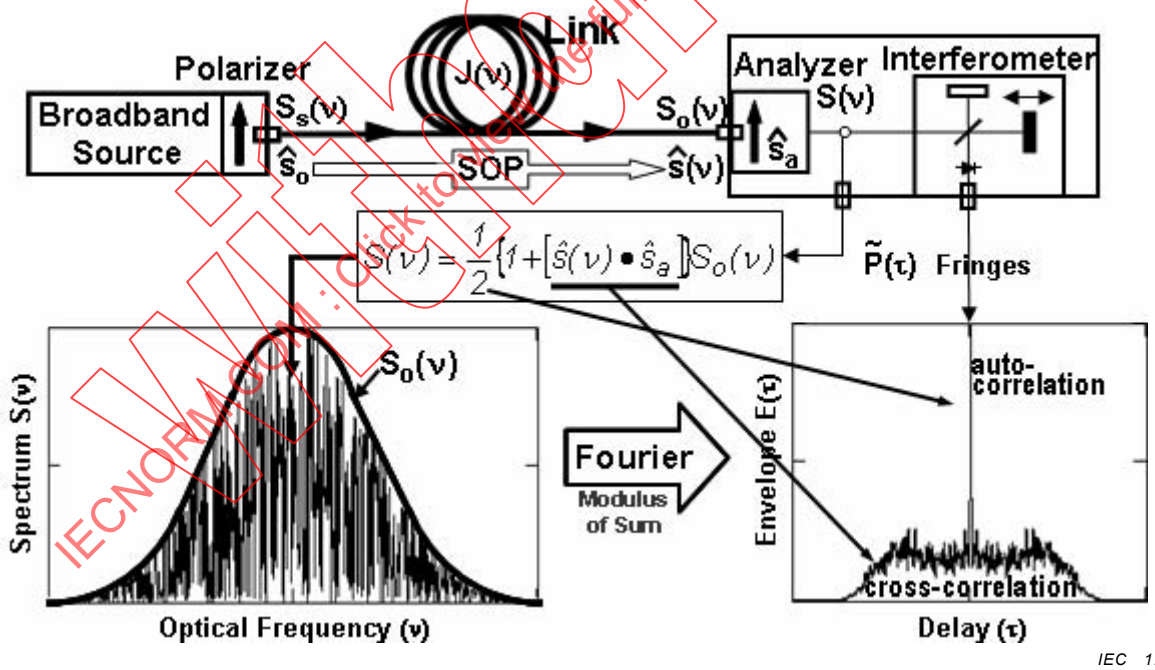

IEC 1269/06

Figure 20 – Generic set-up for the measurement of polarization mode dispersion using the interferometric test method

where

τ is the difference of round-trip delay between the two arms of the interferometer;

$\hat{E}_s(\nu)$ is the complex amplitude of the optical field at DUT input;

$\hat{E}_0(\nu)$ is the complex amplitude of the optical field at DUT output and analyser input;

IECNORM.COM : Click to view the full PDF of IEC TR 61282-9:2006
Withdrawn

$E(\nu)$ is the complex amplitude of the optical field at analyser output and interferometer input;

$\hat{E}_d(\nu,\tau)$ is the complex amplitude of the optical field at interferometer output;

$\hat{s}_0$ is the input SOP (unit Stokes vector) at DUT input;

$\hat{s}(\nu)$ is the DUT output SOP;

$\hat{s}_a$ is the analyser transmission axis;

$x(\nu) \equiv \hat{s}_a \bullet \hat{s}(\nu)$ is the Stokes parameter giving the projection of $\hat{s}(\nu)$ on the analyser axis; it is this $x(\nu)$ parameter that contains the information on PMD;

$S_s(\nu)$ is the DUT input optical spectrum ≡ spectral density of $\hat{E}_s(\nu)$, the source spectrum;

$S_0(\nu)$ is the DUT output optical spectrum (and at the analyser input);

$S(\nu)$ is the analyser output optical spectrum (and at the interferometer input);

$J(\nu)$ is the Jones matrix of the DUT as in Equation (93), so that

$$\hat{E}_0(\nu) = J(\nu) \cdot \hat{E}_s(\nu) \tag{158}$$

NOTE In a single-mode fibre, the DOP is assumed equal to 1.

$P(\tau)$ is the interferometer output optical power, as a function of delay τ;

$\tilde{P}(\tau)$ is the τ-dependent part of $P(\tau)$ ("a.c." part), or $P(\tau)$ minus the τ-independent part ("d.c." part), or the zero-mean oscillating fringes;

$E(\tau)$ is the interferogram envelope, i.e. amplitude or RMS value of the oscillating fringes (AM demodulation); the envelope may also be labelled as "fringes visibility";

$E_0(\tau)$ is the autocorrelation envelope

$E_x(\tau)$ is the cross-correlation envelope defined below.

As illustrated in Figure 20, the analyser transmission, $S(\nu)/S_0(\nu)$, consists of two parts:

- a constant part;
- an SOP-dependent part.

Therefore, the spectrum at the output of the analyser, $S(\nu)$, also consists of two parts, and as a consequence, the interferogram, $\tilde{P}(\tau)$, also consists of these two parts since it is the FT of the spectrum $S(\nu)$. In summary:

- constant part gives:

  autocorrelation ≡ FT of spectrum $S_0(\nu)$ at input of analyser.

- SOP-dependent part:

  cross-correlation ≡ FT of $[\hat{s}(\nu) \bullet \hat{s}_a] S_0(\nu)$.

where

$\hat{s}(\nu)$ is the unit Stokes vector that represents the SOP at the output of the DUT (output-SOP);

$\hat{s}_a$ is the unit Stokes vector that represents the analyser axis.

In all cases, the interferometer must be configured so that orthogonal SOPs can interfere. There are many ways to achieve this.

IECNORM.COM : Click to view the full PDF of IEC TR 61282-9:2006
Withdrawn

A first way is to put a polarizer at the input of the interferometer, as depicted in the generic set-up above. However, if no polarizer is placed at input and both arms of the interferometer have no effect on the SOPs, no cross-correlation interferogram representative of PMD is observed. If no polarizer is set at the interferometer input, something else must be done.

Second, a waveplate in one interferometer arm may be used in case of an air-type interferometer. Generally speaking, the roundtrip in the two interferometer arms of any dual-path interferometer can be represented by Jones matrices J_1 and J_2. This is equivalent to a waveplate with Jones matrix $J = J_1 J_2^+$ in one arm only. In case of a fibre interferometer, a Lefebvre loop may be put in one arm and adjusted until $J = J_1 J_2^+$ gives the desired effect (a given cross-correlation-to-autocorrelation ratio).

One particular case consists of putting a quarter waveplate in one arm of a Michelson interferometer (or a half waveplate in one arm of a Mach-Zehnder interferometer); with this configuration, only the cross-correlation interferogram is observed.

5.5.2 Basic formulation and assumptions

The following subclauses provide the basic formulation and assumptions for the generic INTY application.

5.5.2.1 The device under test

A DUT with no PDL is assumed. In this case, the Jones matrix can be written as,

$$J(\nu) = \exp[z_J(\nu)]\, U(\nu) \tag{159}$$

where

$U(\nu)$ is a unitary matrix, i.e.

$$U^+(\nu)U(\nu) = I \tag{160}$$

z_J is a complex number, i.e.

$$z_J(\nu) = [\alpha_J(\nu) + i\phi_J(\nu)] \tag{161}$$

The complex number z_J represents the mean attenuation and phase shift of the optical field from the DUT input to output, averaged over all possible input SOPs, $\hat{s}_0$. The mirror image of $U(\nu)$ in the Stokes representation is the reduced 3x3 Mueller matrix, $M(\nu)$. The equivalent of the property

$$U^+(\nu)U(\nu) = I \tag{162}$$

is that $M(\nu)$ acts as a pure rotation operator on the Stokes vectors representing the SOP. Therefore, angles between different input SOPs are maintained at the DUT output.

NOTE This property will be useful as follows: if $\hat{s}_0$ is a random variable (such as in the case of I/O SOP scrambling), $\hat{s}(\nu)$ has the same statistical properties as $\hat{s}_0$.

Given the above DUT property, the equation of motion of the output SOP, $\hat{s}(\nu)$, as a function of optical frequency ν is found in Equation (12) replacing ω by ν.

IECNORM.COM : Click to view the full PDF of IEC TR 61282-9:2006
Withdrawn

Also implicitly assumed in:

$$z_J(\nu) = [\alpha_J(\nu) + i\phi_J(\nu)] \tag{163}$$

is that $z_J(\nu)$ is time independent. The derivation can be generalised for a time-dependent $z_J(\nu,t)$; but it is assumed to be time-independent for simplicity.

$M(\nu)$ can also be time dependent. A time-dependent $M(\nu)$ represents an unstable DUT. It is also assumed time-independent here for simplicity. However, the results can be generalised to take this time-dependence into account: basically, a time-dependent $M(\nu)$ have the same effect as I/O-SOP scrambling, and if the PMD to be measured is itself unstable, the result will simply be the average over the time of the measurement.

5.5.2.2 Representation of a broadband source

In order to successfully apply TINTY analysis, the BBS spectral shape is required to be approximately Gaussian, without ripples that could influence the autocorrelation function of the emerging light. GINTY does not require such characteristics: any shape can be used. The BBS used is assumed having no deterministic amplitude or phase modulation, as for example a periodic modulation. Mathematically, the required condition is the following: the optical field $\hat{E}_s(t)$ emitted by the source (DOP = 1) is a random process which autocorrelation is time independent. Then the autocorrelation and the spectrum can be expressed as follows:

- autocorrelation (time independent):

$$R_s(\tau) = \left\langle \hat{E}_s(t) \bullet \hat{E}_s^*(t-\tau) \right\rangle \tag{164}$$

- spectrum:

$$S_s(\nu) = \int_\nu R_s(\tau) \exp(-i2\pi\nu\tau) \tag{165}$$

NOTE The autocorrelation and the spectrum are an FT pair:

$$R_E(\tau) = \int_\nu S_s(\nu) \exp(i2\pi\nu\tau) \leftrightarrow S_s(\nu) = \int_\nu R_E(\tau) \exp(-i2\pi\nu\tau) \tag{166}$$

In the remainder of this document:

$$\int_z f(z) = \int_{-\infty}^{\infty} f(z)dz \tag{167}$$

The DUT is also assumed not affecting this property, so that, in the same way,

$$R_0(\tau) = \left\langle \hat{E}_0(t) \bullet \hat{E}_0^*(t-\tau) \right\rangle \tag{168}$$

$$R(\tau) = \left\langle \hat{E}(t) \bullet \hat{E}^*(t-\tau) \right\rangle \tag{169}$$

$$R_0(\tau) = \int_\nu S_0(\nu) \exp(i2\pi\nu\tau) \leftrightarrow S_0(\nu) = \int_\nu R_0(\tau) \exp(-i2\pi\nu\tau) \tag{170}$$

$$R(\tau) = \int_\nu S(\nu) \exp(i2\pi\nu\tau) \leftrightarrow S(\nu) = \int_\nu R(\tau) \exp(-i2\pi\nu\tau) \tag{171}$$

IECNORM.COM : Click to view the full PDF of IEC TR 61282-9:2006
Withdrawn

5.5.2.3 General expression of the auto- and cross-correlation envelopes

The raw interferogram, $P(\tau)$, is proportional to the optical power at the interferometer output as a function of delay τ. Given the definitions and basic assumptions provided in the previous clauses, the τ-dependent part of the interferogram, $\tilde{P}(\tau)$, is given by

$$\tilde{P}(\tau) = R(\tau) = \int_{\nu} S(\nu) \exp(i2\pi\nu\tau) \tag{172}$$

where $S(\nu)$ is the spectrum at analyser output and interferometer input.

On the other hand, the transmission of the analyser can be written

$$\frac{S(\nu)}{S_0(\nu)} = \frac{1}{2}\left(1 + \mathrm{x}(\nu)\right) \tag{173}$$

where $x(\nu) \equiv \hat{s}_a \bullet \hat{s}(\nu)$ is the projection of $\hat{s}(\nu)$ onto the analyser axis $\hat{s}_a$.

Thus $S(\nu)$ can also be written as:

$$S(\nu) = \frac{1}{2}\left[S_0(\nu) + S_x(\nu)\right] \tag{174}$$

where

$$S_x(\nu) \equiv x(\nu)\, S_0(\nu) \tag{175}$$

Therefore

$$\tilde{P}(\tau) = R_0(\tau) + R_x(\tau) \tag{176}$$

where

$$R_0(\tau) = \int_{\nu} S_0(\nu) \exp(i2\pi\nu\tau) \tag{177}$$

$$R_x(\tau) = \int_{\nu} S_x(\nu) \exp(i2\pi\nu\tau) \tag{178}$$

Since $\tilde{P}(\tau)$ is complex, its amplitude or envelope is represented by its modulus, as follows:

$$E(\tau) = \left| R_0(\tau) + R_x(\tau) \right| \tag{179}$$

NOTE 1 $|R_0(\tau)|$ and $|R_x(\tau)|$ are respectively the autocorrrelation and cross-correlation envelopes, such as:

- the autocorrrelation envelope is

$$E_0(\tau) = \left| R_0(\tau) \right| \tag{180}$$

- the cross-correlation envelope is

$$E_x(\tau) = \left| R_x(\tau) \right| \tag{181}$$

IECNORM.COM : Click to view the full PDF of IEC TR 61282-9:2006
Withdrawn

NOTE 2 The overall envelope $E(\tau)$ in Equation (179) is not the sum of the modulus but the modulus of the sum: that the two interferograms interfere; the envelope is not the sum of the two envelopes.

NOTE 3 $S_x(\nu)$ represents the zero-mean fluctuations of the output spectrum related to the fluctuations of the output SOP, i.e. related to PMD. Its ensemble, statistical average is zero.

NOTE 4 The variance σ_0^2 of the autocorrelation envelope can be written as a function of the output spectrum as follows:

$$\sigma_0^2 = \frac{\int_\tau \tau^2 |R_0(\tau)|^2}{\int_\tau |R_0(\tau)|^2} = \frac{\int_\nu \left(\frac{d}{d\omega} S_0(\nu)\right)^2}{\int_\nu S_0^2(\nu)} \quad (182)$$

(See Annex D: "Generalised Parseval theorem".)

5.5.2.4 Statistical properties related to input/output state-of-polarization scrambling

Ensemble averages may be performed over all possible occurrences of the random variables $\hat{s}_0$ and $\hat{s}_a$. The ensemble averages will be represented by brackets $\langle\ \rangle$.

$\hat{s}_0$ and $\hat{s}_a$ are assumed to be independent random variables, representing uniformly distributed SOPs on the Poincaré sphere. Mathematically, this is related to

- correlation:

$$\langle \hat{s}_a \bullet \hat{s}_0 \rangle = 0 \quad (183)$$

- PDF:

$$f_{s0}(s_{0q}) = f_{sa}(s_{aq}) = \frac{1}{2} \text{ for } -1 \le s_{0q}, s_{aq} \le 1 \quad (184)$$

where

$$q = 1..3 \quad (185)$$

$$f_{s0}(s_{0q}) = f_{sa}(s_{aq}) = 0 \quad (186)$$

elsewhere.

5.5.2.4.1 Corollaries related to input/output state-of-polarization scrambling

Since $M(\nu)$ acts as a rotation of the Stokes vectors, $\hat{s}(\nu) = M(\nu)\hat{s}_0$ has the same statistical properties as $\hat{s}_0$, i.e.

$$\langle x(\nu) \rangle = \langle \hat{s}_a \bullet \hat{s}(\nu) \rangle = 0 \qquad f_s(s_q) = \frac{1}{2} \quad (187)$$

for $-1 \le s_q \le 1$.

Given the above relations, it can be shown that

$$\langle s_q \bullet s_{q'} \rangle = \langle s_{aq} \bullet s_{aq'} \rangle = \frac{1}{3}\delta_{q,q'} \quad (188)$$

IECNORM.COM : Click to view the full PDF of IEC TR 61282-9:2006
Withdrawn

The different Stokes parameters are uncorrelated

$$\left\langle \frac{d}{d\omega}\hat{s}(\nu)\right\rangle = \hat{\Omega}(\nu)\times\left\langle \hat{s}(\nu)\right\rangle = 0 \tag{189}$$

$$\left\langle x^2(\nu)\right\rangle = \frac{1}{3} \tag{190}$$

$$\left\langle \frac{d}{d\omega}x(\nu)\right\rangle = \left\langle \hat{s}_a \bullet \frac{\mathrm{d}}{\mathrm{d}\omega}\hat{s}(\nu)\right\rangle = 0 \tag{191}$$

(192)

$$\int_\nu \left\langle \mathrm{S}_x^2(\nu)\right\rangle = \int_\nu \left\langle x^2(\nu)\right\rangle \mathrm{S}_0^2(\nu) = \frac{1}{3}\int_\nu \mathrm{S}_0^2(\nu) \tag{193}$$

These different corollaries will prove useful in the GINTY calculations below.

5.5.2.4.2 Implementation of input/output state-of-polarization scrambling

When GINTY or TINTY analysis is performed using the set-up shown in Figure 20, a single envelope is obtained (a squared envelope in case of GINTY), corresponding to a single I/O-SOP combination and a single interferometer scan. When GINTY or TINTY analysis is performed using the set-up shown in Figure 21, an ensemble of I/O-SOP combinations is obtained in conjunction with the following:

- for GINTY, both autocorrelation and cross-correlation interferograms are obtained separately;
- the envelopes (squared for GINTY) are averaged over the ensemble of I/O-SOP combinations. In this case, a mean envelope (mean-squared for GINTY) is obtained and a dramatic improvement over the uncertainty is obtained (see single-scan uncertainty below).

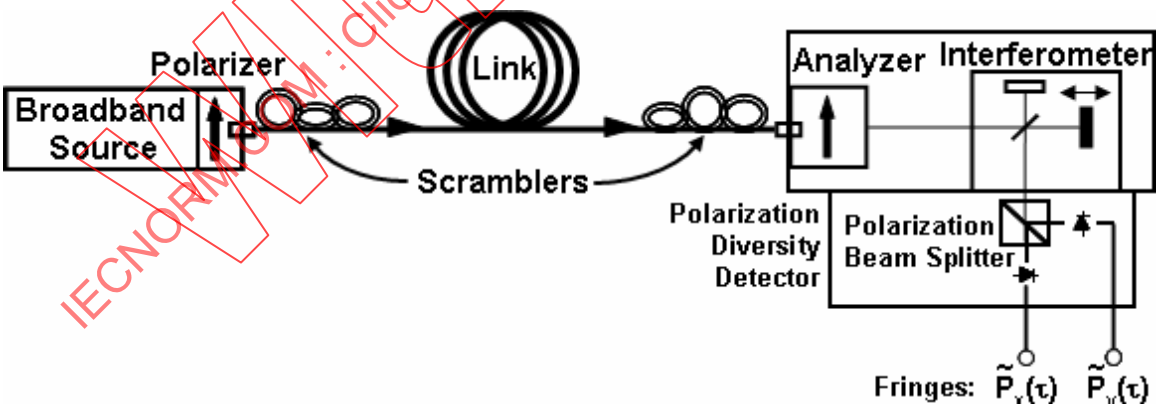

IEC 1270/06

Figure 21 – Schematic diagram for GINTY analysis using input/output state-of-polarization scrambling

Physically, SOP scrambling consists of inserting controllable polarization scramblers or controllers, one at the input and one at the output of the DUT, so that different input-SOPs and analyser axes (output SOP) are set for an interferometer scan. Multiple I/O SOPs can be selected to obtain a more complete interferometric envelope, the mean-squared envelope, than would be possible for a single I/O-SOP setting. While a measurement obtained from a single setting is an option, doing multiple settings will improve the accuracy of the result. Conceptually, the scrambling process can be viewed as follows:

IECNORM.COM : Click to view the full PDF of IEC TR 61282-9:2006
Withdrawn

- the input polarizer followed by the scrambler acts as a single unit, an equivalent elliptical polarizer whose axis is set at any point on the Poincaré sphere in order to define the input SOP;
- the scrambler followed by the polarization beam splitter (PBS)/analyser acts as an equivalent elliptical analyser whose axis is set at any point on the sphere in order to define the output SOP.

One set of input-SOP/analyser-axis combination will be labelled as one I/O SOP. The aim is to get the mean envelope (mean-squared for GINTY) averaged over uniformly distributed I/O SOPs. In practice, there exist a number of possible ways to achieve this goal, as shown below:

a) the 9-states Mueller set

The sum of nine envelopes (squared for GINTY) observed with nine specific I/O SOPs is rigorously equal to the uniformly scrambled mean envelope (mean-squared for GINTY). These nine I/O SOPs are: three analyser axes forming a right-angled trihedron, for each three input SOPs also forming a right-angled trihedron.

b) uniform grid

If the necessary hardware is available (waveplates, loops, etc.), I/O-SOP scrambling may also be performed using a uniformly-spaced grid on the Poincaré sphere. An example of results obtained with such uniformly-spaced grid is shown in Figure 22. The GINTY mean-squared envelope was obtained with 96 I/O-SOP combinations.

c) random scrambling

Random scrambling may be accomplished using the following techniques:

- scan-to-scan scrambling: automatic/manual setting of the scramblers at each scan;
- continuous scrambling: when envelopes (squared for GINTY) are summed, scrambling can be performed while scanning. Automated scramblers are set to cover the sphere continuously as a function of time;
- fast, single-scan scrambling: if scramblers are sufficiently fast, well-scrambled envelopes (squared for GINTY) can be observed in a single-scan. However, this requires special provisions to avoid crosstalk between the a.c. part and the previously d.c. part of the interferogram.

Continuous scrambling while scanning is by far preferable and easier to implement in the field, for instance, because good scrambling is achieved easily and in a much shorter time.

When the DUT is itself very unstable, as is often the case with links having aerial sections, the DUT is also providing "self-scrambling" in addition to the intentional scrambling with the I/O scramblers. In this case, the reduction of the uncertainty is even better, but obviously, specifying by exactly how much (factor 100 or 200) demands that the fluctuations of the link be characterised as well as the characteristics of the scramblers.

The critical parameter is the "scrambling bandwidth." It can be determined for given scramblers by launching a polarized input, with a polarizer at the scramblers output, and looking at the transmitted power with an OSA, or by sampling and Fourier transforming (with a digital oscilloscope for example). Typically, the transmitted power is a band-limited white noise (i.e. as white noise passed through a lowpass filter). The ratio between this bandwidth and (v/c) times (spectral width of the optical spectrum) says it all, i.e. gives the accuracy improvement factor over N scan-to-scan settings. But beforehand, the scramblers must be known or measured/characterised.

IECNORM.COM : Click to view the full PDF of IEC TR 61282-9:2006
Withdrawn

5.5.2.4.2.1 Polarization beam splitter

A PBS may be used to obtain interferograms from output states that are orthogonal (opposite on the Poincaré sphere) for the same I/O-SOP combination. These two interferograms allow the calculation of the autocorrelation and cross-correlation as separate functions. Together with the detection system, the PBS forms a polarization diversity detection system. Means other than the PBS may be used to obtain these interferograms from orthogonal output states.

Any interferogram can be basically represented by a weighted sum of two interferograms obtained with the generic set-up (INTY), more precisely, two interferograms observed with two orthogonal analyser-axes (opposite on the Poincaré sphere). Thus, whatever the actual means for separately providing both autocorrrelation and cross-correlation, they are basically given by the following expressions:

- autocorrrelation envelope for a single I/O SOP:

$$E_0(\tau) = \left|\tilde{P}_x(\tau) + \tilde{P}_y(\tau)\right| \quad (194)$$

The squared envelope being $E_0^2(\tau)$ for a single I/O SOP and the mean-squared envelope being $\left\langle E_0^2(\tau)\right\rangle$ for an ensemble of I/O-SOP combinations (I/O-SOP scrambling);

- cross-correlation envelope for a single I/O SOP:

$$E_x(\tau) = \left|\tilde{P}_x(\tau) - \tilde{P}_y(\tau)\right| \quad (195)$$

The squared envelope being $E_x^2(\tau)$ for a single I/O-SOP and the mean-squared envelope being $\left\langle E_x^2(\tau)\right\rangle$ for an ensemble of I/O-SOP combinations (I/O-SOP scrambling)

where $P_x(\tau)$ and $P_y(\tau)$ are the raw interferograms observed (directly or indirectly) along two orthogonal analyser-axes for a single I/O-SOP combination.

Raw interferograms consist of a d.c. part (independent of delay τ), and an a.c. part (zero-mean fringes oscillating as a function of τ). In Equations (194) and (195), $\tilde{P}_x(\tau)$ and $\tilde{P}_y(\tau)$ represent the a.c. parts of their respective raw interferograms.

5.5.2.4.3 Single-scan versus input/output state-of-polarization scrambling uncertainty

A single-scan measurement (a single I/O-SOP combination) has a greater uncertainty than if no I/O-SOP scrambling is performed. This is true and applicable if either TINTY or GINTY is used, independent of the stability of the device or DUT.

This uncertainty has nothing to do with the statistical nature of PMD. It is a procedural uncertainty due to the fact that a single I/O SOP combination gives only partial, basically insufficient information, however absolutely perfect the actual instrument may be (it is not an instrumental uncertainty; it is neither "noise," nor instrument instability nor imperfection). The distribution of single-scan, single I/O-SOP results obtained with a set of distinct I/O SOPs (single-scan statistics) has nothing to do with the distribution of DGDs, for example. It is not "PMD statistics," it is procedural, single-scan statistics. Multiple I/O SOPs or scrambling must be used to retrieve complete information that will dramatically reduce uncertainty compared to single-scan uncertainty.

IECNORM.COM : Click to view the full PDF of IEC TR 61282-9:2006
Withdrawn

Generally speaking, unless very large PMD values in the ns range are measured, single-scan uncertainly is overwhelmingly larger than any other uncertainty from other causes, but:

- this is not INTY uncertainty;
- it is single-scan, single I/O-SOP uncertainty, which can be virtually eliminated via I/O-SOP scrambling. One sees the "PMD" dramatically changing when "moving the patchcord." No more of that with I/O-SOP scrambling.

The GINTY analysis yields the RMS result that is rigorously equivalent to the result that is obtained from reporting the RMS metric from the Stokes parameter evaluation (SPE) method. It does not, however, report the average DGD (which may be specified), but must be linked to this metric by way of assuming a Maxwell distribution. It means that, at any given time, the RMS DGD within a given spectral window is a deterministic value.

5.5.2.4.3.1 Expression of the mean single-scan uncertainty

In the general case,

$$\frac{\sigma_{Single}}{PMD} = \sqrt{\frac{1-\frac{8}{3\pi}}{1+\frac{1}{4}\left(\frac{PMD}{\sigma_A}\right)^2}} \tag{196}$$

In the asymptotic case, when $PMD >> \sigma_A$,

$$\frac{\sigma_{Single}}{PMD} \sim b\sqrt{\frac{\sigma_A}{PMD}} \tag{197}$$

where

$$b = \sqrt{2\left(1-\frac{8}{3\pi}\right)} \sim 0{,}55 \tag{198}$$

σ_A is the RMS width of the autocorrelation envelope.

An example is shown in Figure 22, where 1-ps PMD emulator is used consisting of 10 concatenated segments of PMF. The segments are spliced with their axes at ~ 45 °. The autocorrelation and cross-correlation envelopes are measured with 96 I/O SOPs performing a SOP matrix equally and uniformly spaced, simulating a complete covering of the Poincaré sphere. The autocorrelation and cross-correlation mean-square envelopes are obtained by simply adding the 96 square envelopes (each normalised to total input power, i.e. maximum of the autocorrelation envelope, in case the total power changes with time).

IECNORM.COM : Click to view the full PDF of IEC TR 61282-9:2006
Withdrawn

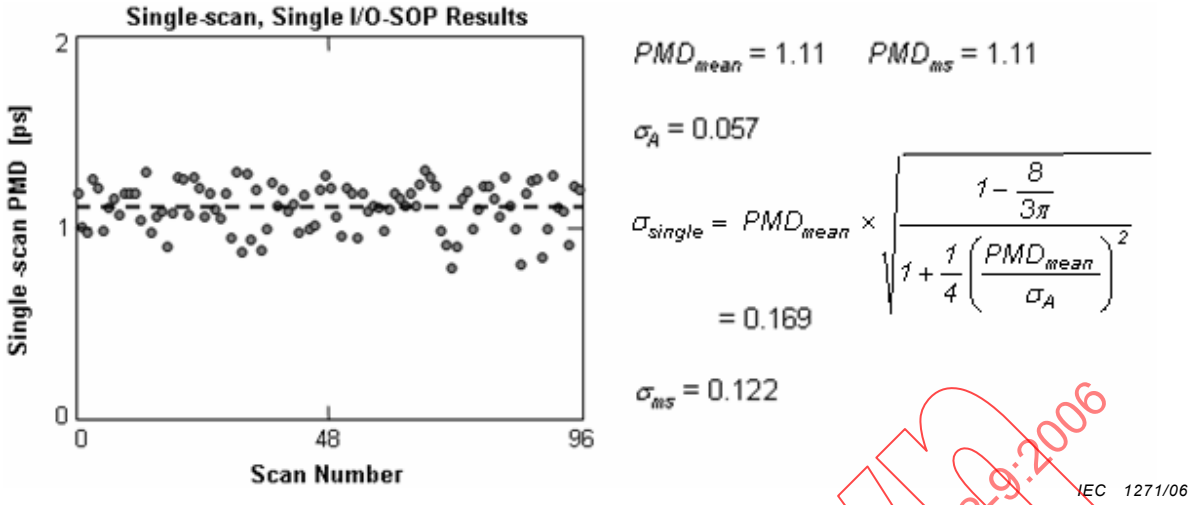

Figure 22 – Comparison between single-scan and scrambling uncertainties

5.5.2.4.3.2 Uncertainty with input/output state-of-polarization scrambling

In the case of scan-to-scan scrambling, the uncertainty after averaging is decreased by the following factor:

- $1/\sqrt{N}$ when using random scrambling;
- $\sim 1/N$ with I/O SOPs distributed over a uniformly-spaced grid on the Poincaré sphere.

Basic uncertainty is reduced to nothing with the 9-states Mueller set described above. However, this is assuming that the DUT is stable. If the DUT is unstable, the ideal averaging provided by the 9-states Mueller set is impaired. On the other hand, the fact that the DUT is unstable is equivalent to providing "self-scrambling."

Continuous scrambling, random or deterministic, can also be precisely characterised, but this discussion will be skipped in the present document. In the general case, especially for outside plant applications where the DUT cannot be assumed stable, continuous scrambling is the best solution and provides an almost ideal scrambling with a reasonable number of scans.

In any case, a reasonably good, well-done, systematic scrambling, performed according to the considerations described in this document, easily and dramatically reduces the basic uncertainty by a factor of 10 to100, towards the noise floor where instrumental imperfections may finally come into play.

5.5.3 Determination of polarization mode dispersion

The following subclauses describe the mathematical formulation for the determination of PMD for TINTY and GINTY in different cases of mode coupling.

5.5.3.1 Negligible mode coupling

In the case of negligible mode coupling, the PMD delay is determined in the same way for TINTY and GINTY: from the separation of the two satellite coherence peaks, each delayed from the centre by the DGD of the DUT, as shown, for example, in Figure 23.

IECNORM.COM : Click to view the full PDF of IEC TR 61282-9:2006
Withdrawn

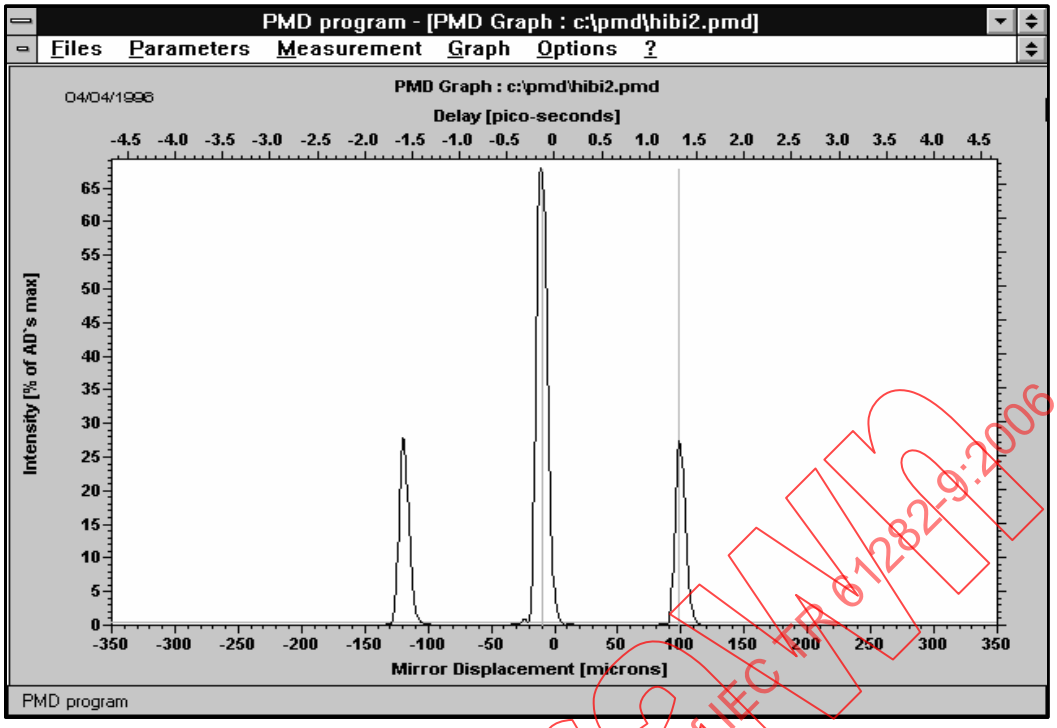

IEC 1272/06

a) With a polarization maintaining fibre and one I/O SOP)

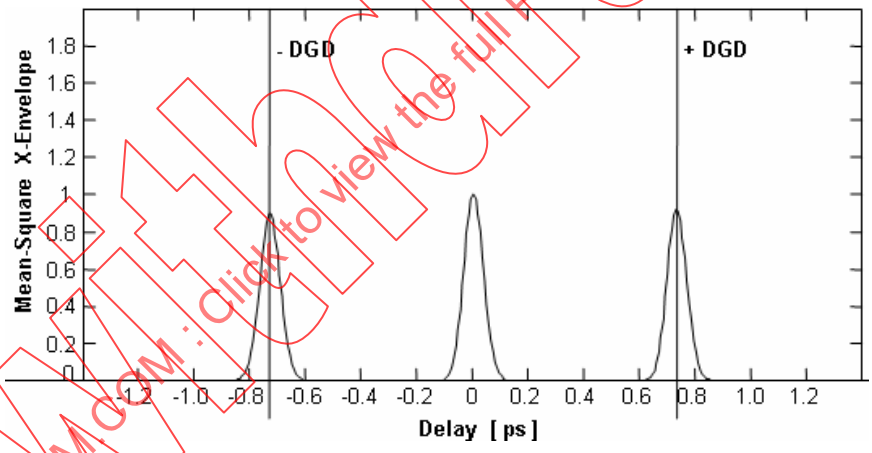

IEC 1273/06

b) With I/O-SOP scrambling (L/h << 1, DGD = 0,732 ps, σ_A = 50 fs, DGD/σ_A ~ 14,7)

Figure 23 – Example of negligible-mode-coupling result using a) TINTY analysis and b) GINTY analysis

In this case, the DGD is equivalent to the PMD delay:

$$PMD = <\Delta\tau> = \frac{2\Delta L}{c_0} \tag{199}$$

where

ΔL is the moving path of the optical delay line between the two satellite coherence peaks;

c_0 is the light velocity in free space.

$<\Delta\tau>$ in Equation (199) is typically quoted in units of ps. The PMD coefficient is given by $<\Delta\tau>/L$, where L is the DUT length (such as a fibre length) in km.

IECNORM.COM : Click to view the full PDF of IEC TR 61282-9:2006
Withdrawn

5.5.3.1.1 Random mode coupling

In the case of random mode coupling, TINTY and GINTY diverge in their analysis and results depending on their assumptions, as described below.

5.5.3.1.1.1 Traditional analysis

In the case of random mode coupling using TINTY, the determination of the PMD delay is based on the envelope of the fringe pattern interferogram. An example of such an interferogram is shown in Figure 24.

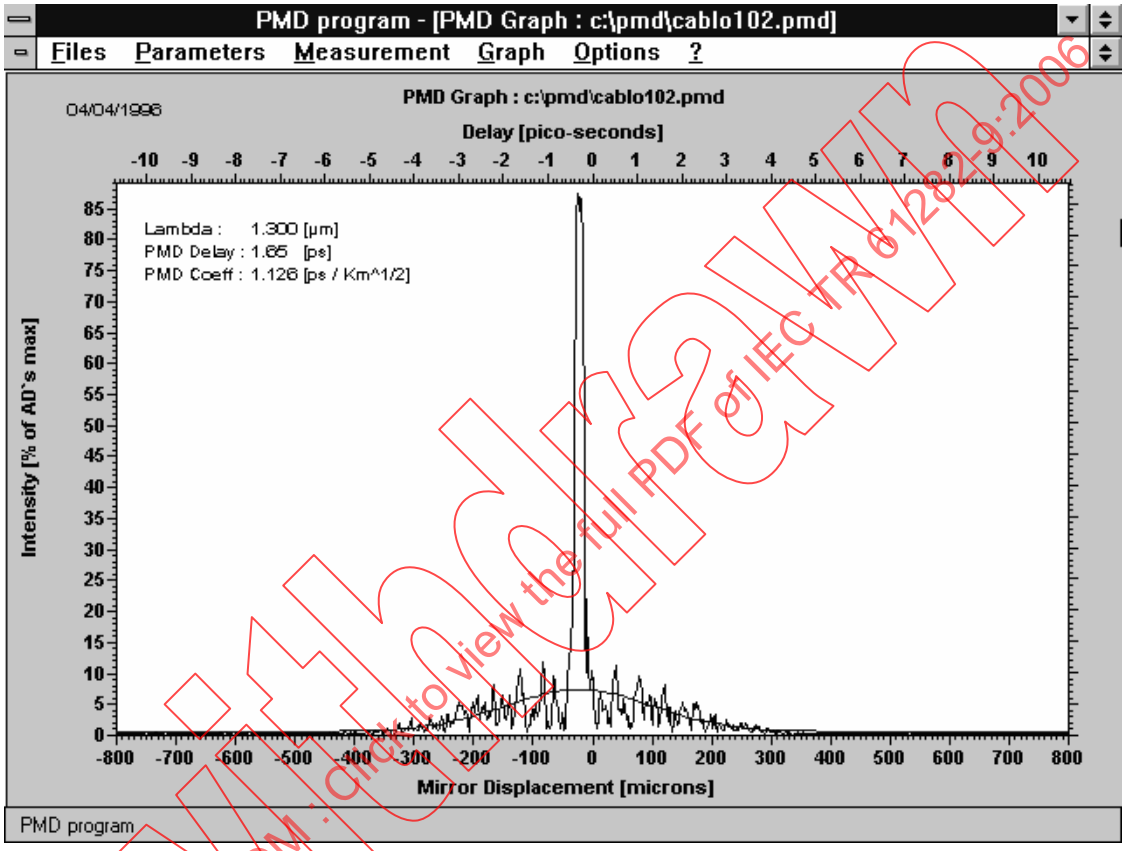

IEC 1274/06

Figure 24 – Example of random-mode-coupling result using TINTY analysis

The PMD delay $<\Delta\tau^2>^{1/2}$ is determined from the second moment (RMS width) of the cross-correlation interferogram:

$$<\Delta\tau^2>^{1/2} = \left(\sqrt{\frac{3}{4}}\right)\sigma_\varepsilon \qquad (200)$$

where σ_ε is the RMS width of the cross-correlation envelope.

$<\Delta\tau^2>^{1/2}$ in Equation (200) is typically quoted in units of ps. The PMD coefficient is given by $<\Delta\tau^2>^{1/2}/\sqrt{L}$, where L is the DUT length (such as a fibre length) in km. Equation (200) applies to a RMS DGD definition; a different coefficient may be necessary for an average DGD definition.

Equation (200) is obtained from the theory [11,29,30] given the following assumptions. These are generally true for testing typical installed fibre links using modern commercially available test equipment.

IECNORM.COM : Click to view the full PDF of IEC TR 61282-9:2006
Withdrawn

- random mode coupling (installed optical fibre cable sections greater than 10 km will generally exhibit random mode coupling);

  NOTE 1 Ideal random coupling means $L/h \to \infty$, and a uniformly distributed birefringence axis. L is the device length, and h is the polarization coupling-length. For a device consisting of N concatenated birefringent segments of length h, this corresponds to $N \to \infty$ with uniformly distributed axes.

  NOTE 2 Analysis of no or negligible mode coupling is possible.

- a Gaussian interferogram;
- PMD >> σ_A;
- Equation (200) is a statistical RMS DGD, not a wavelength average;

  NOTE 3 A conceptual, statistical RMS DGD is assumed to be measured, not a well-defined average over a finite wavelength range. Thus, Equation (200), obtained through TINTY, is not exactly equivalent to DGD measurements over a finite wavelength range.

  NOTE 4 In the case of a statistical RMS DGD, the DGD is considered as a local random variable at each given wavelength value. Averages are not performed over wavelength but over all possible occurrences of the conceptual random variables. For this to represent the reality of a measurement, i.e. some kind of wavelength average, the statistical properties (mean, variance, PDF) of the locally random DGDs are assumed to be wavelength-independent, and that wavelength and time averages are equal to the wavelength-independent local averages (ergodicity). As long as the envelope itself is analysed, no formulas such as Equation (183) can be obtained if assumed otherwise.

  NOTE 5 When considering a wavelength average, DGDs outside the source spectrum do not obviously contribute to the average when performing a measurement. But typical spectra are not rectangular windows. In other words, how the average (RMS DGD) is actually weighted by the spectrum is not specified in the traditional analysis. Because in order for Equation (200) to be obtained, we are supposed to measure a local statistical-mean assumed to be wavelength-independent; not an average of the concrete DGD(λ), locally deterministic at a given time. Averaging a constant over wavelength is assumed, therefore any weighting is irrelevant in this context and thus remains unspecified. No wavelength averaging is needed to obtain Equation (200). The theory does not assume and never assumed "uniform averaging within a finite range;" it assumes that the observed interferogram is an average over all possible DUTs with the same conceptual PMD, which gives the equivalent of having a uniform DGD, not a uniform averaging of the actual DGD of a single DUT. The theory never mentioned what is supposed to be the weighting with TINTY or even that there is a weighting, because there is in fact a weighting. The theory had forgotten to specify it.

- analysed envelope = unrealisable average;

  NOTE 6 Equivalent to averaging over all possible DUTs with the same conceptual PMD; this is performed through averaging as described in Note 4.

  NOTE 7 Even if $L/h \to \infty$, a real, single DUT gives a "noisy" envelope even if overall Gaussian-shaped: a pure Gaussian is obtained only if averages are preformed as described in Note 4.

- smooth spectrum: notably with no large, fast ripples (peaks in the interferogram).

Equation (200) applies to a RMS PMD definition. Equation (201) applies to the linear average PMD definition under the assumption that the DGD values are distributed with a Maxwell probability density function.

$$< \Delta\tau > = \left(\frac{8}{3\pi} \right)^{1/2} < \Delta\tau^2 >^{1/2} \qquad (201)$$

The following gives an example of an algorithm to determine the PMD delay $<\Delta\tau^2>^{1/2}$ from an interferogram. Other algorithms are possible for instance based on cumulative integration.

Let $\tilde{I}_j$ denote the measured intensity of the interferogram at increasing positions, t_j, in ps, with j = 1…N.

Step 1: computation of the zero intensity $\tilde{I}_0$ and the noise amplitude Na

Definition: N_s = round (5 N/100) is the integer at which is $\tilde{I}_j$ approximately 5 %.

IECNORM.COM : Click to view the full PDF of IEC TR 61282-9:2006
Withdrawn

$$\tilde{I}_0 = \frac{\sum_{j=1}^{N_S}\left(\tilde{I}_j + \tilde{I}_{N_S-j}\right)}{2N_S} \tag{202}$$

$$X_2 = \frac{\sum_{j=1}^{N_S}\left(\tilde{I}_j^2 + \tilde{I}_{N_S-j}^2\right)}{2N_S} \tag{203}$$

$$Na = \sqrt{X_2 - \tilde{I}_0^2} \tag{204}$$

Step 2: definition of the shifted intensity, I_j

$$I_j = \tilde{I}_j - \tilde{I}_0 \qquad \text{if } \tilde{I}_j - \tilde{I}_0 > 4\text{Na} \tag{205}$$

$$I_j = 0 \qquad \text{if } \tilde{I}_j - \tilde{I}_0 \leq 4\text{Na} \tag{206}$$

Step 3: computation of the centre, C, of the interferogram

$$C = \frac{\sum_{j=1}^{N_s} t_j I_j}{\sum_{j=1}^{N_s} I_j} \tag{207}$$

Step 4: removal of the autocorrelation peak

Definition:

j_l = the largest index j so that $C - t_j > \tau_c$ (208)

j_r = the smallest index j so that $t_j - C > \tau_c$ (209)

where τ_c is the source coherence time.

NOTE For cross-correlation interferograms, the following definition is to be applied:

$$j_r = j_l + 1 \tag{210}$$

Step 5: Computation of the second moment S of the interferogram

$$S = \frac{1}{2}\left\{\sqrt{\frac{\sum_{j=1}^{j_l}(t_j - C)^2 I_j}{\sum_{j=1}^{j_l} I_j}} + \sqrt{\frac{\sum_{j=j_r}^{N}(t_j - C)^2 I_j}{\sum_{j=j_r}^{N} I_j}}\right\} \tag{211}$$

Step 6: Truncate the interferogram

- Set $j_{\min}$ to the largest index j so that $C - t_j > 2S$
- Set $j_{\max}$ to the smallest index j so that $t_j - C > 2S$

IECNORM.COM : Click to view the full PDF of IEC TR 61282-9:2006
Withdrawn

Step 7: Computation of the second moment σ_ε of the interferogram

$$\sigma_\varepsilon = \frac{1}{2}\left\{\sqrt{\frac{\sum_{j=j_{min}}^{j_l}(t_j - C)^2 I_j}{\sum_{j=j_{min}}^{j_l} I_j}} + \sqrt{\frac{\sum_{j=j_r}^{j_{max}}(t_j - C)^2 I_j}{\sum_{j=j_r}^{j_{max}} I_j}}\right\} \quad (212)$$

Step 8: Computation of the σ_ε of the Gaussian $e^{-\frac{(t-C)^2}{2\sigma^2}}$ so that

$$\sigma_\varepsilon = \frac{1}{2}\left\{\sqrt{\frac{\int_{t_{j_{min}}}^{t_{j_l}}(t-C)^2 e^{-\frac{(t-C)^2}{2\sigma^2}}dt}{\int_{t_{j_{min}}}^{t_{j_l}} e^{-\frac{(t-C)^2}{2\sigma^2}}dt}} + \sqrt{\frac{\int_{t_{j_r}}^{t_{j_{max}}}(t-C)^2 e^{-\frac{(t-C)^2}{2\sigma^2}}dt}{\int_{t_{j_r}}^{t_{j_{max}}} e^{-\frac{(t-C)^2}{2\sigma^2}}dt}}\right\} \quad (213)$$

σ is computed by iteration from Equation (213) and PMD is computed from Equation (200).

5.5.3.1.1.2 General analysis

The determination of PMD obtained by the GINTY analysis is based on the square envelopes of the cross-correlation and autocorrelation interferograms. This determination may be obtained in any mode coupling regime or with any spectral shape characteristic at the receiver. This means that it can be used to measure links with amplifiers.

The envelopes, $E_0(\tau)$ and $E_x(\tau)$, are first formed for instance from Equations (194) and (195), from the raw interferograms and a single I/O-SOP combination.

Second, the squared envelopes $E_0^2(\tau)$ and $E_x^2(\tau)$ are then computed.

Third, for a single I/O-SOP combination, the PMD is calculated from the following:

$$\langle \Delta\tau^2 \rangle^{1/2} = \sqrt{\frac{3}{2}\left(\sigma_x^2 - \sigma_0^2\right)} \quad (214)$$

where

σ_0 is the RMS width of the squared envelope $E_0^2(\tau)$ of the autocorrelation interferogram;

σ_x is the RMS width of the squared envelope $E_x^2(\tau)$ of the cross-correlation interferogram;

both being defined as:

$$\sigma_0^2 = \frac{\int_\tau \tau^2 E_0^2(\tau)d\tau}{\int_\tau E_0^2(\tau)d\tau} \quad (215)$$

IECNORM.COM : Click to view the full PDF of IEC TR 61282-9:2006
Withdrawn

$$\sigma_x^2 = \frac{\int_\tau \tau^2 E_x^2(\tau) d\tau}{\int_\tau E_x^2(\tau) d\tau} \tag{216}$$

In case an ensemble of I/O-SOP combinations (I/O-SOP scrambling) is used, the first step (getting the $E_0(\tau)$ and $E_x(\tau)$ envelopes) and the second step (getting the $E_0^2(\tau)$ and $E_x^2(\tau)$ squared envelopes) above are performed for each I/O-SOP combination. It is important to make sure that the ensemble used be representative of sufficient coverage of the Poincaré sphere.

The mean-squared envelopes $\langle E_0^2(\tau) \rangle$ and $\langle E_x^2(\tau) \rangle$ are then formed, and the PMD is computed using Equation (214), where this time,

σ_0 is t RMS width of the mean-squared envelope $\langle E_x^2(\tau) \rangle$ of the cross-correlation interferogram.

Both are defined as:

$$\sigma_0^2 = \frac{\int_\tau \tau^2 \langle E_0^2(\tau) \rangle d\tau}{\int_\tau \langle E_0^2(\tau) \rangle d\tau} \tag{217}$$

$$\sigma_x^2 = \frac{\int_\tau \tau^2 \langle E_x^2(\tau) \rangle d\tau}{\int_\tau \langle E_x^2(\tau) \rangle d\tau} \tag{218}$$

An example of a test result is provided in Figure 25 for random mode coupling (L/h = 100 and PMD/σ_A ~ 100; PMD = 4,94 ps, σ_A = 50 fs; still not "ideal", but nearly-Gaussian smoothed envelope; smoothing is for guiding the eye only: analysis is not performed on any kind of fit).

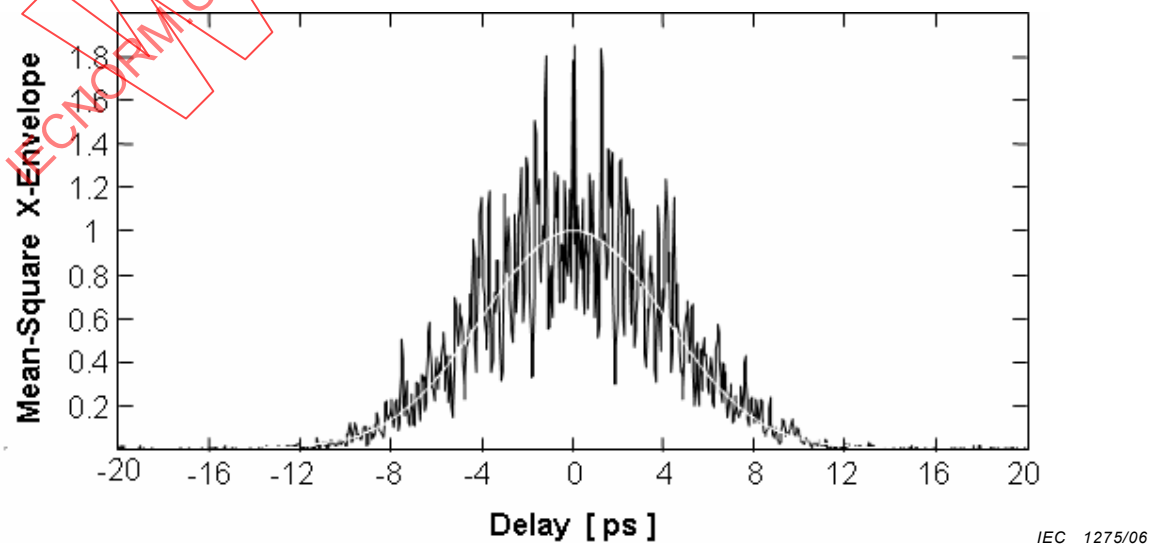

Figure 25 – Example of random-mode-coupling result using GINTY analysis with I/O-SOP scrambling

IECNORM.COM : Click to view the full PDF of IEC TR 61282-9:2006
Withdrawn

The RMS widths, σ_x and $\sigma_{0,}$ of these envelopes can be obtained using an algorithm such as the one described below.

Equation (214) is obtained from the theory [31] given the following enhancement features (notably):

- mean squared envelope = realisable average from I/O-SOP scrambling;
- basically exact for any mode coupling: 1, 2,...,N-segment DUT, anything;
- basically exact for any interferogram shape: no exception;
- same result as Equation (200) if TINTY assumptions are met as defined in 5.5.3.1.1;
- result from mean squared envelope exactly equivalent to RMS DGD measured with a reference test method (RTM) such as SPE, using typical standard reference materials (SRM) provided by national calibration laboratories. An example is shown in Figure 26 where the artifact is the same as the one used for the case shown in Figure 22. The DGD is measured as a function of optical frequency using the PSA polarimetric PMD test method. A smoothed mean-square envelope is plotted for guiding the eye only. TINTY analysis gives a PMD of 0,94 ps.

NOTE Equivalence means that the result exactly compares to RMS DGD deduced from DGD measurements within a practical, finite wavelength range, using the expression given hereinafter, answering the question: how exactly is DGD weighted when performing Interferometric PMD measurement? It does not mean that the result from TINTY is not weighted by the spectrum. It is, but it is not specified.

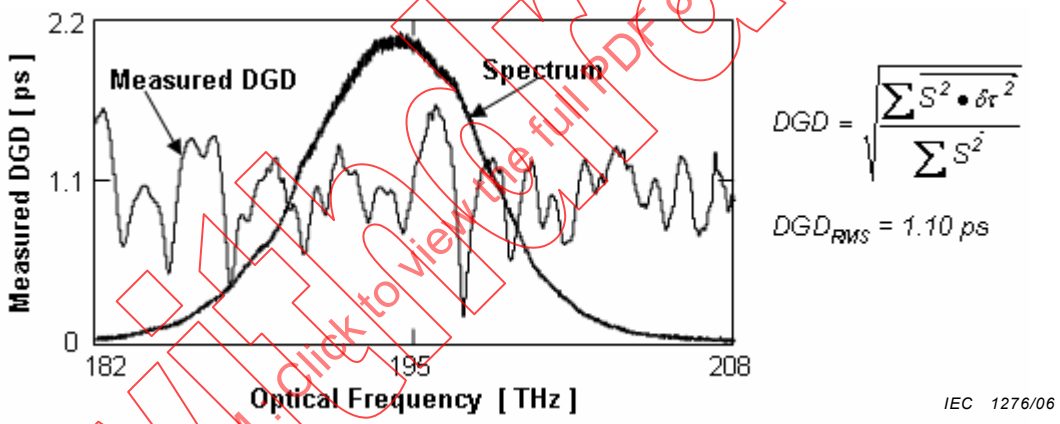

a) RMS DGD obtained from PSA analysis

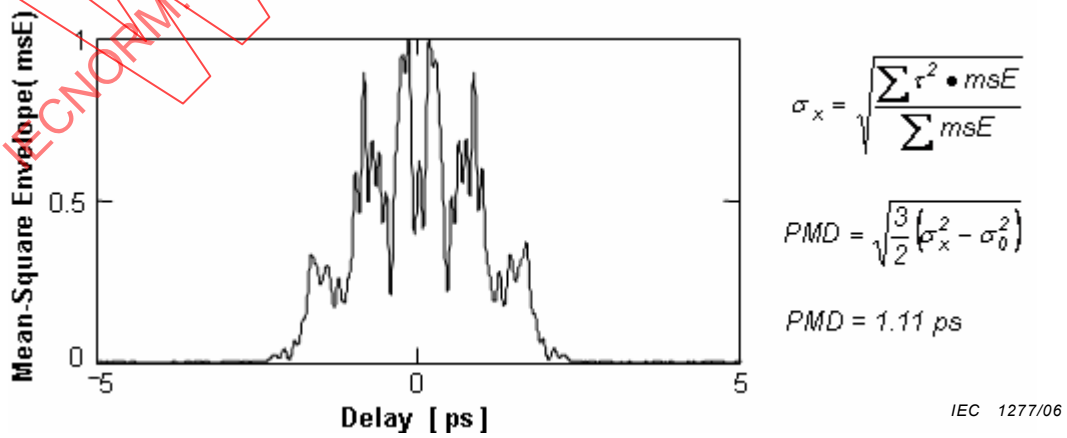

b) PMD obtained from GINTY analysis with the mean-square envelopes

Figure 26 – Equivalence between a) Stokes parameter evaluation method PSA analysis and b) GINTY analysis

IECNORM.COM : Click to view the full PDF of IEC TR 61282-9:2006
Withdrawn

- the measured PMD, i.e. RMS DGD $<\Delta\tau^2>^{1/2}$ given by Equation (214), is related to DGD $\Delta\tau$ by Equation (219):

$$Measured\_PMD = <\Delta\tau^2>^{1/2} = \sqrt{\frac{\int_\nu w_0^2(\nu)\Delta\tau^2(\nu)}{\int_\nu w_0^2(\nu)}} \tag{219}$$

where $w_0(\nu)$ is the FT of the autocorrelation interferogram (fringes).

If no normalisation of the spectra is performed, $w_0(\nu)$ is the physical spectrum $S_0(\nu)$ at the output of the DUT. But since $S_0(\nu)$ is known because the autocorrelation is known, $w_0(\nu)$ can be a user-selected window. Through respective applications of forward FT and inverse FT, the spectra are multiplied by $w_0(\nu)/S_0(\nu)$, and the corresponding interferograms retrieved. This is essentially identical to the spectrum normalisation in the FA method [16,27,28], under the following conditions:

a) $w_0(\nu)$ must not extend in a range where the measured physical spectrum $S_0(\nu)$ falls into the noise floor;

b) $w_0(\nu)$ can be nearly rectangular or narrow, but the resulting autocorrelation must not extend outside the delay travel.

Along the same lines (for instance, small PMD/σ_0 ratio), a good estimate of the DGD curve may be made via multiple-windowing. This consists of analysing the same raw data using a number of narrow, shifted windows. Ultimate practical limits remain to be assessed, but there is no theoretical limit. A few tenths of ps uncertainty is easily achieved with windows having a width of 100 GHz (~0,78 nm at 1 550 nm).

The weighting on DGD used in the SPE method is typically uniform, even when the source is an LED, because the spectrum is normalised when measuring the SOPs; the power along each polarimeter axis is divided by the total power. The exact same thing can be done with GINTY, as well as it is done, for example, with the generalised PSA implemented with an interferometer used as a FT spectrum analyser. Equivalence between GINTY (with mean-squared envelope) and SPE is ensured, and there is no source shape dependence of PMD. The expected value of a uniformly weighted RMS is the same as the expected value of a non-uniformly weighted RMS.

- subtraction of the offset σ_0^2.

NOTE When σ_0^2 is subtracted from σ_x^2, all that matters about the output spectrum is the RMS width of its FT (autocorrelation), which acts as an offset. Values obtained via Equation (214) are basically exact whatever the shape or width of the spectrum, should there be large ripples or not, thanks to the offset subtraction:

There is no theoretical requirement for spectrum smoothness, absence of ripples, etc; there are no particular requirements for the source spectral shape.

Noise-limited PMD value can basically be measured if a set-up is provided so that both autocorrelation and cross-correlation are obtained separately;

Measurement through amplified links is possible, i.e. with an unknown, narrowed and/or ill-shaped output spectrum.

The same consideration applies here in the case of Equation (200).

The following is an example of an algorithm for determining the PMD delay $<\Delta\tau^2>^{1/2}$ from the squared envelope of an interferogram.

Let $\tilde{I}_j$ denote the measured intensity of the interferogram at increasing positions t_j in units of ps, j = 1…N.

IECNORM.COM : Click to view the full PDF of IEC TR 61282-9:2006
Withdrawn

Step 1: computation of the zero intensity $\tilde{I}_0$

Definition: N_s = round (5 N/100) is the integer at which $\tilde{I}_j$ is approximately 5 %.

$$\tilde{I}_0 = \frac{\sum_{j=1}^{N_S} \left(\tilde{I}_j + \tilde{I}_{N_S - j} \right)}{2N_S} \tag{220}$$

Step 2: definition of the shifted intensity, I_j:

$$I_j = \tilde{I}_j - \tilde{I}_0 \tag{221}$$

Step 3: computation of the centre C of the interferogram:

$$C = \frac{\sum_{j=1}^{N_s} t_j I_j}{\sum_{j=1}^{N_s} I_j} \tag{222}$$

Step 4: computation of the second moment σ_x of the squared cross-correlation envelope over the full scan scale:

$$\sigma_x = \sqrt{\frac{\sum_{j=1}^{N} (t_j - C)^2 I_j}{\sum_{j=1}^{N} I_j}} \tag{223}$$

Step 5: truncate the scan scale

- Set $j_{\min}$ to the largest index j so that $C - t_j > 4\sigma_x$
- Set $j_{\max}$ to the smallest index j so that $t_j - C > 4\sigma_x$

Now the total number of points over the new scale is

$$N = (j_{\max} - j_{\min}) + 1 \tag{224}$$

Step 6: recomputation of the zero intensity $\tilde{I}_0$ within the new scan scale

Step 7: redefinition of the shifted intensity I_j

Step 8: recomputation of the second moment, $\sigma_{x,}$ of the of the squared cross-correlation envelope over the new adjusted scan scale

Redo Step 5 to Step 8 until there is no substantial variation of the second moment, i.e. second moment and scan become compatible (maximum delay of the scan scale ~4σ_x)

Step 9: Computation of the RMS width σ_0 of the squared envelope of the autocorrelation of the interferogram

Step 10: The PMD delay $\langle \Delta\tau^2 \rangle^{1/2}$ is computed using Equation (194).

IECNORM.COM : Click to view the full PDF of IEC TR 61282-9:2006
Withdrawn

5.5.3.1.2 Mixed mode coupling

In the case of mixed mode coupling, only GINTY applies with the same considerations as described in 5.5.3.1.1.1. An example of a test result is provide in Figure 27 for mixed mode coupling (one random-mode-coupling section with L/h = 10 + one negligible-mode-coupling section with $DGD = PMD_{\text{Random}}/4$; PMD = 9,97 ps, σ_A = 50 fs with nearly-flat envelope).

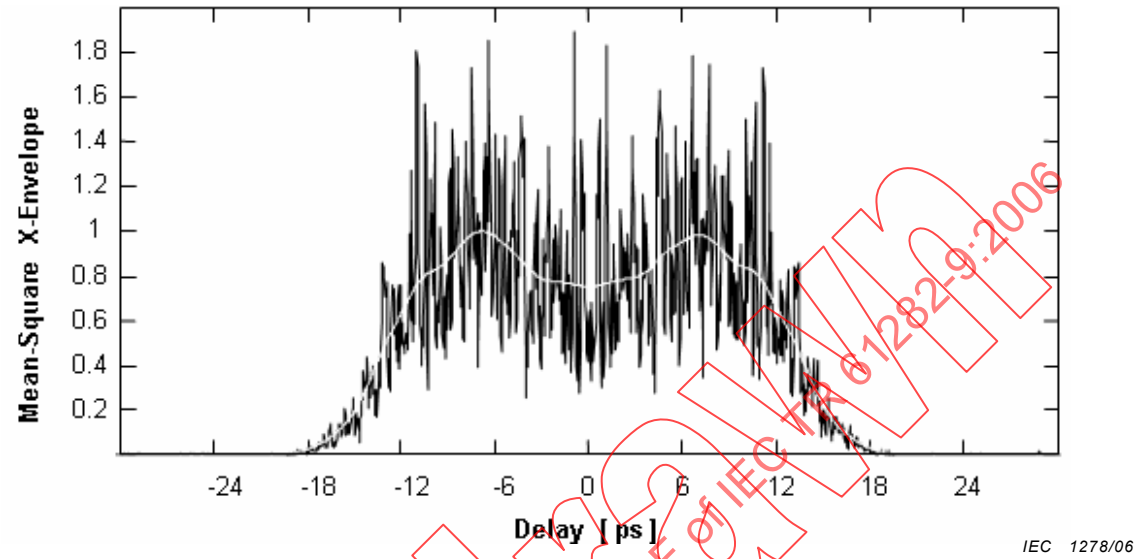

Figure 27 – Example of mixed-mode-coupling result using GINTY analysis

5.5.3.1.3 Comparison between TINTY and GINTY analyses for various degrees of coupling

The GINTY analysis is exact for any degree of coupling. The analysis is valid in all cases. Thus, "type of coupling" or "degree of coupling" labels are no longer necessary to qualify what can be measured when using GINTY. However, in order to compare the validity of TINTY results with GINTY, a Gaussian compliance factor (g) may be introduced. This factor would define by how much TINTY results are off-target simply knowing the shape of the interferogram. The following provides a basis for some useful definitions:

$$g \equiv \frac{PMD_{\text{TINTY}}}{DGD_{\text{RMS}}} = \frac{\text{TINTY Result}}{\text{GINTY Result}} \tag{225}$$

$$PMD_{\text{TINTY}} = g \, x \, DGD_{\text{RMS}} \tag{226}$$

The Gaussian compliance factor, g, can be expressed as follows:

$$g \equiv \frac{g_v g_S}{\sqrt{g_v^2 - g_S^2}} \tag{227}$$

where

$g_S \equiv \frac{1}{\sqrt{2}} \frac{\sigma}{\sigma_x}$ is a shape factor (a Gaussian interferogram corresponds to g_S = 1);

$g_v \equiv \frac{1}{\sqrt{2}} \frac{\sigma}{\sigma_0}$ is a value factor;

σ is the RMS width of the cross-correlation envelope;

σ_x is the RMS width of the squared cross-correlation envelope;

σ_0 is the RMS width of the squared autocorrelation envelope.

IECNORM.COM : Click to view the full PDF of IEC TR 61282-9:2006
Withdrawn

In case of large PMD, g_v>>1 and, consequently, $g \sim g_S$.

Table 3 provides some values of g_S for various types or degrees of coupling. Typical labels are given here for illustration only. These labels concerning types or degrees of coupling have developed fuzzy meanings, and tend to create misunderstandings and to generate an artificial appearance of complexity which is in fact simple. There simply cannot be a label for any device or interferogram shape that is possible, where indeed anything is possible in practice. The shapes mentioned in Table 3 refer to the shape of the RMS envelope (averaged over I/O SOPs).

Table 3 – Values of g_S for various types or degrees of coupling

Shape factor g_S	Interferogram shape	Mode coupling	Comments
1	Gaussian	Ideal random with $N = L/h \to \infty$	1-ps emulator: g = 85 %
$\sqrt{2^{\frac{1}{n}-1}}$	Super-Gaussian	Mixed/intermediate	
<1	Flat	Mixed/intermediate	
>1	Sharp	Mixed/intermediate	
$< \frac{1}{\sqrt{2}}$	Concave	Negligible: small L/h with large N and correlated axes	
$< \frac{1}{\sqrt{2}}$	Concave	Random: small L/h with small N and uncorrelated axes	g ~ 67 %
$\frac{1}{\sqrt{2}}$	3 peaks	No coupling (N = 1): PMFs, waveplates, etc.	
$\frac{1}{\sqrt{2}} = 0{,}707$	Rectangular window	Mixed/intermediate	"Flat-top", g = 71 % Figure 31: g = 75 %
$\sqrt{2} = 1{,}141$	Exponential	Mixed/intermediate	Sharp
$\sqrt{\frac{21}{50}} = 0{,}648$	Truncated parabola	Mixed/intermediate	Concave
$\sqrt{\frac{5}{6}} = 0{,}913$	Triangle	Mixed/intermediate	

Figure 28 further shows an example of the difference between TINTY and GINTY results.

IECNORM.COM : Click to view the full PDF of IEC TR 61282-9:2006
Withdrawn

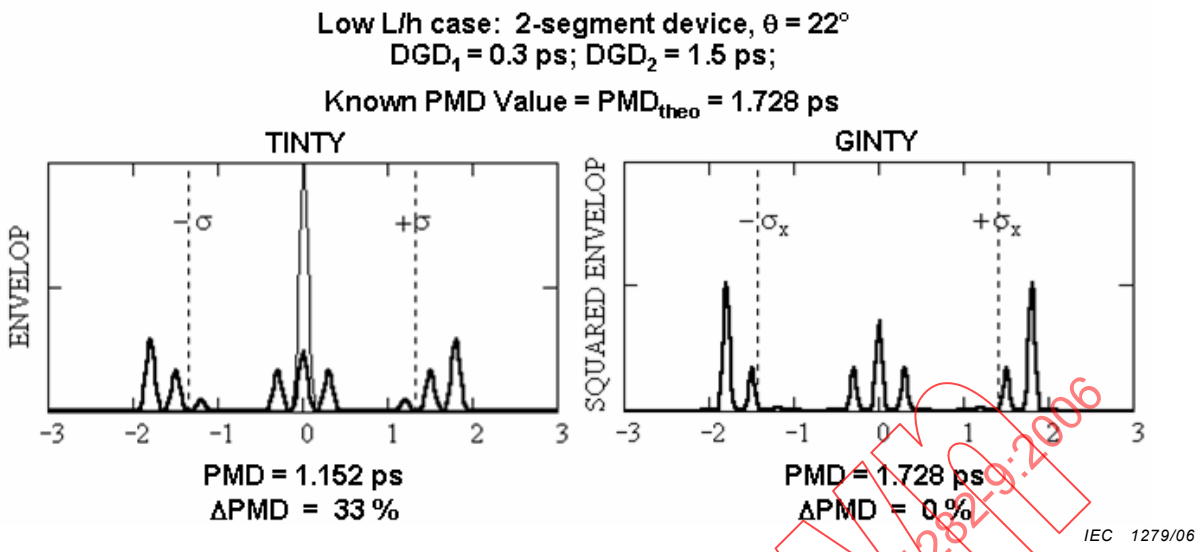

Figure 28 – Comparison between polarization mode dispersion results from TINTY and GINTY analyses

5.5.3.1.4 Three steps from root-mean-square width to root-mean-square differential group delay

NOTE $\langle\ \rangle$ represents an ensemble average over I/O SOPs

Step 1:

The mean-squared envelope, averaged over I/O SOPs, gives

$$\left\langle E^2(\tau)\right\rangle = R_0^2(\tau) + \left\langle E_x^2(\tau)\right\rangle \tag{228}$$

where $\left\langle E_x^2(\tau)\right\rangle = \left\langle \left|R_x(\tau)\right|^2 \right\rangle$ is the mean-square cross-correlation envelope.

The mean-square envelope is the sum of the two mean-square envelopes, as opposed to when the envelope is not averaged, and a single-scan, single I/O-SOP envelope is obtained. When averaged over I/O SOPs, the mean-square envelope is the sum of the two mean-square envelopes because $\langle R_x(\tau)\rangle = 0$.

Now, since $R_x(\tau)$ and $S_x(\nu)$ are forming a FT pair, it follows that

$$\int_\nu S_x^2(\nu) = \int_\tau |R_x(\tau)|^2 \tag{229}$$

is the Parseval theorem.

$$\int_\nu \left\langle \left(\frac{d}{d\omega} S(\nu)\right)^2 \right\rangle = \int_\tau \tau^2 \ |R_x(\tau)|^2 \tag{230}$$

is the generalised Parseval theorem (see Annex D). Thus, combining Equations (228), (229) and (230), step 3 equation follows.

IECNORM.COM : Click to view the full PDF of IEC TR 61282-9:2006
Withdrawn

σ_x^2

$\Downarrow$

mean square-derivative of spectrum $S_x(\nu) = x(\nu)\, S_0(\nu)$

$$\sigma_x^2 \equiv \frac{\int_\tau \tau^2 \left\langle E_x^2(\tau) \right\rangle}{\int_\tau \left\langle E_x^2(\tau) \right\rangle} = \frac{\int_\nu \left\langle \left(\frac{d}{d\omega} S_x(\nu) \right)^2 \right\rangle}{\int_\nu \left\langle S_x^2(\nu) \right\rangle}$$

(See Annex D: generalized Parseval theorem)

Step 2:

Starting from the $S_x(\nu)$ definition in Equation (175) and using the different corollaries in 5.5.2.4.1, it follows that

$$\left\langle \left(\frac{d}{d\omega} S_x(\nu) \right)^2 \right\rangle = S_0^2(\nu) \left\langle \left(\frac{d}{d\omega} x(\nu) \right)^2 \right\rangle + \left\langle x^2(\nu) \right\rangle \left(\frac{d}{d\omega} S_0(\nu) \right)^2 + 2 S_0(\nu) \frac{d}{d\omega} S_0(\nu) \left\langle x(\nu) \frac{d}{d\omega} x(\nu) \right\rangle$$

$$\left\langle \left(\frac{d}{d\omega} S_x(\nu) \right)^2 \right\rangle = S_0^2(\nu) \left\langle \left(\frac{d}{d\omega} x(\nu) \right)^2 \right\rangle + \frac{1}{3} \left(\frac{d}{d\omega} S_0(\nu) \right)^2 \tag{231}$$

Dividing Equation (231) by the integral of $\left\langle S_x(\nu) \right\rangle$, and using Equation (193) in the right member of Equation (231), then Equation (182) of σ_0^2, the step 2 equation follows.

mean square-derivative of spectrum $S_x(\nu)$

$\Downarrow$

mean square-derivative of Stokes parameter *x(ν)*

$x(\nu) \equiv \hat{\mathbf{s}}_a \bullet \hat{s}(\nu)$

$$\frac{\int_\nu \left\langle \left(\frac{d}{d\omega} S_x(\nu) \right)^2 \right\rangle}{\int_\nu \left\langle S_x^2(\nu) \right\rangle} = \sigma_0^2 + 3 \frac{\int_\nu S_0^2(\nu) \left\langle \left(\frac{d}{d\omega} x(\nu) \right)^2 \right\rangle}{\int_\nu S_0^2(\nu)}$$

Step 3:

The equation of motion of $\hat{s}(\nu)$, Equation (12), can be written as:

$$\hat{s}_\omega(\nu) = \hat{\Omega}(\nu) \times \hat{s}(\nu) = DGD(\nu) \left[\hat{p}(\nu) \times \hat{s}(\nu) \right] \tag{232}$$

where

$\hat{\Omega}(\nu)$ is the PDV;

$\hat{p}(\nu)$ is the PSP (unit vector, direction of the PDV).

IECNORM.COM : Click to view the full PDF of IEC TR 61282-9:2006
Withdrawn

Thus

$$\frac{d}{d\omega}x(\nu) \;=\; DGD(\nu)\;\hat{s}_a \bullet \left[\hat{p}(\nu)\times\hat{s}(\nu)\right] \tag{233}$$

$$\left\langle\left(\frac{d}{d\omega}x(\nu)\right)^2\right\rangle \;=\; DGG^2(\nu)\left\langle\left(\hat{s}_a \bullet \left[\hat{p}(\nu)\times\hat{s}(\nu)\right]\right)^2\right\rangle \tag{234}$$

Since $\hat{s}_a$, $\hat{s}(\nu)$ and $\hat{p}(\nu)$ are independent random variables, and $\left\langle s_{aq} \bullet s_{aq'}\right\rangle = \frac{1}{3}\delta_{q,q'}$ according to Equation (188), a corollary in 5.5.2.4.1,

$$\left\langle\left(\frac{d}{d\omega}x(\nu)\right)^2\right\rangle \;=\; DGD^2(\nu)\frac{1}{3}\left[\left\langle(p_2 s_3 - p_3 s_2)^2\right\rangle + \left\langle(p_3 s_1 - p_1 s_3)^2\right\rangle + \left\langle(p_1 s_2 - p_2 s_1)^2\right\rangle\right] \tag{235}$$

and since $\left\langle s_q \bullet s_{q'}\right\rangle = \frac{1}{3}\delta_{q,q'}$ also according to the corollary in 5.5.2.4.1, then,

$$\left\langle\left(\frac{d}{d\omega}x(\nu)\right)^2\right\rangle \;=\; DGD^2(\nu)\frac{2}{9}\left[p_1^2 + p_1^2 + p_3^2\right] \tag{236}$$

Finally, since $\hat{p}(\nu)$ is a unit vector, step-3 equation is obtained as follows:

mean square-derivative of Stokes parameter *x(ν)*

$$\Downarrow$$

$$DGD^2(\nu)$$

$$\left\langle\left(\frac{d}{d\omega}x(\nu)\right)^2\right\rangle \;=\; \frac{2}{9}\mathrm{DGD}^2(\nu)$$

Combining the equations shown in the three steps above, the link between RMS DGD and the RMS width of the cross-correlation squared-envelope is established, giving the exact-analysis formula as follows:

$$\sigma_x^2 = \sigma_0^2 + \frac{2}{3}\overline{DGD^2} \tag{237}$$

where

$$\overline{DGD^2} \;=\; \frac{\int_\nu S_0^2(\nu)\,DGD^2(\nu)}{\int_\nu S_0^2(\nu)} \tag{238}$$

IECNORM.COM : Click to view the full PDF of IEC TR 61282-9:2006
Withdrawn

5.6 Poincaré sphere arc method

This procedure, also called SOP analysis, is based on finding $\Delta\theta$ (see Figure 10) from one trajectory on the Poincaré sphere, or from a number of trajectories but treating them independently from each other. The method is fundamentally correct and will give the right result if $d\hat{\Omega}/d\omega \approx 0$; but it will give a false result if $d\hat{\Omega}/d\omega \neq 0$. Consequently, the method is fundamentally valid and has no bias in negligible mode coupling, but it is not valid in random mode coupling.

Its existence has propagated from a number of references in scientific literature [32-34].

It has never been verified in random mode coupling (example: 10 ps PMD over >20 nm), with no simulations and no comparison with the SPE. It is expected that since the SOP method counts extrema (like the FA method); a k correction factor would be required in order to make the method valid in the presence of random mode coupling.

However, there are a number of known facts available:

- the result depends on the local DGD but also depends on the local derivatives of $\hat{\Omega}$;
- in some cases, $\hat{\Omega}$ has very fast local changes with the local DGD giving any value, depending on how $\hat{\Omega}$ moved locally;
- the local DGD varies randomly, and there is a bias on the mean DGD, about 20 %, depending on the ratio of 1st order to 2nd order PMD.

The PS arc method is consequently only valid in negligible mode coupling.

5.6.1 Calculation or interpretation results

After the SOP fluctuation is measured by a polarimeter (Stokes analyser or rotating analyser), it can be transformed into the SOP curve as a function of wavelength (frequency).

The SOP is expressed as [35]:

$$SOP = \frac{1-\eta^2}{1+\eta^2} \tag{239}$$

where

$$\eta = \tan\left[0{,}5\tan^{-1}\left(s_3 / \sqrt{s_1^2 + s_2^2}\right)\right] \tag{240}$$

Here, η is the polarization ellipticity; s_1, s_2 and s_3 are Stokes parameters.

Here, the relationship between beat length and SOP is shown in Figure 29. Also, the relationship between Stokes parameter on the Poincaré sphere and the SOP is shown in Table 4 and Figure 30.

IECNORM.COM : Click to view the full PDF of IEC TR 61282-9:2006
Withdrawn

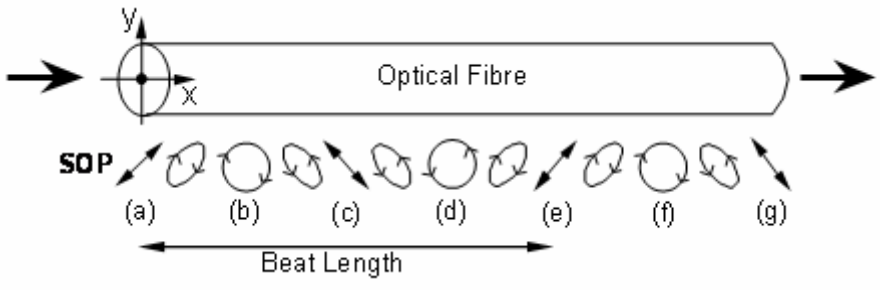

Figure 29 – Relationship between beat length and state of polarization

Table 4 – Values of 45 ° power, Stokes parameters and SOP corresponding to Figure 29

SOP	(a)	(b)	(c)	(d)	(e)	(f)	(g)
S_2/S_0	1 (max)	$\cos^2 45^o$	0 (min)	$\cos^2 45^o$	1 (max)	$\cos^2 45^o$	0 (min)
(s_1,s_2,s_3)	(0,1,0)	(0,0,1)	(0,-1,0)	(0,0,-1)	(0,1,0)	(0,0,1)	(0,-1,0)
SOP	1	0	1	0	1	0	1

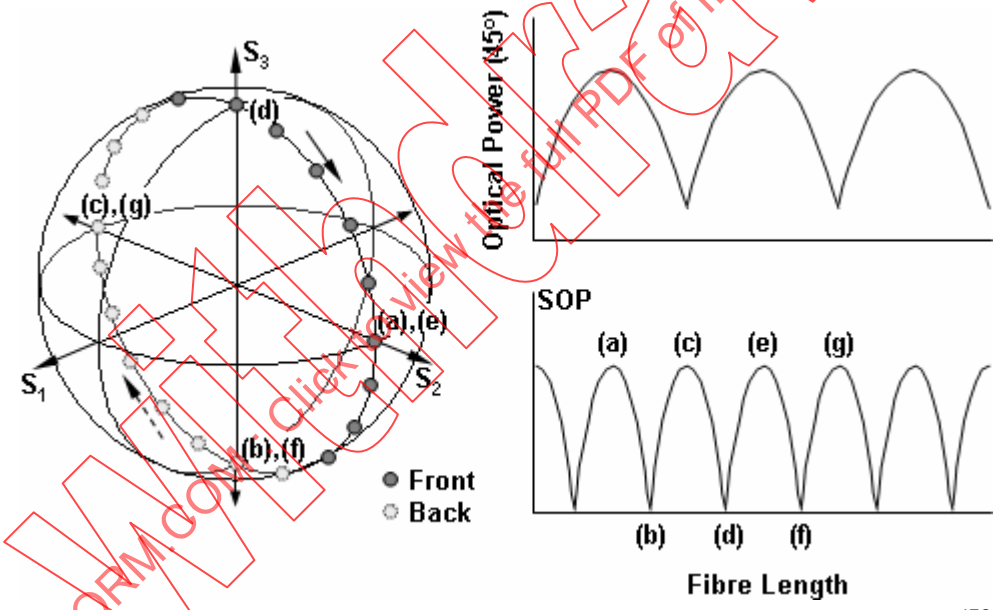

Figure 30 – Relationship between Stokes parameter and state of polarization on the Poincaré sphere

The DGD or PMD $\Delta\tau$ is given by [35]:

$$\Delta\tau = \frac{N}{2} \bullet \frac{1}{\Delta f} = \frac{N}{2} \bullet \frac{\lambda_1 \lambda_n}{c\Delta\lambda} \tag{241}$$

where N represents the numbers from extrema to extrema of the SOP curves.

IECNORM.COM : Click to view the full PDF of IEC TR 61282-9:2006

5.6.2 Possible ambiguity in the measurements

Depending on how the launch polarization relates to the PSP, there can be a factor-two ambiguity in the measured PMD.

It can be shown from Equations (240) and (241) that $(1 - \eta^2)(1 + \eta^2)$ is equal to $(1 - s_3^2)^{1/2}$, which is plotted versus s_3 in Figure 31. This plot assumes the use of a Stokes analyser in the SOP method and a circular polarizer/detector in the FA method.

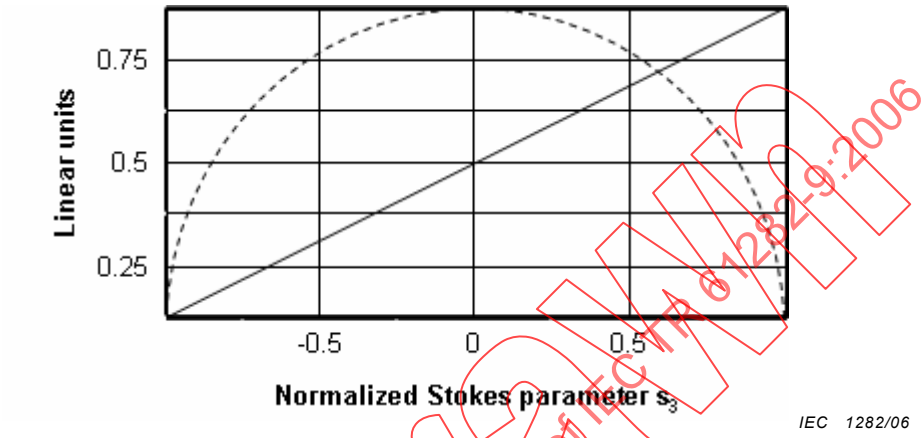

Figure 31 – Relationship between fixed analyser method with circular analyser (—) and Poincaré sphere arc method (---)

As the wavelength of the source is scanned, the output SOP traces a circle on the Poincaré sphere. Each time the circle is traced, s_3 goes through one cycle oscillation. The number of extrema in $(1 - \eta^2)(1 + \eta^2)$ per wavelength increment is counted, and this number is used to calculate the PMD.

If the output SOP circle is traced only on the upper hemisphere of the Poincaré sphere, there is exactly one maximum and one minimum in S_3 for each oscillation period. In this case, only the right half of Figure 31 is used, and $(1 - s_3^2)^{1/2}$ will also have only one maximum and one minimum. The same argument applies if the output SOP circle is traced only on the lower hemisphere of the Poincaré sphere. In this case, only the left half of Figure 31 is used.

Suppose, however, that the circle is large enough to extend into both hemispheres of the Poincaré sphere. In this case, the $s_3 = 0$ plane (i.e., the equator) is crossed twice in each oscillation cycle. From Figure 31, we see that $(1 - s_3^2)^{1/2}$ now has *two* maxima and *two* minima for each oscillation cycle. Counting extrema will then lead to a PMD value that is twice as large as before.

Thus the measured PMD value depends on a relationship between the SOP and PSP that is generally not known during the measurement. In the presence of random mode coupling, the error can still occur, but it is no longer a simple factor of two. This is not a flaw of all extrema counting methods – it can be seen in Figure 35 that the problem does not exist with the FA method.

Figure 32 illustrates experimental results showing that the SOP method results in a doubling of the peak count when the output polarization cycles back and forth across the equator of the Poincaré sphere ($s_3 = 0$).

IECNORM.COM : Click to view the full PDF of IEC TR 61282-9:2006
Withdrawn

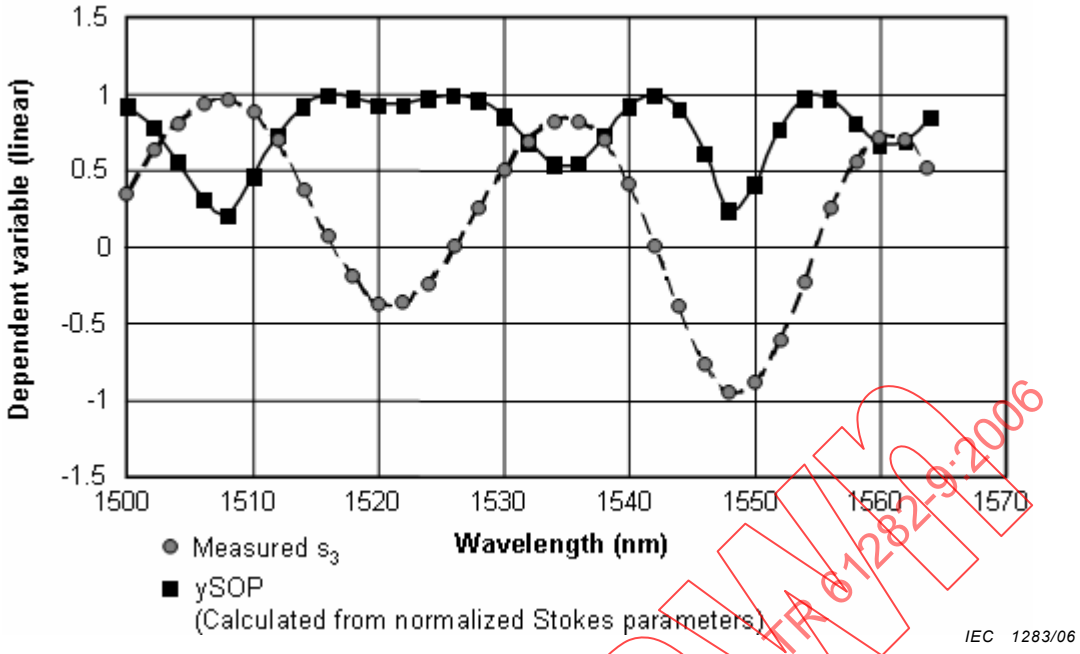

Figure 32 – Relationship of state of polarization (SOP) analysis to normalised Stokes s_3 parameter

The normalised Stokes parameters were measured using a polarimeter as the optical receiver. The curve labelled $ySOP$ is calculated from the measured normalised Stokes parameters using the published SOP formula.

The curve labelled s_3 gives the normalised Stokes parameter s_3 for comparison. Two cases are evident:

a) a peak or valley in the s_3 curve produces a single extremum in the $ySOP$ curve. This is evident at 1 508 nm, 1 534 nm, 1 548 nm and 1 561 nm;

b) an excursion across $s_3 = 0$ and back again produces a pair of extrema. This is evident for the negative s_3 valleys at 1 521 nm and 1 548 nm.

The impact of this behaviour is that polarization variations that extend back and forth across the $s_3 = 0$ boundary produce twice as many extrema as polarization variations that are confined to positive (or negative) s_3 values. In actual measurements, there is no way to predict where the polarization excursions will occur. Therefore, correction by a scale factor is not feasible.

In conclusion, there is a possibility of as much as a factor-two error occurring in the Poincaré sphere arc (SOP) method, confirming its non-validity for the random mode coupling.

5.7 Poole formula method

Poole [7] did not give a name to his method. However a number of facts are available:

- the method requires a $\Delta\lambda$ increment 4 to 5 times smaller than SPE for obtaining the same standard deviation independently from the noise;
- but Poole analysis and SPE are formally and fundamentally equivalent;
- the result with Poole analysis is right but the standard deviation is larger than with SPE if $\Delta\lambda \neq 0$.

Poole analysis estimates DGD by approximating the derivatives of T with finite differences.

In SPE using JME for instance, Equation (51) is obtained.

IECNORM.COM : Click to view the full PDF of IEC TR 61282-9:2006
Withdrawn

If the previous procedure is applied, the same standard deviation will be obtained with the Poole analysis, and the following conclusions stand:

- Poole's analysis = JME, fundamentally, in cases where $\Delta\lambda$ tends to 0;
- but even if $\Delta\lambda \neq 0$, the result with Poole's analysis is good, but the standard deviation will be larger.

5.8 Single-end test methods

Various techniques have been proposed for single-end PMD measurement:

- one is based on SPE (JME) analysis of the back-reflected field from the fibre far-end (Fresnel reflection) [36];
- another one is based on FA method [37] of the back-reflected field from the fibre far-end (Fresnel reflection);
- a third one is based on the use of a polarimetric optical time domain reflectometer (OTDR) for the identification of bad PMD section in a cable plant using correlation between DOP and the h factor [38].

5.8.1 Single-end test method using the Jones matrix eigenanalysis procedure

When a continuous optical wave is injected into a fibre, the total backscattered power is given by the sum of two contributions: the Rayleigh scattering and the Fresnel reflection due to the fibre far-end face. The Rayleigh backscattered power can be expressed as follows [39]:

$$P_S = P_0 \frac{S\alpha_R}{2\alpha}\left(1 - e^{-2\alpha L}\right) \tag{242}$$

where symbols have the following meaning (values are typical for step-index single-mode fibres at 1 550 nm): P_0 is the input power [W]; L is the fibre length [m]; $S \cong 1{,}5 \cdot 10^{-3}$ represents the recapture factor; $\alpha_R \cong 2{,}76 \cdot 10^{-5}$ m^{-1} is the Rayleigh scattering loss coefficient, and $\alpha \cong 5 \times 10^{-5}$ is the attenuation coefficient.

Similarly, the contribution due to the power reflected by the fibre end face is given by

$$P_F = P_0 \rho_F e^{-2\alpha L} \tag{243}$$

where ρ_F is the reflection coefficient ($\cong 0{,}035$) of the glass-air interface (a straight connector termination is assumed).

In order to perform PMD measurement based on the power reflected by the fibre far-end face, it should be assumed that P_F is the backscattered power dominant component. Setting a minimum acceptable value of the ratio P_F/P_S, the maximum fibre length is consequently fixed. From now on, it will be assumed that the total backscattered power is due to P_F only. The maximum fibre length can be further increased by placing a perfect reflector at the fibre far-end (i.e. $\rho_F \rightarrow 1$). This solution is mandatory when the fibre is terminated with an angled connector.

Let $\hat{s}_0$ be the unitary Stokes vector of the input field and R the Mueller matrix of a single-mode fibre; the SOP of the output field can be expressed as $\hat{s} = R\hat{s}_0$. The evolution of $\hat{s}$ as a function of frequency is well known [6]:

$$\frac{d\hat{s}}{d\omega} = \frac{dR}{d\omega} R^{-1}\hat{s} = \hat{\Omega} \times \hat{s} \tag{244}$$

IECNORM.COM : Click to view the full PDF of IEC TR 61282-9:2006
Withdrawn

where

R^{-1} represents the inverse matrix of R;

$\hat{\Omega}$ $= (\Omega_1, \Omega_2, \Omega_3)$ is the PDV;

$\Delta\tau$ $= \left|\hat{\Omega}\right|$ is the DGD.

A similar result can be obtained for the SOP of the backreflected field, $\hat{s}_B$. Indeed, it can be demonstrated that [35]:

$$\hat{s}_B = R_B \hat{s}_0 = MR^T MR\hat{s}_0 \tag{245}$$

where

M = diag(1,1,- 1) is a diagonal matrix;

R^T is the transpose of R.

The analogy can be pushed further, as it is easy to demonstrate that the evolution of $\hat{s}_B$ as a function of frequency is described by the following equation [40]:

$$\frac{d\hat{s}_B}{d\omega} = \left(\frac{dR_B}{d\omega}\right) R_B^{-1} \hat{s}_B = \hat{\Omega}_B \times \hat{s}_B, \tag{246}$$

where

$\hat{\Omega}_B$ may be written as

$$\hat{\Omega}_B = 2MR^T \begin{pmatrix} \Omega_1 \\ \Omega_2 \\ 0 \end{pmatrix} \tag{247}$$

Since M and R are orthogonal matrices, it is easy to obtain [40]:

$$\Delta\tau_B = \left|\hat{\Omega}_B\right| = 2\sqrt{\Omega_1^2 + \Omega_2^2} \tag{248}$$

It is well known that, when the fibre is in the *long-length regime*, Ω_i, i = 1, 2, 3, are Gaussian distributed random variables, statistically independent of each other, with zero mean and the same standard deviation [41]. Because of this, $\Delta\tau$ is Maxwellian while $\Delta\tau_B$ results Rayleigh distributed, and its PDF reads as follows [40]:

$$f(\Delta\tau_B) = \frac{2\Delta\tau_B}{\pi\langle\Delta\tau\rangle^2} \exp\left(-\frac{\Delta\tau_B^2}{\pi\langle\Delta\tau\rangle^2}\right) \tag{249}$$

where $\langle\Delta\tau\rangle$ is the mean value of $\Delta\tau$.

Finally the following relationship holds:

$$\langle\Delta\tau_B\rangle = \frac{\pi}{2}\langle\Delta\tau\rangle \tag{250}$$

IECNORM.COM : Click to view the full PDF of IEC TR 61282-9:2006
Withdrawn

It can be noticed that the motion equation of the round trip, (247), formally coincides with the motion equation of forward propagation (245). Consequently $\Delta\tau_B$ can be measured applying the same techniques used for forward measurements. Even if Equation (251) is independent of the particular measurement technique, the JME method is preferred because of its intrinsic high dynamic range and easy implementation in single-end configuration.

5.8.2 Single-end test method using the fixed analyser procedure

With the single-end technique, the PMD of the fibre can be calculated using the following formula:

$$\langle\Delta\tau\rangle = 1{,}555\frac{N_e - 1}{\Delta\omega} = 0{,}495(N_e - 1)\frac{\lambda_1\lambda_2}{2c(\lambda_2 - \lambda_1)} \quad (251)$$

where

$<\Delta\tau>$ is the fibre PMD;

N_e is the number of extrema of the signal $P(\lambda)$ in the spectral increment $\Delta\omega$;

c is the speed of light;

λ_1, is the initial wavelength of the spectral increment $\Delta\omega$ [42];

λ_2 is final wavelength of the spectral increment $\Delta\omega$ [42].

This formula is slightly different from that derived in [42] (i.e. N_e–1 instead of N_e), but is compliant with the ITU-T Recommendation G.650.2 [43]. As the purpose of these measurements is to demonstrate the coherence of two different measurement schemes, this formula has been chosen to adopt the same extrema counting criterion in the single-end and in the both-end configurations.

The intrinsic measurement uncertainty, due to the finite width of the spectral increment over which the extrema counting is performed, is given by

$$\frac{\sigma^2}{\langle\Delta\tau\rangle^2} \cong 0{,}19\frac{2\pi}{\langle\Delta\tau\rangle\Delta\omega} \cong \frac{0{,}19}{\langle\Delta\tau\rangle}\frac{\lambda_1\lambda_2}{c(\lambda_2 - \lambda_1)} \quad (252)$$

where σ is the standard deviation of the measurement results in the spectral increment, $\Delta\omega$.

With the both-end technique, the PMD can be calculated using the following formula [43]:

$$\langle\Delta\tau\rangle = 2{,}589\frac{N_e - 1}{\Delta\omega} = 0{,}824(N_e - 1)\frac{\lambda_1\lambda_2}{2c(\lambda_2 - \lambda_1)} \quad (253)$$

with the same meaning of symbols as illustrated before.

The intrinsic measurement uncertainty, due to the finite width of the spectral increment over which the extrema counting is performed, is given by

$$\frac{\sigma^2}{\langle\Delta\tau\rangle^2} \cong 0{,}21\frac{2\pi}{\langle\Delta\tau\rangle\Delta\omega} \cong \frac{0{,}21}{\langle\Delta\tau\rangle}\frac{\lambda_1\lambda_2}{c(\lambda_2 - \lambda_1)} \quad (254)$$

IECNORM.COM : Click to view the full PDF of IEC TR 61282-9:2006
Withdrawn

5.8.3 Single-end test method using polarization optical time domain reflectometry

A polarization sensitive OTDR (P-OTDR) can be used for field measurements along installed fibre links on the localisation and classification of fibre sections with respect to their PMD characteristics [44]. The technique relies on the statistical analysis of the local DOP obtained from the backscattered signal. It allows classifying fibre sections as low-, medium- and high-PMD contributors.

Most recent efforts [45-47] are derived from the P-OTDR initially proposed by Rogers for fibre sensing applications [48]. The simplest P-OTDR is nothing but an OTDR with a polarizer analyser inserted in the return path just before the detector. An interesting variation using a TLS is an extension of the FA PMD measurement methods [46]. Although conceptually simple and capable of directly measuring the DGD along a fibre, the technique is not well adapted to the task because of its long measurement time (one P-OTDR trace per wavelength) and complex and expensive hardware, but more importantly because it extracts the birefringence properties of the fibre from the measurement of the evolution of the SOP which is difficult to measure on high-PMD fibres.

The SOP of the light transmitted through a fibre is known to rotate about the birefringence axis at a rate that depends on the local birefringence of the fibre. The beat length, L_b, represents the period of this rotation and is defined by

$$L_b = \frac{\lambda}{\beta c} \tag{255}$$

where

λ is the wavelength of light;

β is the local birefringence of the fibre;

c is the speed of light.

For fibres with large birefringence (>1 ps/km), the SOP of the backscattered light completes one turn around the birefringence axis in less than 2,5 m, so that short P-OTDR laser pulses are required (<10 ns) to resolve the fast rotation. (The beat length of the backscattered signal is $L_b/2$ because of the round-trip.) Short pulse implies small dynamic range, and consequently high birefringence fibres (that necessarily exhibit high-PMD) are difficult to characterise. Only rather low-PMD fibres (<0,2 ps/km$^{1/2}$) have so far been tested with these techniques.

The limitation of the SOP-based technique has been recognised by Huttner et al. [49]. They suggested that the DOP is a more appropriate parameter for the characterisation of long or high birefringence fibres. They used the DOP and its standard deviation to estimate the fibre beat length, whereas its power spectral density was used to estimate coupling length. The interesting characteristic is that long OTDR pulse can be used since the resolution only has to remain smaller that the coupling length. This DOP method yields only order-of-magnitude estimates but allows identifying bad fibres amongst good ones.

The DOP method is based on temporal depolarization not to be confused with spectral depolarization. In practice, for each sample point, the backscattered light impinging upon the detector arrives from many scatterers distributed along the (half-) length of the pulse (L_p) within the fibre. If L_p and the beat length, L_b, are comparable, the polarization coming from each individual scatterer differs from the others, and the resulting measured SOP is a smoothed average of the true local SOPs. The evolution of the measured SOP is no longer directly related to the change in birefringence along the fibre, and this is why SOP-based methods fail in presence of large birefringence. It is instead the variations of the DOP, brought about by the variation of the SOP within the pulse, which will yield information on the local birefringence. It is important to note that this depolarization is dependent on the local birefringence only, and that it is not affected by the accumulated PMD.

IECNORM.COM : Click to view the full PDF of IEC TR 61282-9:2006
Withdrawn

Three particular regimes may be distinguished based on the relations between the pulse length L_p, the beat length L_b and the coupling length h.

a) $L_p << L_b$

No depolarization occurs within the pulse and the DOP stays close to unity whatever is h. This case is characteristic of low-PMD fibres.

b) $L_p >> L_b$

When the pulses are longer than the backscattering beat length, several SOP rotations occur within the pulse, which yield a decrease in measured DOP. For a very long pulse, $L_p >> h$, the transmitted DOP will tend toward zero, but the backscattered DOP approaches 1/3. The returned pulse gets partially re-polarized on its way back. Deventer [50] presented the complete explanation of this phenomenon with arguments based on Mueller matrix calculations. This case is characteristic of medium-PMD fibres.

c) $L_b << L_p << h$

The SOP rotates rapidly around the birefringence axis, but the orientation of the axis does not change much within the pulse. The measured local DOP can be anywhere between 0 and 1, since it will depend on the angle between the SOP and the birefringence axis. For a short section of fibre, the backscattered SOP collapses toward zero and the resultant DOP is small when the SOP and the birefringence axis are far apart (Figure 33a)). On the other hand, when the SOP and the birefringence axis are nearly aligned, the backscattered SOP will not cover a large part of the sphere and even if the P-OTDR pulse is long, the DOP will remain close to 1 (Figure 33b)). This case is characteristic of high-PMD fibres.

IECNORM.COM : Click to view the full PDF of IEC TR 61282-9:2006

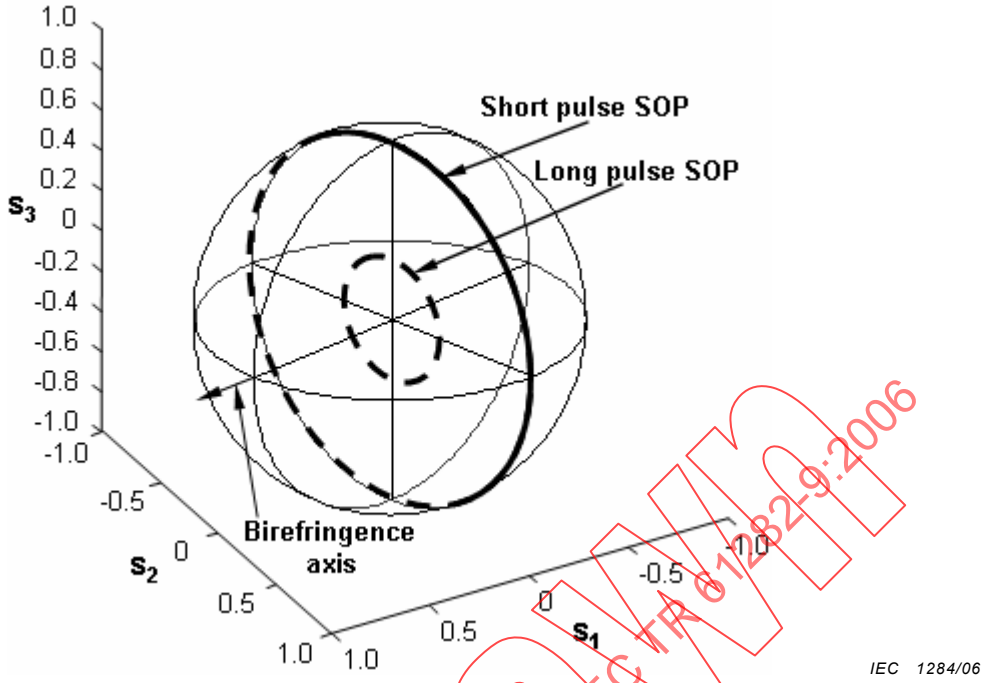

a) For wide SOP-to-birefringence axis angle

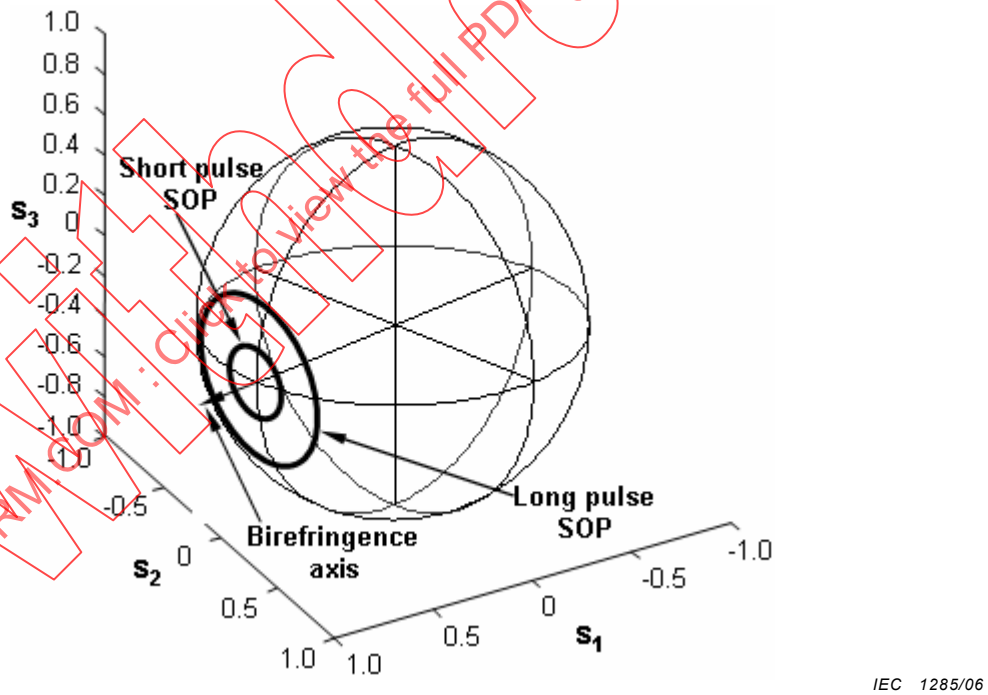

b) For a small SOP-to-birefringence axis angle

Figure 33 – Backscattered state of polarization (SOP) for short and long pulses versus distance

The mean DOP measured with the P-OTDR give some insights of the mean local birefringence of a fibre. An estimate of the mean DOP can be calculated based on the fading in signal that is expected from the ratio between the P-OTDR resolution and the backscattering beat length by the following formula:

IECNORM.COM : Click to view the full PDF of IEC TR 61282-9:2006
Withdrawn

$$\overline{DOP} = 0{,}33 + \frac{0{,}67}{\sqrt{1+\left(\frac{2 \cdot L_p}{L_b/2}\right)^2}} \qquad (256)$$

where

L_p is the spatial resolution of the P-OTDR;

$L_b/2$ is the beat length of the backscattering signal.

L_p is defined as FWHM of the impulse response of the P-OTDR, measured at a Fresnel reflection. The simple estimate in Equation (256) yields a relatively good estimate of the mean DOP, but is not exact since it does not take into account the impact of mode coupling.

The SOP of the light rotates about the birefringence axis of the fibre upon propagation. However, the birefringence vector varies both in amplitude and orientation over the length of the fibre, which gives rise to mode coupling and the notion of coupling length. The coupling length is roughly defined as the length for which the birefringence axis has changed significantly or alternatively, for which a significant portion of energy in one mode (fast or slow) is transferred to the other mode.

The PMD itself is obtained from the knowledge of both the beat length and the coupling length through the following approximation (which holds for long fibres $L > L_b$ and h):

$$PMD = \frac{\lambda\sqrt{hL}}{cL_b} \qquad (257)$$

It is interesting to note that the L_b and h have opposite effects on the PMD. Large L_b *(small birefringence)* leads to low PMD whereas large coupling length leads to high-PMD. Recent fibres have rather long beat length and short coupling length. Older fibres tend to have significantly longer coupling lengths for similar beat lengths. Therefore, the detection of a long coupling length should allow the identification of most of the high PMD sections in a fibre link.

In practice, for fibre with negligible mode coupling (high h value), the DOP is expected to vary slowly against distance with values between 0 and 1. But the DOP will not change as long as the orientation of the fibre birefringence axis does not change with distance (relative to an initial point). If the orientations of the slow and fast axes move, the DOP will vary. Slow fluctuations with large DOP amplitude are seen on fibres with a very long coupling length, h, as can be seen in the centre section of Figure 34.

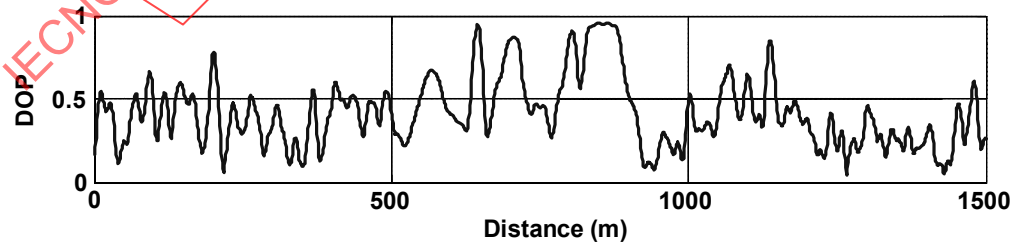

IEC 1286/06

Figure 34 – Degree of polarization (DOP) vs. distance for a concatenation of three 500-m fibres, with a centre fibre that exhibits a high *h* value

The rate of change of the DOP is thus related to the rate of change of the orientation of the birefringence vector, which is itself related to the coupling length, h. In order to quantify the rate of change of DOP against distance, the DOP correlation length is used, a quantity that is refered to as h_{DOP}. h_{DOP} has a definition similar to the coupling length and it has been shown

IECNORM.COM : Click to view the full PDF of IEC TR 61282-9:2006
Withdrawn

to be linearly related to h for values of h that are higher than the resolution of the P-OTDR [51].

6 Measurement issues

The following paragraphs will discuss some of the critical issues related to the measurement techniques described in this document.

6.1 Degree of polarization and amplified spontaneous emission

The methods described in this document using a TLS together with a step-wavelength technique such as the SPE JME or the FA, $\Delta\lambda$ being the wavelength increment ("step"), or with a swept wavelength system, $\Delta\lambda$ being the RBW, require that light emerging from the DUT remains polarized under all measurement conditions and for all DGD values being measured. A DOP of 90 % or greater is preferred, although measurements may be performed with values as low as 25 % with reduced precision.

It is important to understand that the DOP that is mentioned here refers to the DOP at the DUT output, not at the DUT input.

This DOP requirement is particularly critical when testing optical amplifiers (OAs). Although the test source is highly polarized, the DOP at the output of the OA may be significantly reduced by the unpolarized amplified spontaneous emission (ASE) as well as by the OA PMD itself. In this case, the measured signal DOP (at the DUT output) should be at least 25 % within the optical bandwidth of the SOP measurement. This is of particular concern when using a TLS without a tracking optical filter at the OA output, because the total ASE power out of the OA, i.e. the ASE spectrum integrated over all wavelengths, impinges on the photodetectors whatever the selected wavelength. In this case, proper saturation conditions must be ensured in order for the DOP to be high enough for accurate measurement.

An optical fibre amplifier (OFA) such as an erbium doped fibre amplifier (EDFA) will emit more ASE noise but will have higher signal gain if the source signal power is low. Raising the signal power to saturate the amplifier will reduce signal gain but also reduce the ASE power. Figure 35 shows a typical OFA output spectrum from a TLS input as viewed on an OSA with a RBW of 0,5 nm (~65 GHz around 1 550 nm).

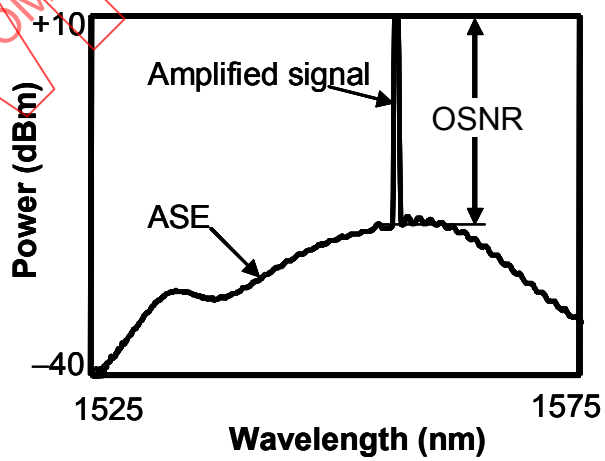

Figure 35 – Power spectrum of a typical optical fibre amplifier output showing the amplified signal, the amplified spontaneous emission (ASE), and the optical signal-to-noise ratio (OSNR)

Normally, the ASE noise is specified in optical systems using OSNR, the ratio of the signal power and the noise power defined when the RBW is 0,1 nm. When using a BBS and

IECNORM.COM : Click to view the full PDF of IEC TR 61282-9:2006
Withdrawn

spectrum analyser (the latter acts as a narrowband optical tracking filter centred about the selected wavelength), or a TLS with a tracking narrowband filter at the output of the amplifier, then the OSNR is the relevant quantity to consider. In this case, the ASE power, within the RBW of the spectral analysis, or output-filter bandwidth, remains low with respect to signal power for a broad range of saturation conditions.

However, when using a TLS without a tracking optical filter at the OA output, the total ASE power out of the OA, i.e. the ASE spectrum integrated over all wavelengths, impinges on the photo-detectors whatever the selected wavelength. In this case, proper saturation conditions must be ensured in order for the output DOP to be high enough for accurate measurement. For this case, it is best to take the ratio of the signal power to the total ASE power. This would be the case when using a TLS and no filter, or BBS and no filter, as in the case of interferometry. Figure 36 shows the relationship between the ratio of signal power to total ASE to the more conventional OSNR (in 0,1nm RBW). This illustrates that the ASE total power is more than the signal power, even for "good" OSNR of 18 db to 20 dB. This can limit the permissible range of amplifier saturation conditions.

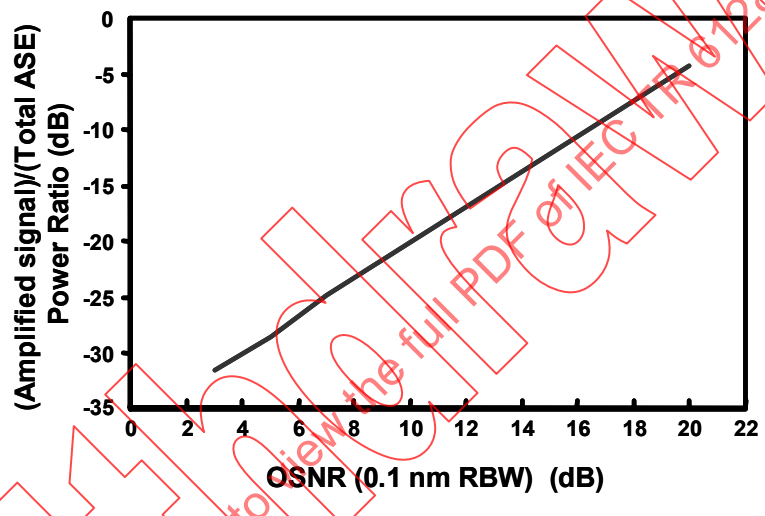

Figure 36 – Power ratio of amplified signal to total amplified spontaneous emission (ASE) versus the optical signal-to-noise ratio (OSNR) in 0,1-nm resolution bandwidth (RBW)

The DOP requirement is consequently less of a concern when using a BBS and spectral analysis (which acts as a narrowband filter centred about the selected wavelength), or a TLS with a tracking narrowband filter at the output of the amplifier. In this case, the ASE power, within the RBW of the spectral analysis, or output-filter bandwidth, remains low with respect to signal power for a broader range of saturation conditions.

With INTY, the DOP at the DUT output, over the spectral width, is typically very small (OA or not), whenever $PMD^{*}\Delta\nu$ is much larger than one. But, the condition $PMD^{*}\Delta\nu >> 1$ is exactly what is being required, as much as possible, to get the best averaging.

Now, regarding the ratio amplified-signal to ASE, it has nothing to do with the DOP requirement; it does not depend on PMD. And it must not be confused with DOP over the spectral width, which is already low, whether there is ASE or not.

Finally, the input must obviously be polarized. Any polarizer will meet this requirement; this is not critical at all. Even a 10-dB extinction ratio can be satisfactory at DUT input. One important criterion to be set should be that the extinction of the input polarizer must be, say, 10 times or larger than the PDL of the DUT. This is particularly important in the case of link testing. When a link exhibits some PDL, a cross-correlation interferogram can be observed even if the input DOP = 0.

IECNORM.COM : Click to view the full PDF of IEC TR 61282-9:2006

Assuming that the signal is highly polarized and the ASE is unpolarized, the DOP is given by the following equation:

$$DOP = \frac{P_s}{P_s + \int N(\lambda) d\lambda} \tag{258}$$

where

P_s is the amplified signal power;

$N(\lambda)$ is the power spectral density of the ASE.

The integral in the denominator is the total ASE power. For an OFA, the value of N at the signal wavelength can be calculated as follows:

$$N = FGh\nu \tag{259}$$

where

F is the OA noise factor;

G is the gain;

h is Plank's constant;

ν is the optical frequency.

Typical values for a heavily saturated amplifier are:

F = 4 (6 dB)

G = 100 (20 dB)

P_s = 10 mW (+10 dBm)

For $h\nu$ = 1,28 x 10^{-19}, N is calculated as follows:

N = 4 x 100 x 1,28 x 10^{-19} = 5,12 x 10^{-17} W/Hz ~ 6,4 x 10^{-6} W/nm = –21,9 dBm/nm.

Assuming a 30 nm bandwidth, the total ASE power is 0,19 mW = –7,2 dBm. Using Equation (251), DOP is calculated as 10/(10+0,19) = 98 %. This value is very adequate for making DGD measurements.

However, if the signal level is lowered, the ASE rises. Here are typical values for an OFA at a lower level of saturation:

F = 4 (6 dB)

G = 1000 (30 dB)

P_s = 1 mW (0 dBm)

N = 4 x 1000 x 1,28 x 10^{-19} = 5,12 x 10^{-16} W/Hz ~ 6,4 x 10^{-5} W/nm = –11,9 dBm/nm.

Again, assuming a 30 nm bandwidth, the total ASE power is 1,9 mw = +2,8 dBm. Using Equation (258), DOP is calculated as 1/(1+1,9) = 34 %. This is marginally adequate for the JME or FA method using a narrowband TLS. It is therefore critical to adequately saturate the OFA to obtain a sufficiently high DOP and a reliable measurement result. Furthermore, filtering and other methods may be needed to maintain the instrument performance.

6.2 Suppression of amplified spontaneous emission using optical or electrical filtering

In 6.1, the ASE noise contribution from the use of OAs within the instrument (e.g. for power boosting) or within a link was considered.

IECNORM.COM : Click to view the full PDF of IEC TR 61282-9:2006
Withdrawn

ASE is characterised by its un-polarized, broadband nature. Normally, ASE is a random noise (characteristically similar to white noise) and, like other types of noise in electrical measurements, requires some specialised methods to suppress or remove its effects. Without control, it acts to swamp or saturate the detector within the instrument or to add a spurious output to the detector photo-current, so limiting the amount of signal gain/sensitivity that can be used or simply adding noise to the overall PMD output.

ASE control is highly effective in PMD instrumentation. Some of these control techniques are discussed here. These may be applied individually or in tandem where required:

- control of OA saturation conditions

This technique can be used most effectively with TLS sources, which have higher power densities. If the TLS can drive the OFA hard into saturation, then ASE will be minimised and signal output maximised. This will maintain both a good OSNR at the instrument detector and maintain a high DOP for SOP measurements;

- reducing the detection optical bandwidth

The optical bandwidth used at the detector can be limited to very effectively filter the ASE. For example, the use of a tuneable optical filter at the detector, tracking in tandem with the source wavelength, will allow a much lower ASE power to arrive at the instrument. The detector will no longer be in danger of becoming saturated, and the amount of ASE noise affecting the wanted signal is reduced, and the instrument performance will be maintained at higher OSNR levels;

- reducing the electrical bandwidth

The optical input must always be detected without the detector circuit becoming saturated or overloaded, or else PMD measurement linearity or bias problems will occur. However, once the signal has been converted to an electrical signal, then electrical filtering methods can be used to limit the effective system bandwidth. This typically requires the PMD light source to be modulated at a high frequency (e.g. when using the MPS method). This enables the signal power to be detected using tuned filters, synchronous demodulation, lock-in amplifier, etc. and the ASE (broadband noise) is rejected except within the signal transmission window;

- discriminating the light source from the ASE

This is essentially the same as reducing the electrical bandwidth, by modulating the source and detecting only the modulation, observed at the detector. The “modulation” may take many forms, typically intensity modulation, or digital keying or encoding methods.

6.3 The use of a broadband source

It is possible to characterise devices, components, sub-systems, systems and networks with the use of BBS and tuneable optical filter (such as OSA). Some filters (analysers) have ≤10-pm RBW (<1,5 GHz around 1 550 nm). The difference here is the power measurement range. Strong ASE sources of ≥ 0 dBm/nm will give approximately –20 dBm (including filter loss) in a 20-pm window, whereas laser sources are generally >0 dBm, thus a 25-dB difference in measurement range. It is worth noting that some ASE sources can give >+20 dBm/nm in some wavelength ranges. Nonetheless, if the sensitivity of the detectors is –80 to –90 dBm, this still gives, in general, 60 dB to 70 dB of measurement range, sufficient for many measurement applications.

If a BBS is used together with a tuneable filter or OSA after or before the DUT and the FT is performed on the OSA output signal, the interferogram or the time signature of the signal is obtained. This approach may be used for instance to perform PMD measurement using the PSA method. In that case, the RBW is the setting parameter. In fact any measure has a RBW, tuneable laser included, that must be known, including the shape of the filter used) if the results need to be accurately determined and properly analysed.

IECNORM.COM : Click to view the full PDF of IEC TR 61282-9:2006
Withdrawn

In the case of the interferogram, the cut-off delay or the coherence time (in the time domain) or the RBW (in the frequency domain) must be specified. This corresponds to specifying the bandwidth of a filter, in order to properly reduce the noise level: the spectrum of the signal (the interferogram) is looked at and is cut-off from the point or area where there is excessive noise, spurious or non-interesting, irrelevant information. In fact, the cut-off frequency of the filter (or its coherence time) is carefully selected by analysing the signal spectrum (the interferogram).

6.4 The Nyquist theorem and optical measurements

Many optical components designed for use in WDM optical systems exhibit, for instance, narrow optical bandwidths with fine spectral structure in their optical characteristics. This fine structure is sometimes critical to the correct interpretation of the suitability of the device to its intended application. This requires adequate sampling of the data in the spectral domain, and this requires some initial consideration of the Nyquist conditions for the device. In order to properly apply the Nyquist theorem to the optical measurement domain, important aspects must be considered first concerning its application to time varying signal as well as to frequency spectrum signals.

6.4.1 The Nyquist theorem

The Nyquist theorem (also referred to as the Nyquist criterion) has been used for a long time and is still generally used for measurements of time varying signals (signals in the time domain); thus its terminology is well adapted to the time domain. However, its validity covers any units used with ordinates or abscises of measurement results (any domain).

The Nyquist theorem stipulates that when sampling a signal in the time domain, the sampling frequency used to reconstruct the signal must be at least larger than or equal to two times the bandwidth of the measured signal.

The bandwidth of the measured signal is defined in its Fourier spectrum by Fourier transforming the signal from the time domain to the frequency domain. Bandwidth here means RBW but also the shape of the signal itself, such as the shape of a filter together with its RBW.

6.4.2 Example of a noise-free time varying signal

Figure 37 shows a signal having symmetry from time "0." This does not affect the generality of the example but simplifies the graphical representation, and will ease the process of going from time domain to frequency domain (Figure 38a and Figure 38b).

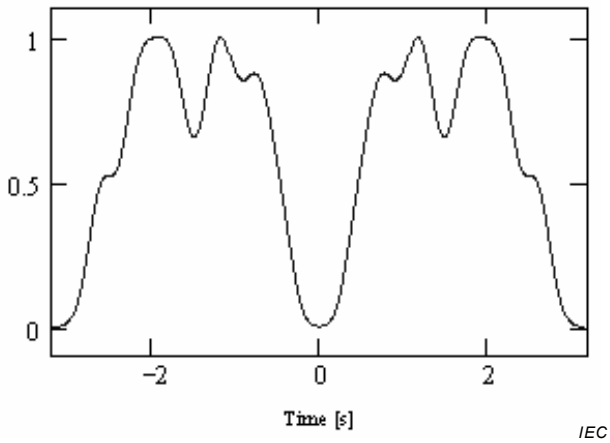

Figure 37 – Time varying signal

IECNORM.COM : Click to view the full PDF of IEC TR 61282-9:2006
Withdrawn

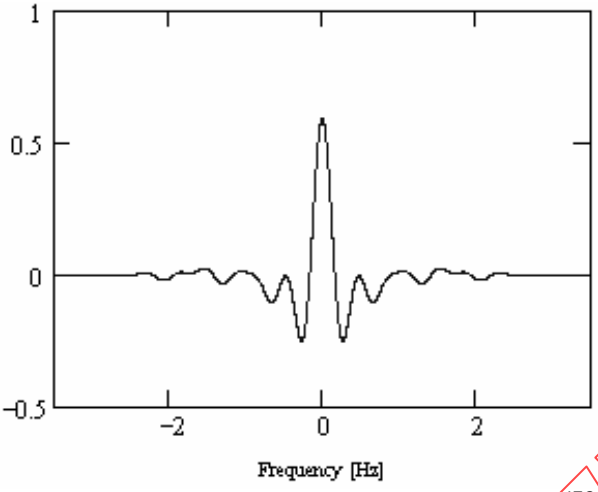

a) Linear scale

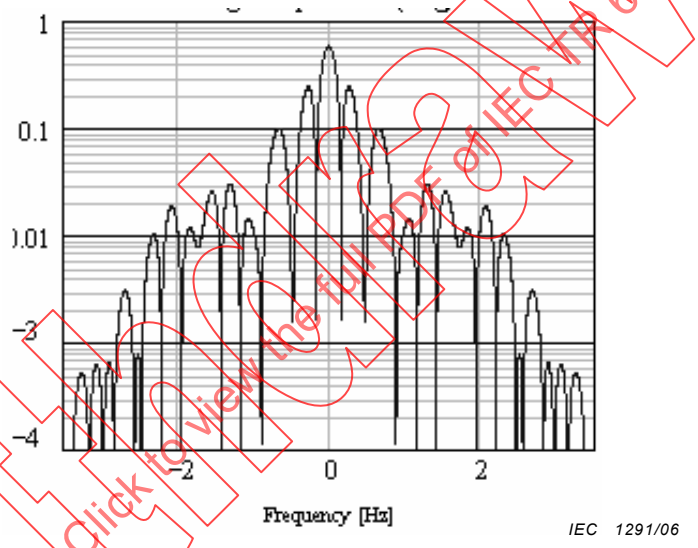

b) Log scale

Figure 38 – Frequency spectrum of Figure 37 signal (its Fourier transform) a) in linear; b) in log scales

IECNORM.COM : Click to view the full PDF of IEC TR 61282-9:2006
Withdrawn

As the signal in Figure 37 has a finite duration, its frequency spectrum (FT) goes to infinity. However, in practice, the measurement accuracy is not infinite (uncertainty exists and is finite), and consequently a spectral width (the signal bandwidth) is chosen proportional to this measurement accuracy.

This signal will then be sampled and then tentatively reconstructed in two different ways:

- first, by following the Nyquist theorem, i.e. by sampling the signal with a frequency at least larger than or equal to two times the signal defined bandwidth;
- second, by using a sampling frequency too low by a factor two (under-sampling).

Figure 38a and Figure 38b show that the signal is essentially defined in a frequency band of about 2,5 Hz. The minimum sampling frequency can consequently be set at 5 Hz in order to follow the Nyquist theorem (Figure 39a), which corresponds to a time increment of 1/(5 Hz) = 0,2 s. If this time increment is used, the signal can be accurately reconstructed (Figure 39b).

If the signal is under-sampled (Figure 40), the reconstruction is inaccurate. The difference is based not only on the fact that part of the signal has been neglected but also because that neglected part has folded and acts now as a perturbation.

Nyquist-followed signal

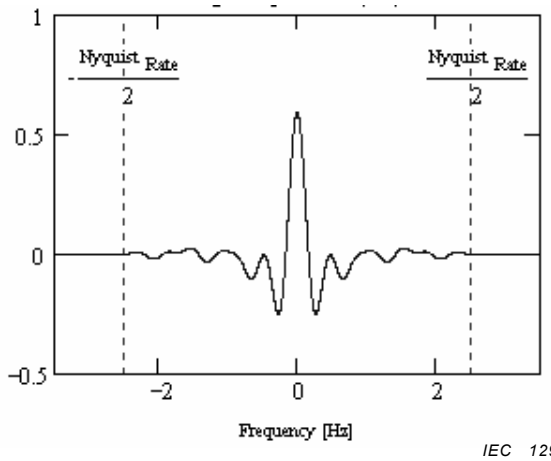

IEC 1292/06

a) Signal frequency spectrum

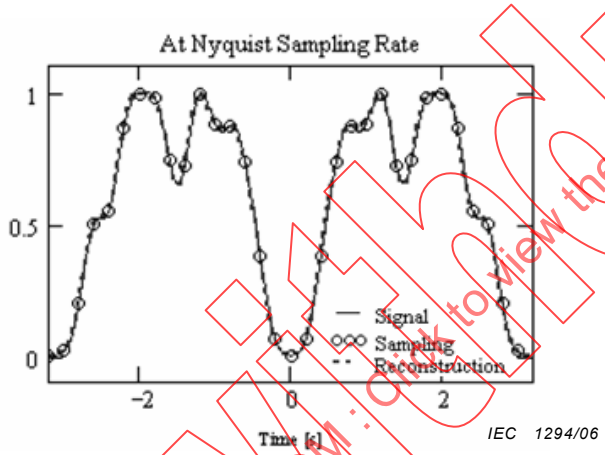

IEC 1294/06

b) Sampled and reconstructed time signal

Figure 39 – Filtered signal with Nyquist-based defined bandwidth

Under-sampled signal (factor 2)

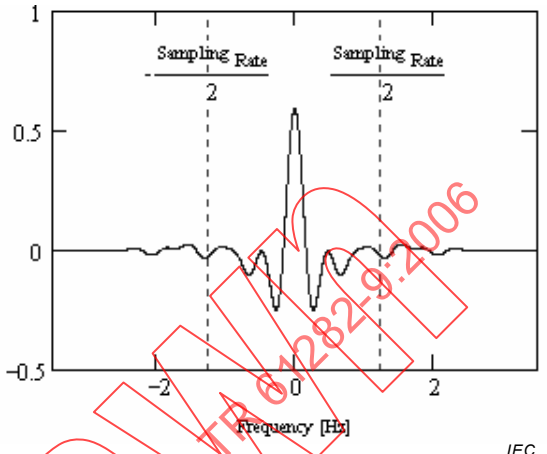

IEC 1293/06

a) Signal frequency spectrum

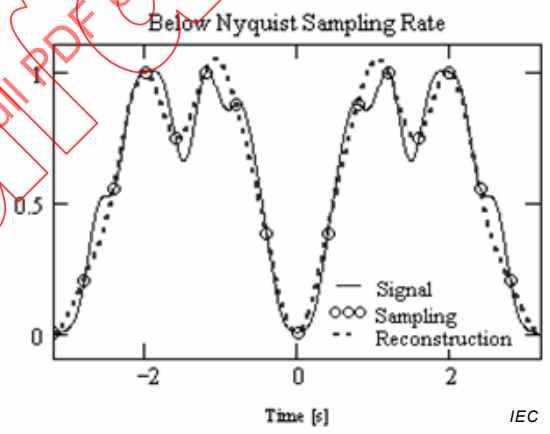

IEC 1295/06

b) Sampled and reconstructed time signal

Figure 40 – Unfiltered signal with under-sampled (factor 2) defined bandwidth

IECNORM.COM : Click to view the full PDF of IEC TR 61282-9:2006
Withdrawn

6.4.3 Example of a noisy time varying signal

In practice, all signals come with noise. Following the case discussed in the previous clause, a zero-average Gaussian noise will be added to the time varying signal shown in Figure 37. Figure 41 shows the new noisy signal in the time domain while Figure 42 shows its frequency spectrum (its FT). The frequency spectrum of the new noisy signal is not anymore only defined by its original spectrum (zero-noise average), but the noise now broadens the spectrum almost to infinity (the noise bandwidth is infinite). In order to accurately reconstruct the signal, two alternatives can be considered:

- sample the signal with infinite rate (infinite bandwidth to sample the noise as well); or
- filter the signal before sampling (to remove the noise).

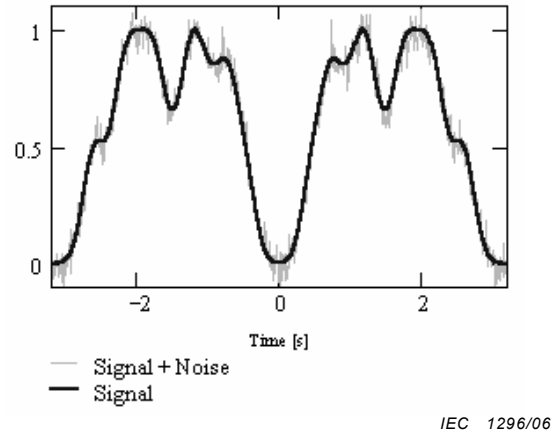

Figure 41 – Figure 37 signal with noise

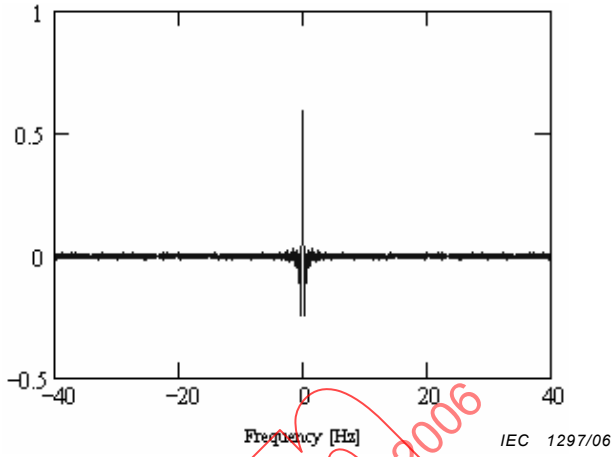

Figure 42 – Frequency spectrum of Figure 41 signal

The signal shown in Figure 41 will now be sampled following the same process as discussed in the previous clause but in two different ways:

- in the first case (Figure 43a), the noisy signal is filtered so as to follow the Nyquist theorem; while
- in the second case (Figure 44a), the noisy signal is not filtered and as such the Nyquist theorem is not followed.

Figure 43b shows the benefit of filtering the signal, as the sampled data points are practically all found on the curve representing the original signal; while in Figure 44b the sampled data points are spread.

Figure 43c shows a reconstructed signal very close to the original one when following the Nyquist theorem (right sampling frequency and filtering), while Figure 44c shows the impact of the folded noise onto the reconstructed signal: signal distortion is obvious.

The Nyquist theorem is followed

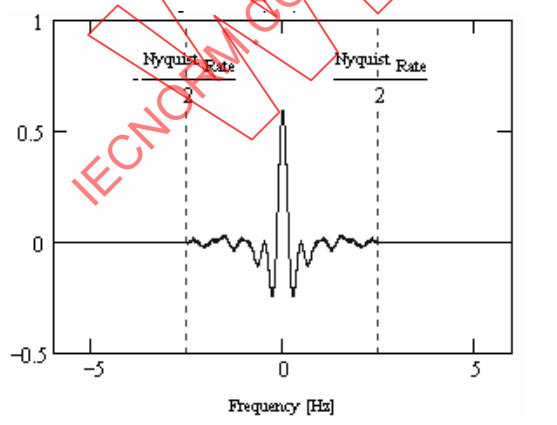

a) Signal spectrum

The Nyquist theorem is not followed

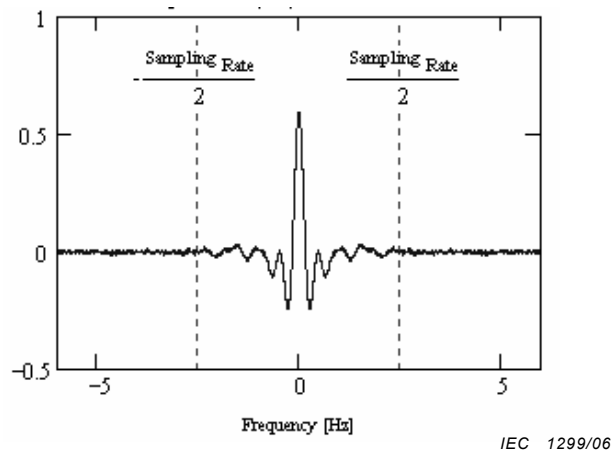

a) Signal spectrum

IECNORM.COM : Click to view the full PDF of IEC TR 61282-9:2006
Withdrawn

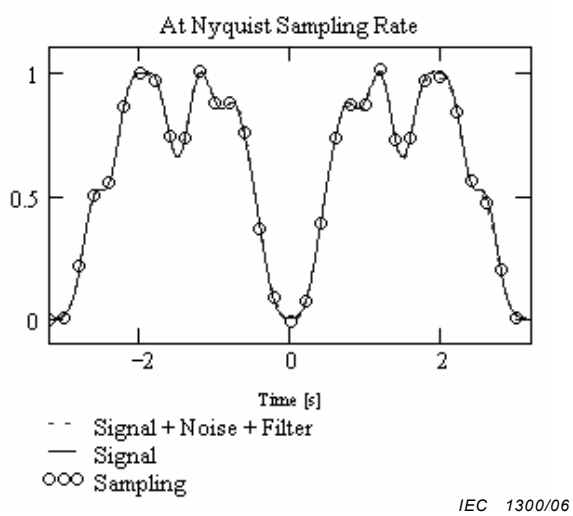

b) Sampled signal

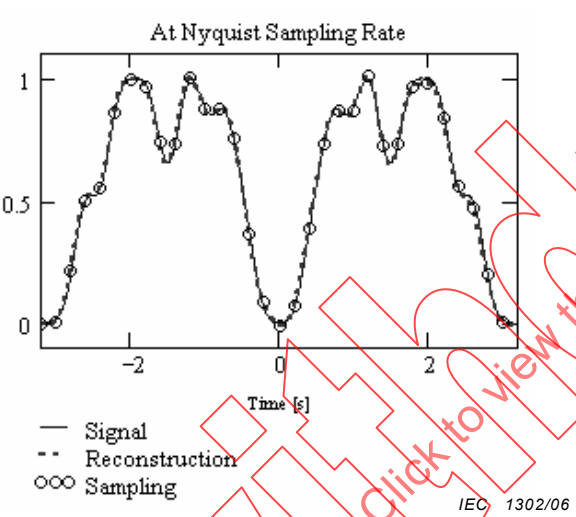

c) Reconstructed signal

Figure 43 – Filtered noisy signal respecting the Nyquist theorem

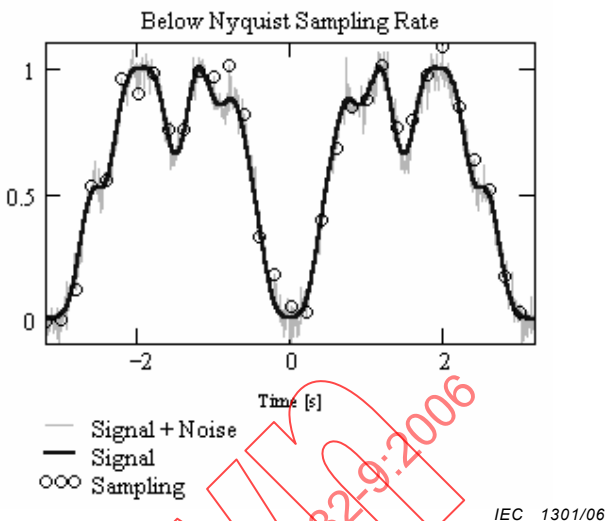

b) Sampled signal

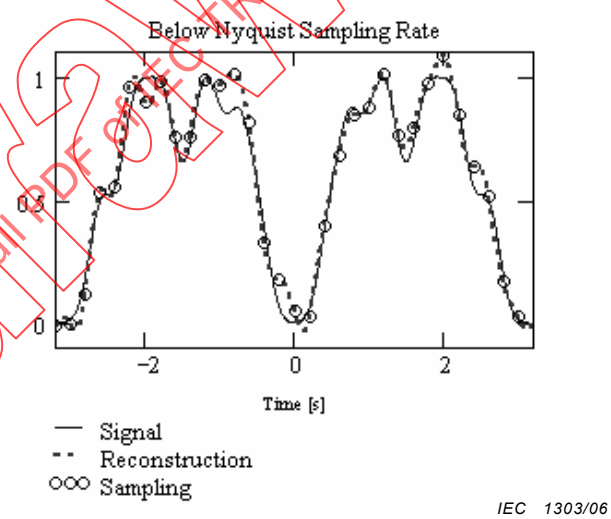

c) Reconstructed signal

Figure 44 – Un-filtered noisy signal spectrum not respecting the Nyquist theorem

IECNORM.COM : Click to view the full PDF of IEC TR 61282-9:2006
Withdrawn

6.4.4 Example of a frequency varying signal

When measuring a transmission spectrum in the frequency domain, the issue is the same. Only the terminology is different.

Figure 45 illustrates a transmission spectrum whose shape is the same in the frequency domain as the one shown in Figure 37 in the time domain. The difference is shown on the "X" axis (the abscissa) now scaled in units of Hz instead of in units of s as shown in Figure 37. The FT of this kind of frequency filter is its time impulse spectrum (Figure 46 – Impulse response from Figure 45). It has the same shape as shown in Figure 38.